秋田県立大学大学院博士学位論文

Design and Preparation of Functional Hydrogels and Their Application in Sensors

（機能性ヒドロゲルの設計と調製およびセンサーへの応用）

陸　春因

2022 年 **3** 月

Abstract

Hydrogel is a soft material with a structure similar to natural biological tissue. It is soft, stretchable and has good biocompatibility. Therefore, hydrogels have received extensive attention as carriers for next-generation flexible wearable devices. However, conventional hydrogels typically lack mechanical properties and functionalities such as toughness, anti-freeze property, adhesion, and self-healing, which will not meet the needs of wearable devices for signal stability, durability, low-temperature adaptability, and so on. Based on the above problems, this thesis designs and develops conductive hydrogels with high toughness, anti-freeze property, adhesion, and self-healing ability, and investigates in detail their application as flexible sensors. The specific research is divided into the following parts:

In Chapter 1, the research background, the application and limitations of hydrogels in sensors, the current status of research on tough hydrogels and functional hydrogels, and the purpose of this research are introduced.

In chapter 2, the properties of experiment materials, as well as experimental methods and characterizations are presented.

In chapter 3, to address the challenge of toughness, ionic conductive hydrogels have been crosslinked by carboxymethyl cellulose and phytic acid via a simple one-pot approach. The unique double crosslinked microstructure ensures that the hydrogel has favorable mechanical performance, resilience (93%, similar to natural resilin), and recovery (20 min, after 7 cycles at 300%) along with less residual strain (6.7%, after 20 successive cycles at 125%). The hydrogel also exhibits outstanding ionic conductivity (6.0 S/m). The combined mechanical performance and ionic conductivity of the prepared hydrogel results in its remarkable performance when used in sensors. The hydrogel-based sensor displays superior sensitivity (GF of 2.86, at a strain of 600%), stability and durability towards both tensile and compressive deformation. In practical applications, the sensor demonstrates a broad strain window to detect both large and

very small human activities, showing the excellent potential of this hydrogel in sensing and flexible devices. The approach in this work has also been optimized to potentially allow for large-area, low-cost fabrication.

In chapter 4, a novel anti-freezing system based on ice structuring proteins and $CaCl_2$ was introduced to enable a conductive hydrogel with low-temperature adaptability. Both formation of ice nuclei and ice growth of the hydrogel at sub-zero temperature could be inhibited. Supported by the anti-freeze system, the hydrogel revealed good flexibility (890% at -20°C), recovery and conductivity (0.50 S/m at −20°C) at both room temperature and sub-zero temperature. The low-temperature adaptability enabled the hydrogel to be used as strain and temperature sensors at both room temperature and sub-zero temperature. The anti-freeze system in this work is expected to open up a new avenue to promote the conductive hydrogel with low-temperature adaptability.

The purpose of chapter 5 is to address two existing challenges. One is to achieve the balance of mechanical properties, adhesion, and self-healing ability in hydrogel used in wearable devices. The other is to use mature products as raw materials and simplify the preparation process of adhesive hydrogels, so as to make it possible for large-scale industrial production. A novel PAA/Fe/PVP hydrogel has been prepared by a simple one-step radical polymerization to meet the above requirements. As the main component of adhesives in daily life, PVP is used to improve the adhesion of the hydrogel. The adhesion as high as 64kPa is achieved in the hydrogel. The adhesion can also withstand multiple uses due to the good mechanical properties of the hydrogel. Furthermore, the hydrogel displays outstanding self-healing ability in terms of both mechanical properties and conductivity. Because of the good mechanical properties, robust adhesion and rapid self-healing ability, the hydrogel-based sensors have demonstrated stability, accuracy and reliability in real-time monitoring of subtle facial micro-expressions and large human activities. In addition, the method uses mature products as raw materials, and the preparation process is simple, so it has the potential for large-area and low-cost production.

In chapter 6, the present study is summarized.

Content

Chapter 1 Introduction

1.1 Background

Hydrogels are viscoelastic, solid-like materials that are the result of entrapment and adhesion of liquids in a large solid three-dimensional surface area matrix [1]. The three-dimensional network of hydrogels can be formed by cross-linking polymer chains through covalent, hydrogen bonding, van der Waals forces, or physical entanglement [2-4]. Since Wichterle [5] first reported hydrogel materials in the 1950s, hydrogels have received close attention from many researchers for their unique wet and soft properties and have subsequently been pervaded in daily life and industrial applications, such as soap, shampoo, toothpaste, hair gel, contact lenses, oil recovery, pharmaceutical, agriculture, textile, and water treatment. [6-10] With years of development, hydrogels now have a wider range of applications in bioengineering, drug delivery, tissue engineering and flexible wearable devices. [11-14]

1.2 Hydrogel in sensors

Novel smart wearable devices use flexible conductive hydrogels as substrates, which possess mechanical properties similar to human skin and can be adhered to the human epidermis for more accurate measurements. Conductive hydrogels are ideal materials for the preparation of wearable sensors because of their good mechanical properties, biocompatibility, and conductivity [15]. Flexible sensors work by converting external deformations into electrical signals [16-19]. Several common electrical signal conversion mechanisms are capacitive, resistive, piezoelectric, friction-generated, and optical effects. Among the hydrogel-based sensors, the transduction principles and fabrication process of resistive and capacitive sensors are much simple potential applications are wide-ranging, and similarities can be easily drawn between studies.

1.2.1 Capacitive Sensor
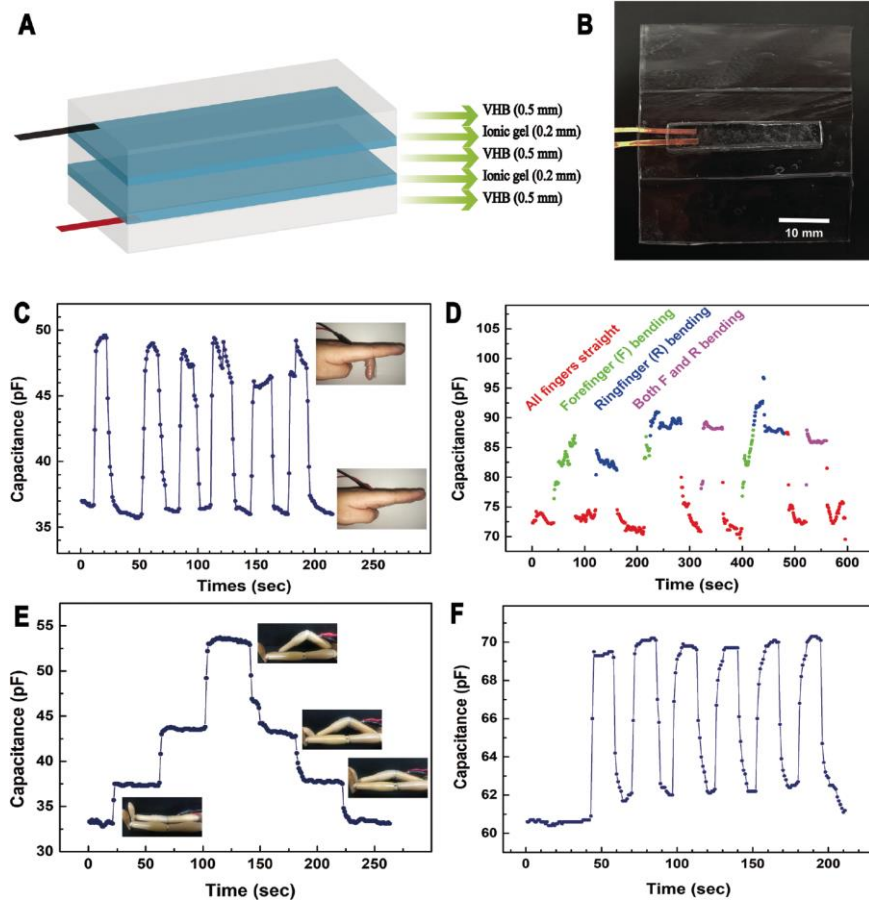
Fig. 1.1 A-B) Schematic diagram and a photo of capacitive strain sensor. C-F) The signals of various deformations monitored by the capacitive strain sensor in real time. [20]

Capacitive sensors are made according to the principle of parallel plate capacitance. The capacitance of a parallel plate capacitor can be calculated by formula (1). The changes in the spacing between parallel plates (d), the area of overlap of the upper and lower plates (A), and the dielectric constant (ε) will affect the capacitance. Therefore, when the sensor is working, its capacitance will change with the deformation of the sensor. For example, our group made a capacitive sensor based on tough polyacrylic acid ionic hydrogel [20]. The hydrogel is used as a conductor for the capacitive sensor. Two sheets of ionic hydrogel are sandwiched between a dielectric layer of acrylic elastomer tape, and two additional layers of VHB are covered on the top and bottom to

protect the sensor and prevent water evaporation from the surface of the ionic hydrogel (Fig. 1.1). The sensor can accurately and quickly discern deformations and monitor body movements such as joint flexion and extension, muscle contraction and relaxation.

$$C = \varepsilon A/d \qquad (1)$$

1.2.2 Resistive Sensor
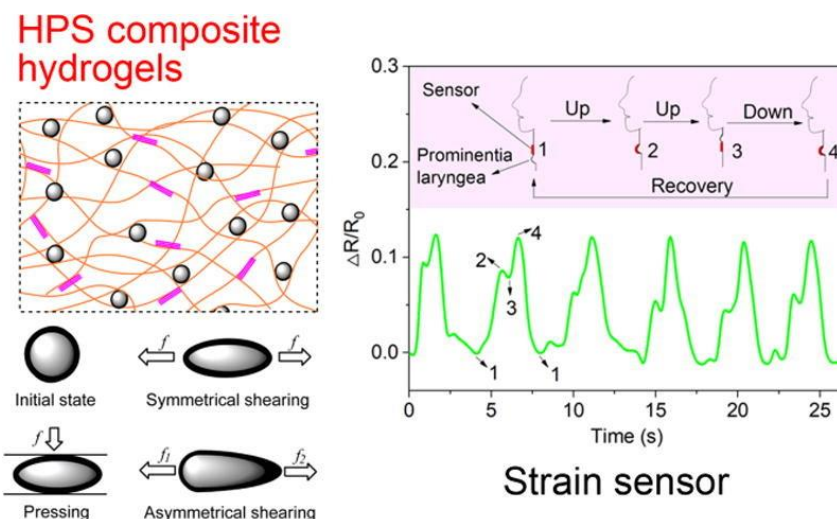
Fig. 1.2 a) Illustration of elastic deformation of HPS under different forces. b) Movement of the laryngeal prominence during swallowing as monitored by resistance sensors. [21]

The working principle of resistive sensor is to convert the change of resistance value caused by external stimulation into electrical signal. Resistive flexible sensors have been widely studied and applied owing to their simple structure and working mechanism, relatively simple fabrication process, and excellent performance. Zhou et al. [21] designed robust and sensitive pressure/strain sensors utilizing a novel composite hydrogel composed of hollow polyaniline spheres (HPS), poly(vinyl alcohol) (PVA) and phytic acid (PA) (Fig. 1.2a). By taking advantages of structure-derived elasticity of hollow spheres, conductivity of doped conducting polymers, flexibility of polymer matrix and physically cross-linked structure, the composite hydrogels based resistive sensor can achieve a gauge factor (GF) of 2.9 in the strain range of 0%~300%, a GF of

7.4 in the strain range of 300%–450%, a response time of 0.22 s and high reliability (1000 cycles). On the basis of their high performances, flexible sensors of the composite hydrogels are applied in monitoring various human motions, physiological activities and bending/vibration deformations in daily life (Fig. 1.2b).

1.2.3 Limitations of hydrogel in sensors

Hydrogel has a network structure like natural life tissue and shows similar physiological properties to human skin. In recent years, many excellent research results have been achieved in hydrogel as a carrier material for flexible wearable devices. [22-27] However, due to the existence of a large amount of water in hydrogels, hydrogels have poor mechanical properties, including poor elongation, toughness, and recovery, which will greatly limit their ability to monitor large-scale and repetitive human movements as wearable monitoring devices. Therefore, it is necessary to prepare hydrogels with high strength, toughness, and recovery for wearable strain sensor applications. In addition, hydrogel tends to freeze in low temperature environments, which greatly limits its flexibility, conductivity, and sensitivity at sub-zero temperatures. Further, for wearable device applications, suboptimal conductivity will result in limited sensitivity. In addition, most hydrogels lack adhesion, requiring additional tape to bond the hydrogel to human skin. The lack of adhesion makes the operation complicated on the one hand, and causes unavoidable friction between the sensor and the bonding surface on the other hand, which affects the accuracy and real time of signal detection. Therefore, there is still much room for improving the performance of hydrogel materials in the preparation of hydrogel-based sensors. The preparation of hydrogel materials with excellent mechanical properties and functional properties is very important for their application in sensors.

1.3 Tough hydrogel

For flexible wearable devices, especially those that fit snugly on the skin, high elasticity,

high flexibility, and good mechanical fatigue resistance are required. [23, 24, 28] However, conventional hydrogel materials are usually either too soft or too mechanically brittle, which extremely limited their potential applications. Therefore, the study of hydrogel toughening has been one of the major research focuses in the past two decades, and many significant results have been achieved. The toughening mechanisms of hydrogels can be classified into the following categories: topological toughening mechanism, hydrophobic association toughening mechanism, macromolecular microspheres toughening mechanism, nanocomposite toughening mechanism and interpenetrating network toughening mechanism.

1.3.1 Topological toughening mechanism
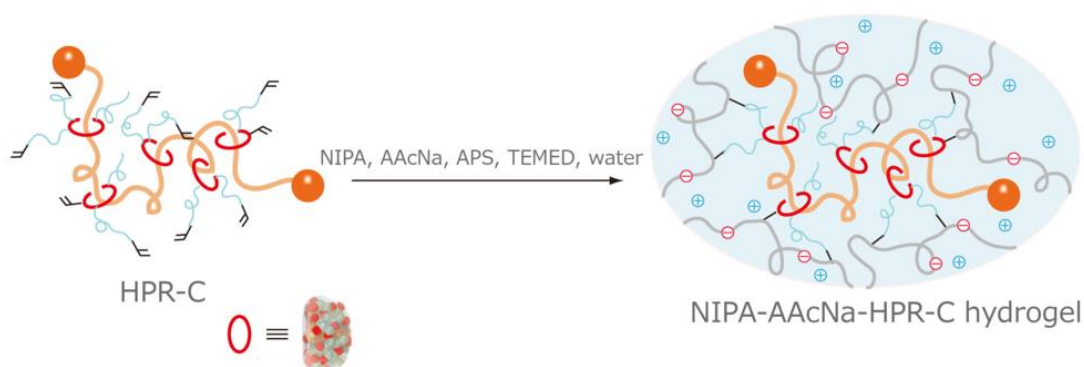
Fig. 1.3 synthesis of topological hydrogel by using nonionic PR cross-linker [29].

Topological hydrogels, also known as "slip chains" or slip ring polymer hydrogels, were first synthesized by Yasushi Okumura and Kohzo Ito in 2001 [30]. Topological hydrogels are topological materials composed of necklace-like macromolecules [31]. The structures of these hydrogels have been compared to pulleys and chains with knots, in which movable ring crosslink slides along the polymer chain. The ends of the chains have blocking molecules (topological constraints) that prevent the ring molecules from dissociating from the axis (Fig. 1.3). The distribution of crosslinking points in sliding ring hydrogels is also random like other types of hydrogels, but their crosslinking points are able to slide with the chain segments. When stress is applied, the crosslinking points

inside the hydrogel can slide arbitrarily like a "pulley". A long molecular chain is divided into several chain segments, thus spreading the stress uniformly to each chain segment [32]. Also, because the hydrogel network is three-dimensional, the "pulley" can spread the stress uniformly throughout the hydrogel network. Slip-ring hydrogel can solve the defect of irregular structure inside the hydrogel, so the slip-ring hydrogel has higher regularity than other types of hydrogels [33]. As a result, slip-ring hydrogels have extremely high stretchability, good recovery, swelling and low viscosity [34-36]. Therefore, compared with ordinary hydrogels, sliding ring hydrogels can bear more stress and dissipate more energy.

1.3.2 Hydrophobic association toughening mechanism

Fig. 1.4 Physically cross-linked network of PEG-DFA hydrogels; DFA hydrophobic aggregates (in red) and PEG chains (in black). RHS is equivalent hard sphere radius according to Percus−Yevick model; RM is mean micellar radius. [37]

Hydrophobic association hydrogels (HA-gels) have physical crosslinking networks, which are generated via hydrophobic association [38]. When hydrophobic groups are introduced into the hydrogel, hydrophobically linked micelles are formed, entangling the hydrophobic chain segments with the hydrophilic groups. The hydrophobically

linked micelles act as physical cross-linking points in the hydrogel system and effectively disperse the stress [39]. Meanwhile, the hydrophobic chains within the micelles can dissipate energy by uncrosslinking or molecular chain slippage, so the hydrophobic effect can lead to a substantial improvement in the mechanical properties of hydrogels [40]. Mihajlovic et al. [37] prepared hydrophobically associated supramolecular hydrogels consisting of a multiblock, segmented copolymer of hydrophilic poly(ethylene glycol) (PEG) and hydrophobic dimer fatty acid (DFA) building blocks. The hydrophobic DFA units form a network in micellar domains by self-assembly, which acts as stable physical cross-link points (Fig. 1.4). Due to the physical cross-links formed by hydrophobic interaction, the hydrogel displays excellent mechanical properties (elongation at break $\varepsilon_B = 1055\%$, tensile strength $\sigma_T = 0.51$ MPa, and tensile toughness $U_T = 4.12$ MJ/m^3).

1.3.3 Macromolecular microspheres toughening mechanism

Hydrogels can be in the form of macroscopic networks or confined to smaller dimensions such as microgels, which are crosslinked polymeric particles. When the size of microgels is in submicron range, they are known as nanogels. Microgels/nanogels are crosslinked polymeric particles, which can be considered as hydrogels if they are composed of water soluble/swellable polymer chains (Fig. 1.5) [41]. The microgels themselves are not hydrogels, but the properties of stimuli-responsive microgels with tuning functions can be transferred to the hydrogels. They possess high water content, biocompatibility, and are mainly used in drug delivery and other biomedical applications [41-43].

When the microspheres of the hydrogel are functionalized and then covalently cross-linked, the original microgel becomes a toughened hydrogel composite. Huang et al. [44] reported a hydrogel toughened by macromolecular microspheres, as shown in Fig. 1.6. The macromolecular microspheres emulsion is irradiated with ^{60}Co γ-rays to form free radicals and initiate polymerization. With the macromolecular microspheres as crosslinker, polymer chains can be chemically bonded to form hydrogels with

extremely high mechanical strength.
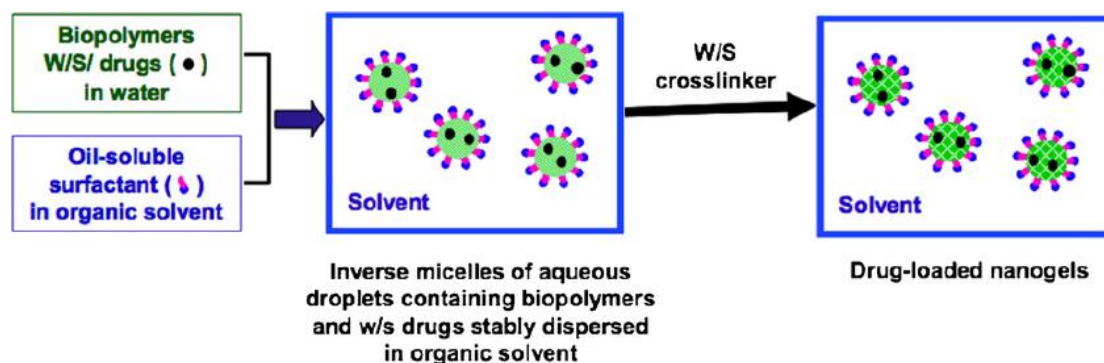
Fig. 1.5 Illustration of the reverse micellar method for the preparation of nanogels. [41]
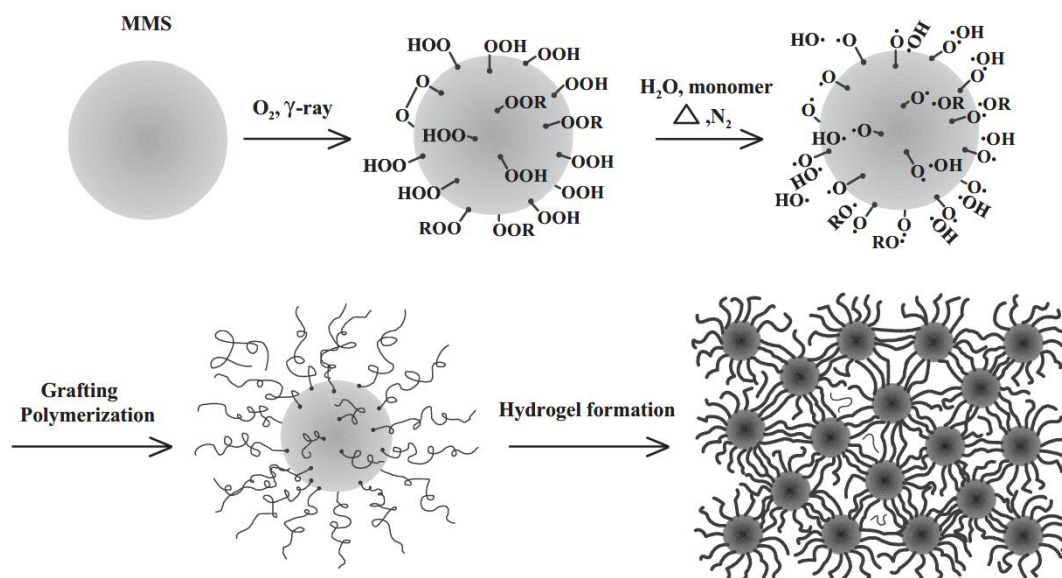
Fig. 1.6 Proposed mechanism for the formation of an MMC hydrogel and an MMC hydrogel microstructure. [44]

1.3.4 Tetra-PEG toughening mechanism

Most of hydrogels from macromonomers are formed from asymmetrical components, which allows the network with a high degree of freedom. However, it is the degrees of freedom of the network that leads to the microstructure, including defects and loops. These different microscopic inhomogeneities deprive the network of cooperativity and lead to weaker hydrogels. [45] Sakai et al. reduced the degrees of freedom of the microscopic network structure by introducing the tetra-PEG structure to form a

homogeneous network [46]. The tetra-PEG hydrogel is formed by combining two well defined symmetrical tetrahedron-like macromonomers of the same size (Fig. 1.7). Each macromonomer has four endlinking groups, and these two macromonomers are alternately linked. The gelation process is a simple A-B type reaction, in accordance with Flory's classical theory. The compressive strength of the tetra-PEG hydrogel formed is in the megapascal range and is much better than agarose or acrylamide hydrogels with the same network concentration.
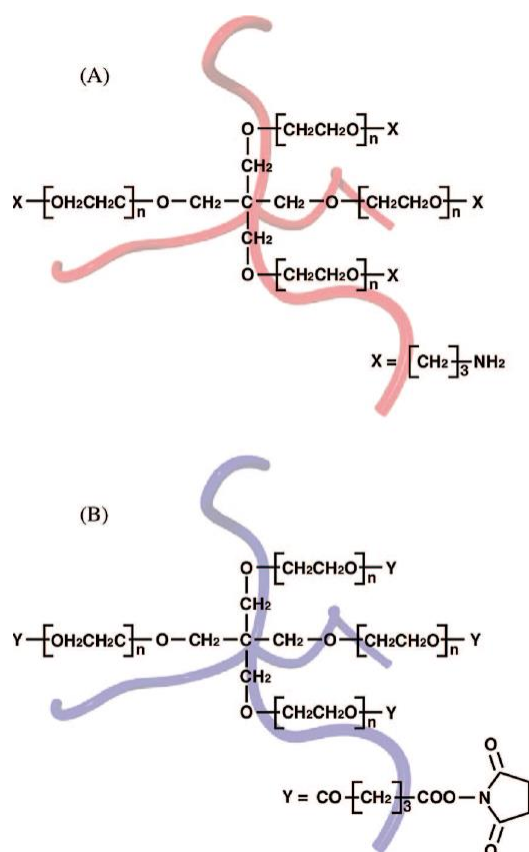
Fig. 1.7 Molecular structures of TAPEG (A) and TNPEG (B). [46]

1.3.5 Nanocomposite toughening mechanism

Nanocomposite hydrogels are a class of hydrogels obtained by compounding inorganic or organic nanoparticles [47], nanorods [48], nanosheets [49] and other nanomaterials [50, 51] with ordinary hydrogels. The high specific surface area and abundant functional groups of nanomaterials make them favorable to improve the interfacial effect with the polymer matrix of the hydrogel. The high mechanical strength of

nanomaterials themselves also makes them excellent reinforcement for hydrogels. Inorganic nanosilica [52], nanoclay sheet [53], titanium dioxide nanoparticles [54], carbon nanotubes [55], graphene [56], hydroxyapatite [57], and organic nanocellulose [58] can be used for hydrogel enhancement purposes.

Hu and co-workers [59] have reported a highly ordered nanocomposite hydrogels with ultrahigh strength. The oriented tunicate cellulose nanocrystals (TCNCs) were locked in polymeric networks (Fig. 1.8). Firstly, a stretchable supramolecular hydrogel was prepared by loosely crosslinking adamantine moiety contained polymers with β-cyclodextrin modified TCNCs through host-guest interaction. Subsequently, dual physically cross-linked hydrogel was constructed by introducing Fe^{3+} ions into the pre-stretched supramolecular hydrogel for the formation of coordination bonds and freezing of oriented TCNCs. The mechanical performance has been largely improved by the introduction of the aligned TCNCs as both multifunctional cross-linking agents and interfacial compatible reinforcements of dual physically cross-linked networks.
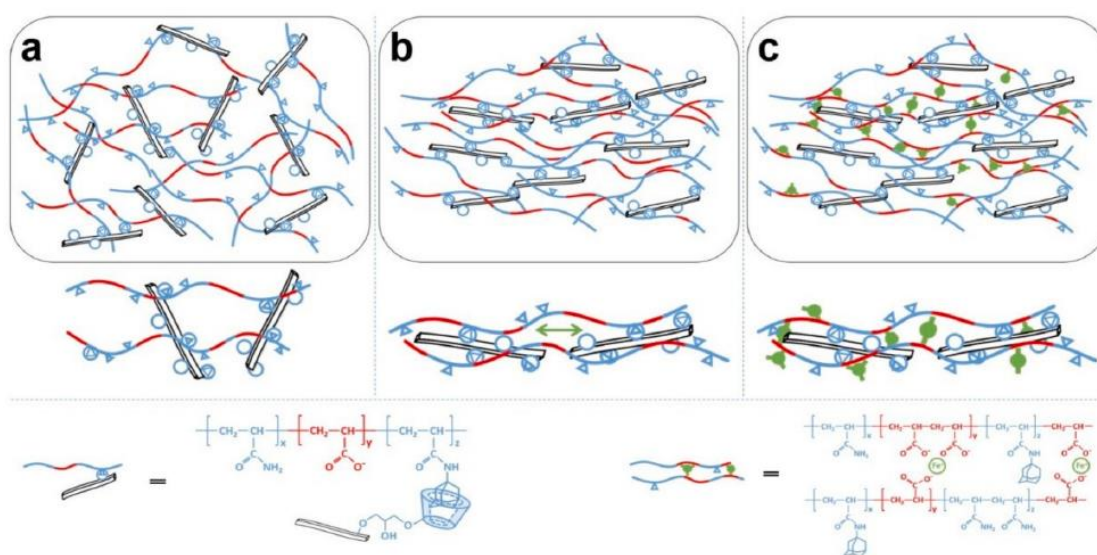
Fig. 1.8 Schematic illustration of hydrogel networks. (a) Highly stretchable mono cross-linked hydrogel (m-Gel) network. (b) Pre-stretched m-Gel network. (c) Anisotropic hydrogel network prepared by freezing oriented TCNCs in dual cross-linked hydrogel (d-Gel). [59]

1.3.6 Interpenetrating network toughening mechanism
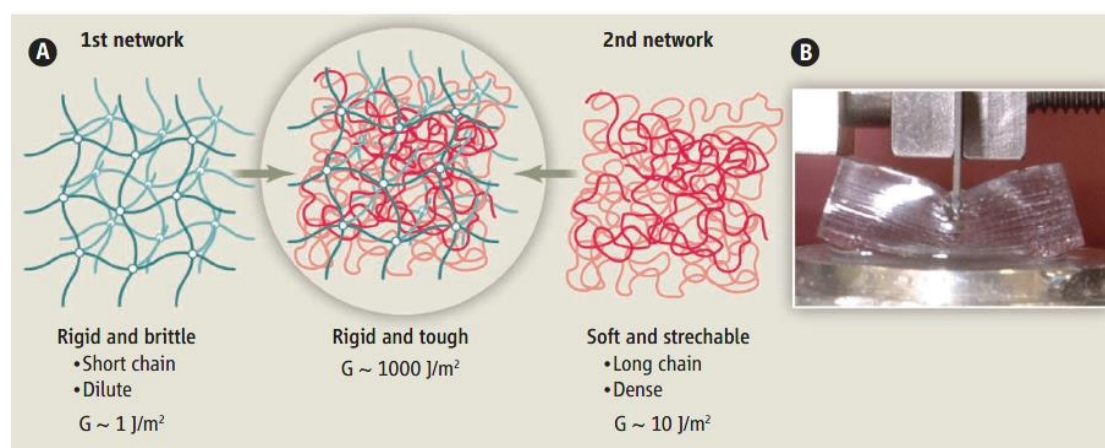
Fig. 1.9 Tougher than its parts. (a) By combining different network materials, tough double-network materials can be created. (b) Photo of a tough double-network hydrogel containing 90 wt % of water (2). The value of the fracture energy G is an indicator of material toughness. [60]

Interpenetrating network hydrogels are usually formed by two or more independent cross-linked networks by entanglement and permeation. Among them, the double network hydrogel proposed by Gong et al. [61] is a typical representative of interpenetrating network hydrogels. The double network hydrogels consist of two interpenetrating polymer networks with contrasting mechanical properties (Fig. 1.9) [60]. The first network is highly stretched and densely cross-linked, providing the hydrogel strength stiff and brittle. The second network is flexible and sparsely cross-linked, allows for energy dissipation at large strains [62]. Double-network hydrogels are tough because the internal fracture of the brittle network dissipates a large amounts of energy under large deformation, while the elasticity of the second network allows it to recover to its original configuration after deformation. The fracture energy of the double network is therefore much larger than those of either of the corresponding single networks. Thus, by sacrificing the rupture of the covalent bonds of the brittle first network, the material gains toughness [63].

Goddard et. al [64]used atomistic molecular dynamics (MD) simulations to investigate

the mechanical and transport properties of the PEO−PAA double network (DN) hydrogel with 76 wt % water content. By analyzing the pair correlation functions for polymer-water pairs and for ion-water pairs and the solvent accessible surface area, the solvation of polymer and ion in the DN hydrogel is found to be enhanced in comparison with both PEO and PAA single network (SN) hydrogels. The effective mesh size of this DN hydrogel is smaller than that of the SN hydrogels with the same water content and the same molecular weight between the cross-linking points (M_c). The mechanical performance of DN hydrogel has also been improved to a much higher level than the sum of the stresses of the two SN hydrogels at the same strain.

1.4 Functional hydrogel

It is well known that the molecular structure and chemical/physical interactions of hydrogels determine their properties, and these properties in turn determine their functional applications. [3, 6, 15, 16] In order to better understand the structure-function relationship of hydrogels, various property-generating mechanisms and the current status of hydrogel research are further described below.

1.4.1 Conductive hydrogel

Imparting conductivity to hydrogels can further expand their applications in electrochemistry, such as supercapacitors and sensors [65, 66]. Considering that most of the polymer networks that constitute hydrogels are insulating, the main strategy to impart conductivity to hydrogels is to add materials with conductivity to them. Current conductive hydrogels can be classified as electronic conductive hydrogel and ionic conductive hydrogel according to the conductivity mechanism. [67, 68]

1.4.1.1 Electronically conductive hydrogel

Electronically conductive hydrogel relies mainly on the directional movement of electrons in the presence of an electric field to obtain conductivity. There are two main

strategies to prepare electronically conductive hydrogels. One is to use conductive polymers, such as poly(3,4-ethylenedioxythiophene) (PEDOT) [69], polythiophene (PTh) [70], polypyrrole (PPy) [71], and polyaniline (PAni) [72], to build a conductive hydrogel network through covalent bonding or physical cross-linking. The other is the introduction of electronically conducting nanomaterials within the hydrogel system, such as graphene [56], carbon nanotubes [73], silver nanowires [74], etc. These types of electronically conducting hydrogels can be used in tissue engineering, energy storage devices and different types of sensors [15, 18, 68, 75, 76].

Electrically conductive, mechanically tough hydrogels based on a double network (DN) comprised of poly(ethylene glycol) methyl ether methacrylate (PPEGMA) and poly(acrylic acid) (PAA) were produced by Naficy and co-workers [77]. Poly(3,4-ethylenedioxythiophene) (PEDOT) was chemically polymerized within the tough DN gel to provide electronic conductivity. The hydrogel with PEDOT reached a maximum conductivity of 4.3 S cm^{-1}. These hydrogels may be useful as soft strain sensors because their electrical resistance changed significantly when cyclically loaded in compression (Fig. 1.10).
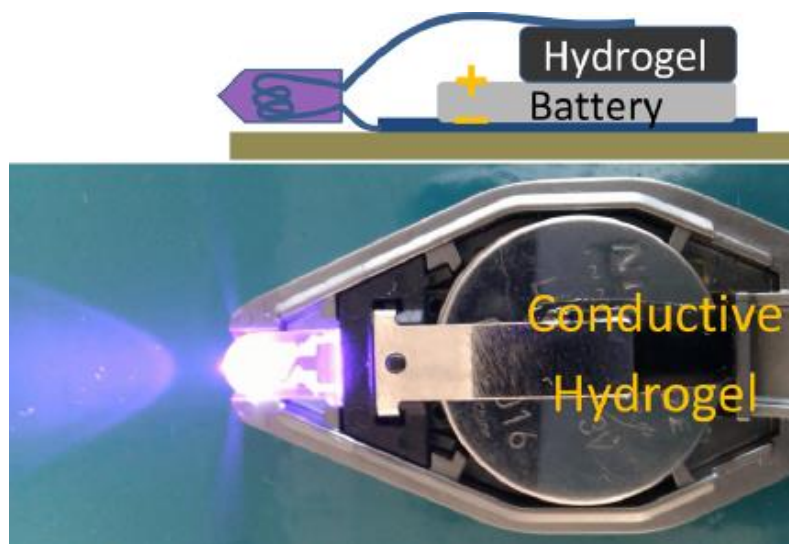
Fig. 1.10 The hydrogel introduced with PEDOT obtained good conductivity. [77]

1.4.1.2 Ionic conductive hydrogel
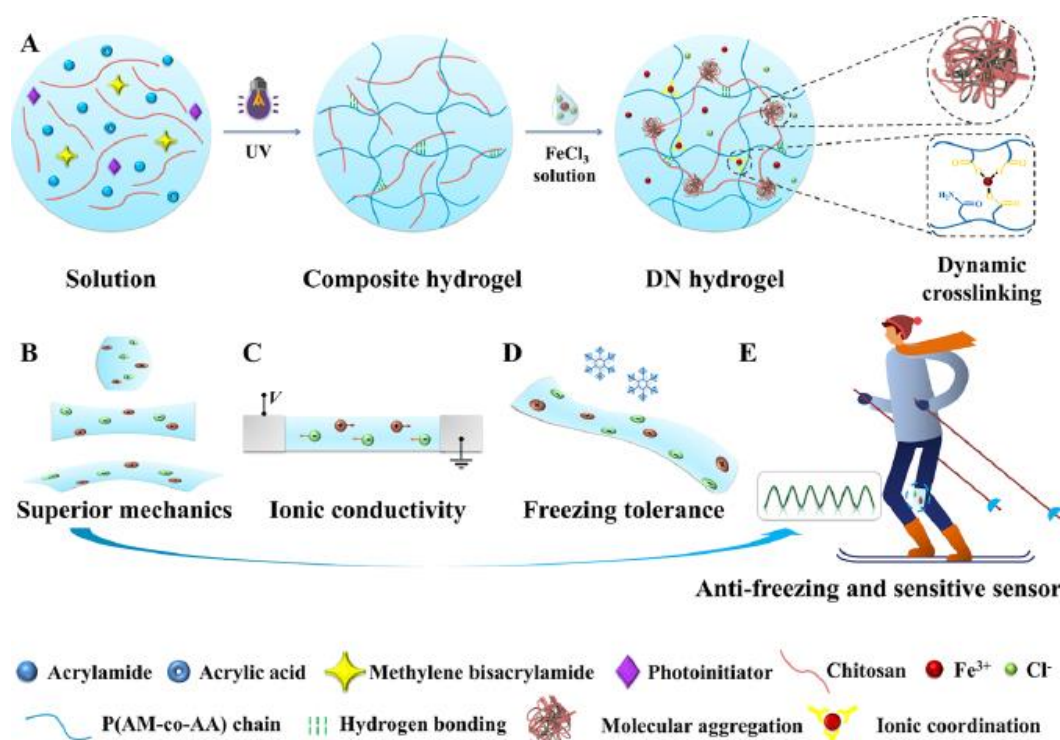
Fig. 1.11 Construction of the ionic conductive hydrogel with dynamic cross-links and the resultant antifreezing and sensitive hydrogel sensor. (A) Preparation of the elastic, antifatigue, and freezing-tolerant CS−P(AM-co-AA) DN hydrogel with dual-dynamic cross-links. (B) Excellent mechanics of the hydrogel to endure various deformations. (C) Ionic migration under electric field. (D) Strong freezing tolerance at subzero temperature. (E) Wearable, antifreezing, and sensitive hydrogel sensor to detect human motion in cold weather.

Conductivity of the ionic conductive hydrogels is mainly achieved through the directional migration of positive and negative ions in hydrogels. The introduction of polyelectrolytes [78] and small molecules of acids [79], bases [80], and salts [81] is the main way to impart ionic conductivity to hydrogels. Depending on the role of ions in the conductive hydrogel, ionic hydrogels are classified as physically doped and chemically doped [82]. Some inorganic ions are simply incorporated into the gel as free ions to enhance the conductivity of the hydrogel without forming new bonds and are

referred to as physical dopants. The other type is chemical doping, where the ions act as ligand centers to cross-link with different polymer chains in the hydrogel to form a hydrogel network. Liu and co-workers [83] introduced ionic conductivity to the chitosan–poly(acrylamide-co-acrylic acid) double-network [CS–P(AM-co-AA) DN] hydrogel with dual-dynamic cross-links (chitosan physical network and ionic coordination [CO_2LFe^{III}]) by soaking the CS–P(AM-co-AA) composite hydrogel in $FeCl_3$ solution (Fig. 1.11). The ions immobilized in dynamic cross-links exerted crucial effects on improving mechanics; meanwhile, the free ions in the hydrogel rendered the hydrogel excellent conductivity and strong freezing tolerance concurrently. The sensor assembled from the DN hydrogel exhibited cycling stability and good durability in detecting pressure, various deformations (elongation, compression, and bend), and human motions even at a low temperature (−20 °C).

1.4.2 Anti-freeze hydrogel

Conventional hydrogels consisting of pure water systems inevitably freeze at low temperatures and thus lose their original properties such as flexibility and conductivity, which limits their practical application at low temperatures. By expanding anti-freezing property to hydrogel, anti-freezing hydrogel-based sensors can maintain their own stability at low temperatures and improve their practicability. In addition, anti-freezing property of hydrogel sensors can also protect human skin from frostbite damage. The most widely used strategy to prepare hydrogels with resistance to low temperatures are to introduce organic solvent or ions to reduce the freezing point of water in the hydrogel network.

1.4.2.1 Binary (organic/water) solvent method

To achieve anti-freeze performance, binary solvents, namely two miscible solvents (organic solvents and water), were introduced into the polymer network of the hydrogel. According to the research of Lin et al. [84] (Fig. 1.12), when prepared in a

water/glycerol binary mixed solvent, the DN hydrogels remained elastic at -30 °C and can be twisted at will. The reason for the anti-freeze performance of the hydrogel is that glycerol molecules contain a large number of hydroxyl groups that can form hydrogen bond interactions with water molecules, thereby inhibiting the crystallization of water molecules and lowering the freezing point of water.
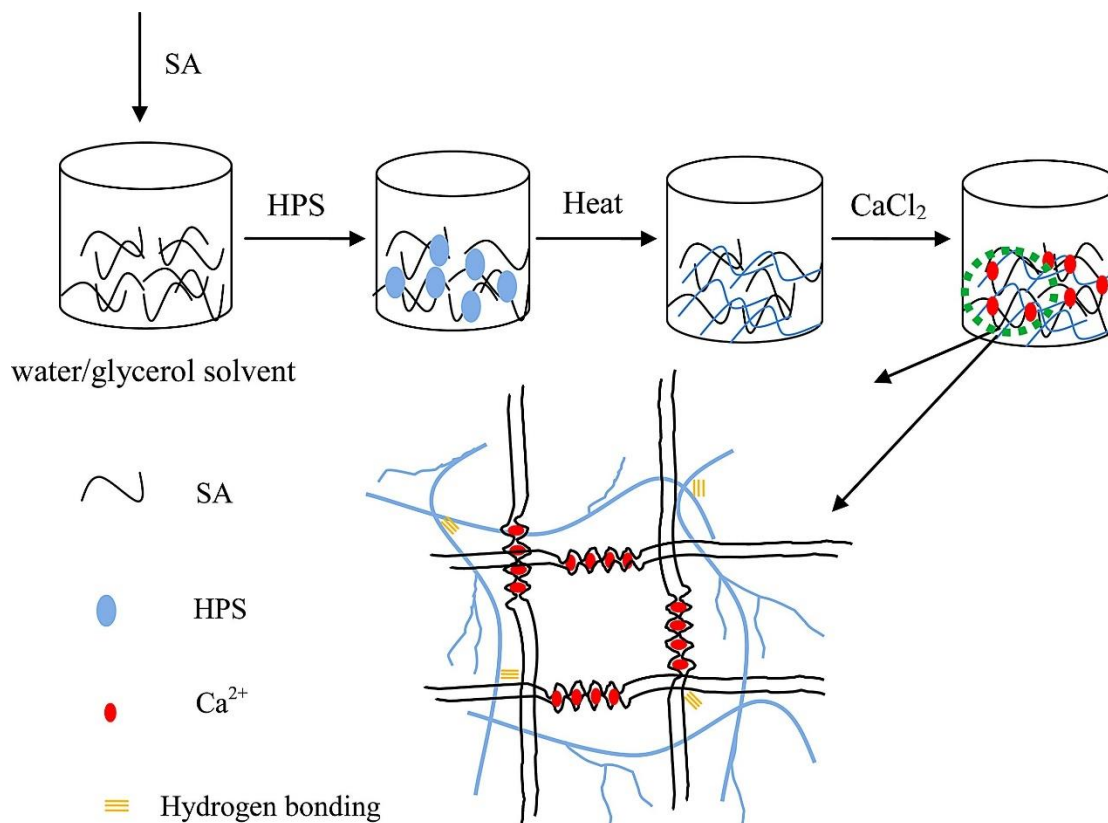
Fig. 1.12 Schematically fabrication of HPS/SA DN hydrogels. [84]

1.4.2.2 Solvent replacement method

Solvent displacement-method is a method that replaces water in the hydrogel with organic solvent through soaking water-based hydrogel into the organic solvent. Li et al. [85] assembled a symmetrical all-solid supercapacitor (called OHEC) with the OHE of double-network PAMPS/PAAm containing organic electrolyte solution (4 m LiCl/EG) (Fig. 1.13). The replacement of water with LiCl/EG mixture enables the OHE achieves mechanical toughness under large deformation behavior and long-term capacitance retention across a wide operating temperature range (from -20 to 80 °C). The OHE

effectively broadens the voltage window and avoids the electrochemical polarization at low temperatures.
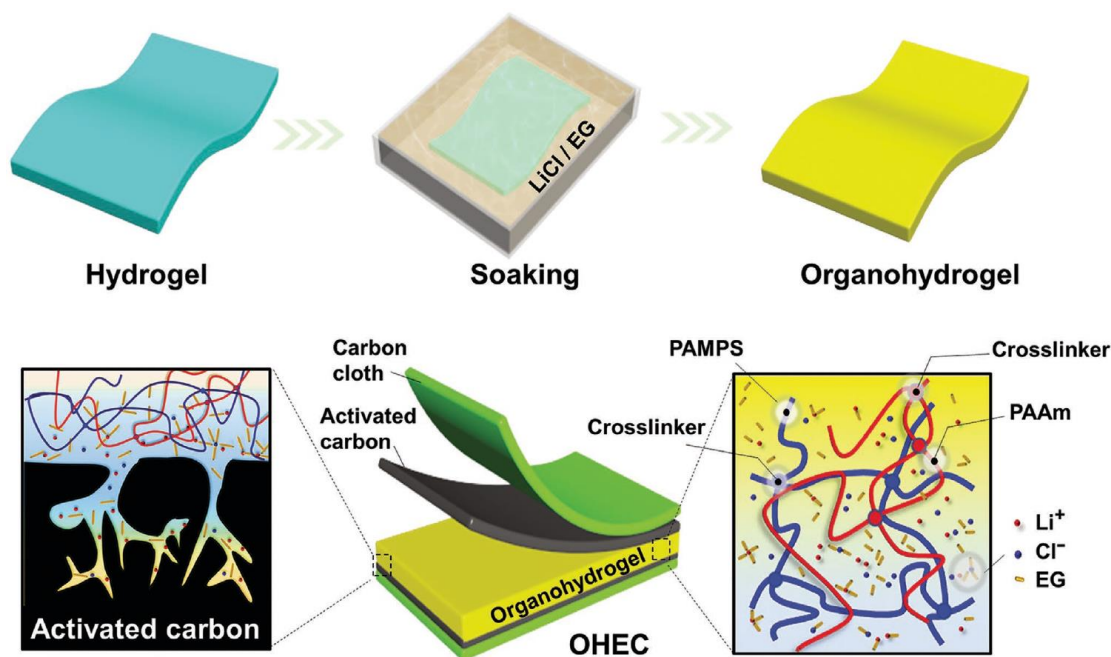
Fig. 1.13 Schematic illustration of the preparation of OHEC. [85]

1.4.2.3 Ionogels

Ionogels can be formed by introducing ionic liquids (IL) or ionic salts into physically or chemically crosslinked polymer matrix networks [86]. Ionogels are widely used in flexible energy storage devices, actuators and sensors because of their unique physical and chemical properties, such as high ionic conductivity, non-flammability, transparency, thermal and electrochemical stability [87-90].

Negre and co-workers[91] have reported an inorganic gel polymer electrolyte based on the confinement of an ionic liquid mixture (1:1 by weight or molar ratio) of N-methyl-N-propylpiperidinium bis(fluorosulfonyl)imide (PIP13FSI) and N-butyl-N-methylpyrrolidinium bis(fluorosulfonyl)imide (PYR14FSI) into a SiO_2 matrix. The synthetized ionogel exhibits a high ionic conductivity over a wide temperature range (from 0.2 mS cm^{-1} at −40 °C up to 10 mS cm^{-1} at 60 °C). Ge and co-workers [92] have synthesized a class of freezing- and dehydration-tolerant PAM/CNF double network hydrogels containing LiCl (Fig. 1.14). The presence of Li$^+$ and Cl$^-$ ions effectively

strengthens the interactions between the water molecules within the hydrogel, preventing both ice formation and water evaporation. Therefore, PAM/CNF/LiCl hydrogels exhibited impressive freezing and dehydration tolerance (Fig. 1.14b). Owing to the corporation of CNF and LiCl salt, the tensile strength and high ionic conductivity were preserved even at temperatures as low as -40 °C. The use of PAM/CNF/LiCl 50% hydrogel electrolyte in an assembly supercapacitor showed stable electrochemical performance and excellent flexibility at low temperatures.
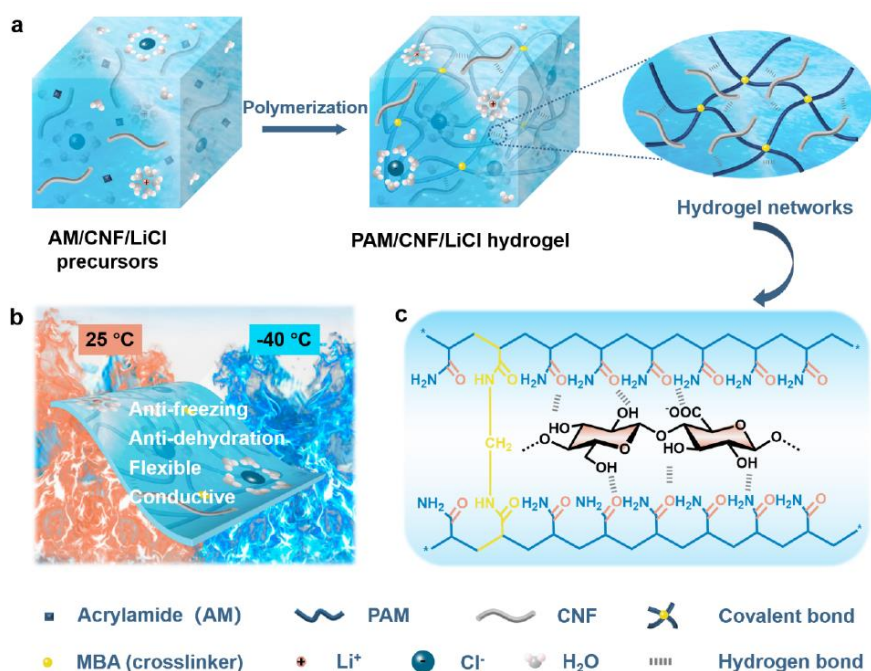
Fig. 1.14 Strategy used in the design of a conductive and stretchable electrolyte hydrogel with low temperature and dehydration tolerance. (a) Schematic illustration of the formation of PAM/CNF/LiCl hydrogel. (b) The PAM/CNF/LiCl hydrogel shows anti-freezing and anti-dehydration performance, is flexible and conductive under cold conditions (-40 °C). (c) Schematic illustration of hydrogen bonding between PAM and CNF chains in the PAM/CNF/LiCl hydrogel. [92]

18

1.4.3 Adhesive hydrogel

Although the number of advanced hydrogels reported in recent years has increased significantly, there are still many opportunities that have not yet been fully explored. For example, for hydrogels used in flexible wearable devices, how to achieve tight fixation while satisfying user comfort or even sensory-free use is one of the key issues to be addressed. The strong and robust adhesion of hydrogels highly desirable for their integration and performance in devices and systems, which remains an ongoing challenge in the field.

The surface adhesion of hydrogels and objects mainly comes from the chemical bonds and/or non-covalent interactions between the active groups in the hydrogels and object surface. The functional groups of hydrogels, such as hydroxyl, ether, amino, carboxyl or catechol groups, can react with object surface functional groups to form imines, amides or other covalent bonds. At the same time, some non-covalent interactions, such as hydrogen bonds, cation-π interactions and mechanical interlocking, are formed at the interface (Fig. 1.15). [93] Covalent bonds are usually strong but irreversible, while non-covalent bonds are relatively weak but reversible and may allow repeated adhesion and peeling.
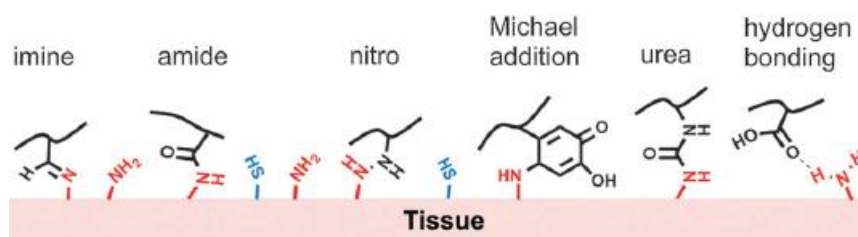
Fig. 1.15 Examples of chemical/physical linkages formed between hydrogels and surrounding tissues. [93]

Currently, the main strategy to increase the adhesion of hydrogels is to introduce compounds with adhesive properties, such as dopamine, proteins, and polysaccharides into the hydrogel system.[94-96] For example, inspired by the catechol-based strategy, Fu et al. [97] prepared a hybrid network hydrogel with underwater adhesion strength as

high as 86.3 ± 7.2 kPa and reduced to 43 ± 3.4 kPa after being immersed in water for 9 days. Alginate hydrogel acted as a "glue" to allow the strong, permanent adhesion of the hydrogel onto the PDMS surface by 1) imparting hydrophilicity to improve compatibility with hydrogels, and 2) providing functional groups for the stable conjugation of hydrogels [98] (Fig. 1.16).
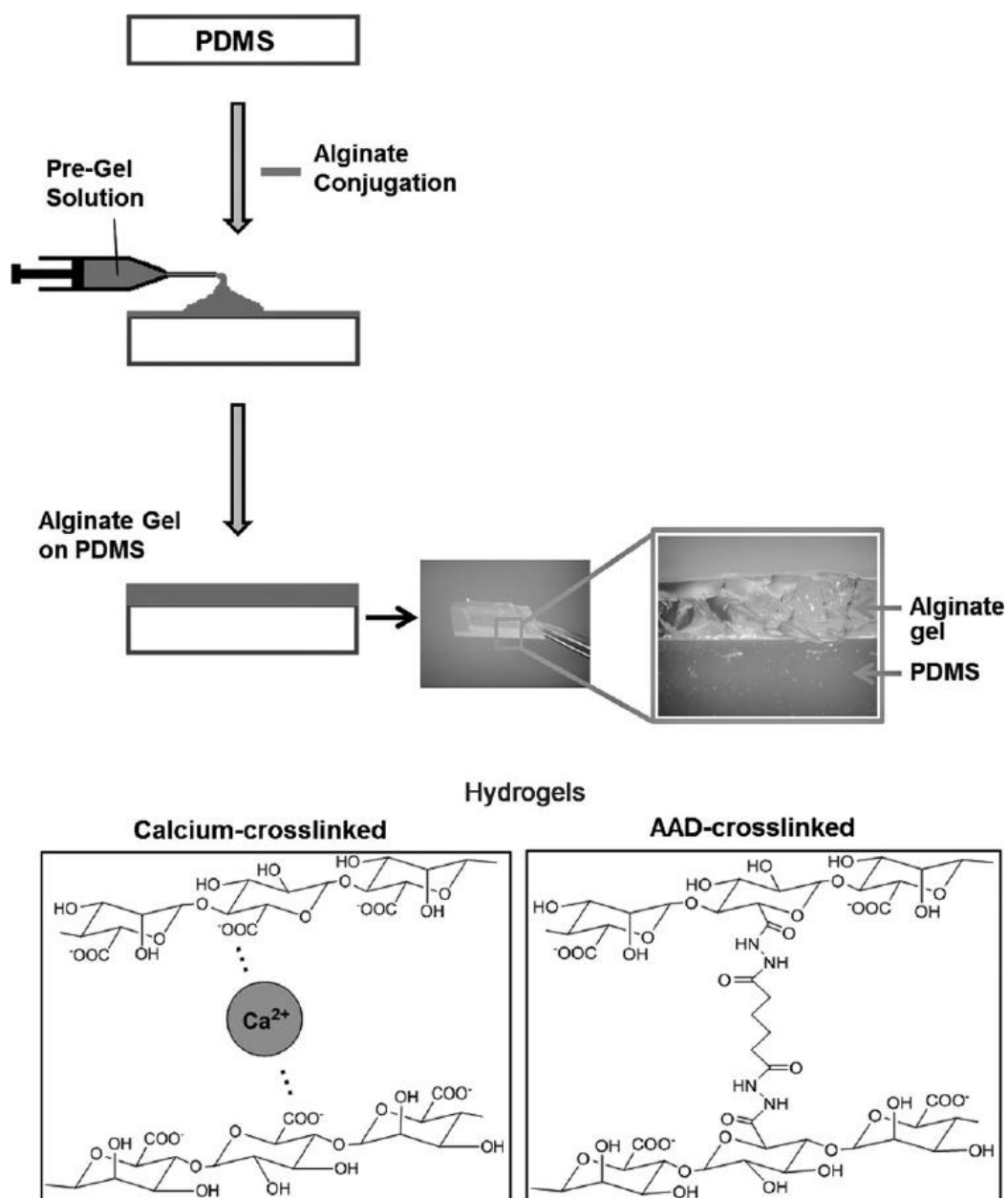
Fig. 1.16 Hydrogels were fabricated on the alginate-PDMS surface by 1) ionic crosslinking with calcium ions or 2) covalent crosslinking with adipic acid dihydrazide (AAD). [98]

1.4.4 Self-healing hydrogel
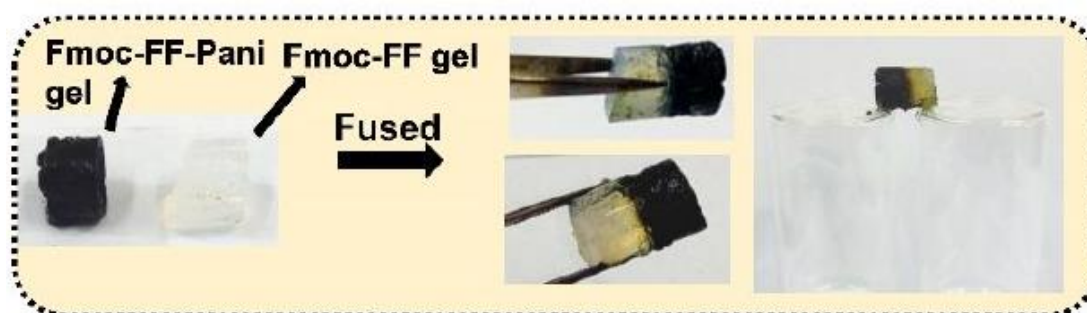
Fig. 1.17 Two separate blocks of Fmoc-FF and Fmoc-FF-PAni hydrogels healed after kept in contact for 5 minutes. [99]

Hydrogel has attracted significant interest in view of the flexible wearable devices. However, the hydrogels currently in use often suffer from insufficient service life to withstand prolonged use. To solve this problem, on the one hand, the mechanical properties of the hydrogel can be further optimized, especially the anti-fatigue performance; on the other hand, the self-healing ability of the device can be realized by giving the hydrogel self-healing ability.

Self-healing is defined as the property that enables a material to heal damages intrinsically and automatically, restoring itself to normality. Self-healing usually occurs in as-prepared materials (with a predefined set of conditions) without the intervention of an external stimulus to promote the onset or magnitude of self-healing. [100] The mechanism of self-healing depends on the reversibility of cross-linking. These crosslinks are mainly constructed by dynamic covalent, hydrogen bonding, ionic, supramolecular host-guest and hydrophobic interactions. [101-103] The number and strength (type) of crosslinks determine the degree of self-healing ability, the stability of the hydrogel and the mechanical properties of the hydrogel.

Chakraborty and co-workers [99] have fabricated a bio-inspired, mechanically rigid and conductive Fmoc-FF-PAni hydrogel by in situ polymerization of Ani inside Fmoc-FF hydrogel matrix. Taking advantage of the inherent tendency of Fmoc-FF fiber to be re-entangled after being detached by mechanical force, the Fmoc-FF-PAni hydrogel has

the ability of self-healing. The Fmoc-FF-PAni hydrogels not only retain their mechanical integrity (Fig. 1.17), but also reinstate their bulk conductivity (Fig. 1.18) after macroscopic disruption.
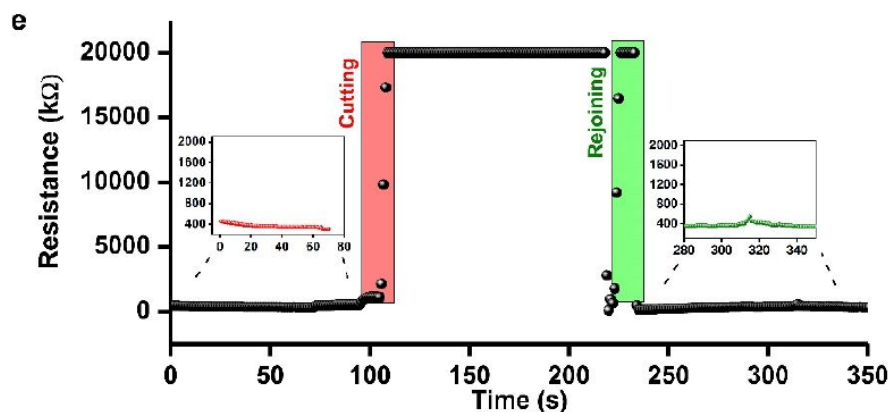
Fig. 1.18 Real-time measurement of the resistance values of Fmoc-FF-PAni hydrogels during cutting and rejoining procedure (Fmoc-FF concentration = 2% w/v). [99]

1.5 Research purpose and content

Hydrogel is a kind of soft material with structure like natural life tissue, which has good flexibility and biocompatibility. The remarkable flexibility in the design of network structure, mechanical properties and functional characteristics of hydrogels makes them one of the ideal flexible substrate materials for the next generation of flexible electronic devices. Based on these special performance advantages, hydrogel has attracted the attention of many researchers and is an ideal choice for flexible wearable sensors. In practical applications, flexible wearable sensors must repeatedly detect all kinds of deformation and pressure in daily activities. For example, electronic skin needs to sense elongation, compression, bending, touch pressure, and even a combination of current and repetitive. Although remarkable efforts have been made in hydrogels, they are still not mechanically and functionally inadequate to meet the practical needs of stability, durability, low temperature adaptability and so on. In this work, we improved the mechanical properties and introduced various functionalities (anti-freeze property,

adhesion, and self-healing) in hydrogels to solve the above problems.

To improve the mechanical properties of the hydrogel, we have designed a double crosslinked hydrogel. The unique double crosslinked microstructure ensures that the hydrogel has favorable mechanical strength, toughness, resilience, and recovery along with less residual strain. The hydrogel also exhibits outstanding ionic conductivity. The combined mechanical performance and ionic conductivity of the prepared hydrogel results in its remarkable performance when used in sensors.

To improve the low-temperature adaptability of the hydrogel, a novel anti-freezing system based on ice structuring proteins and $CaCl_2$ is introduced to a conductive hydrogel. Both formation of ice nuclei and ice growth of the hydrogel at sub-zero temperature can be inhibited. Supported by the anti-freeze system, the hydrogel reveals good flexibility, recovery and conductivity at both room temperature and sub-zero temperature. The low-temperature adaptability enables the hydrogel to be used as strain and temperature sensors at both room temperature and sub-zero temperature.

To meet the requirements of integrated mechanical properties, adhesion, and self-healing ability to hydrogel, a novel PAA/Fe/PVP hydrogel has been prepared. PVP, as the main components of adhesives in daily life, plays a significant role in improving adhesion of the hydrogel. The adhesion can withstand multiple uses due to the good mechanical properties of the hydrogel. Furthermore, the hydrogel displays outstanding self-healing ability in terms of both mechanical properties and conductivity. Because of the good mechanical properties, robust adhesion and rapid self-healing ability, the hydrogel-based sensors have demonstrated stability, accuracy, and reliability in real-time monitoring of subtle facial micro-expressions and large human activities.

References

[1] F. Ullah, M.B.H. Othman, F. Javed, Z. Ahmad, H.M. Akil, Classification, processing and application of hydrogels: A review, Materials Science and Engineering: C, 57 (2015) 414-433.

[2] W.A. Laftah, S. Hashim, A.N. Ibrahim, Polymer hydrogels: A review, Polymer-Plastics Technology and Engineering, 50 (2011) 1475-1486.

[3] M.F. Akhtar, M. Hanif, N.M. Ranjha, Methods of synthesis of hydrogels… A review, Saudi Pharmaceutical Journal, 24 (2016) 554-559.

[4] J. Maitra, V.K. Shukla, Cross-linking in hydrogels-a review, Am. J. Polym. Sci, 4 (2014) 25-31.

[5] O. Wichterle, D. Lim, Hydrophilic gels for biological use, Nature, 185 (1960) 117-118.

[6] E.S. Dragan, Design and applications of interpenetrating polymer network hydrogels. A review, Chemical Engineering Journal, 243 (2014) 572-590.

[7] A. Gupta, M. Kowalczuk, W. Heaselgrave, S.T. Britland, C. Martin, I. Radecka, The production and application of hydrogels for wound management: A review, European Polymer Journal, 111 (2019) 134-151.

[8] P.M. Pakdel, S.J. Peighambardoust, A review on acrylic based hydrogels and their applications in wastewater treatment, Journal of environmental management, 217 (2018) 123-143.

[9] R.A. Ramli, Slow release fertilizer hydrogels: a review, Polymer Chemistry, 10 (2019) 6073-6090.

[10] H. Hamedi, S. Moradi, S.M. Hudson, A.E. Tonelli, Chitosan based hydrogels and their applications for drug delivery in wound dressings: A review, Carbohydrate polymers, 199 (2018) 445-460.

[11] S. Ahmad, M. Ahmad, K. Manzoor, R. Purwar, S. Ikram, A review on latest innovations in natural gums based hydrogels: Preparations & applications, International journal of biological macromolecules, 136 (2019) 870-890.

[12] M. Mahinroosta, Z.J. Farsangi, A. Allahverdi, Z. Shakoori, Hydrogels as intelligent materials: A brief review of synthesis, properties and applications, Materials today chemistry, 8 (2018) 42-55.

[13] S. Van Vlierberghe, P. Dubruel, E. Schacht, Biopolymer-based hydrogels as scaffolds for tissue engineering applications: a review, Biomacromolecules, 12 (2011) 1387-1408.

[14] A. Kumar, S.S. Han, PVA-based hydrogels for tissue engineering: A review, International journal of polymeric materials and polymeric biomaterials, 66 (2017) 159-182.

[15] Q. Rong, W. Lei, M. Liu, Conductive hydrogels as smart materials for flexible electronic devices, Chemistry–A European Journal, 24 (2018) 16930-16943.

[16] Z. Wang, Y. Cong, J. Fu, Stretchable and tough conductive hydrogels for flexible pressure and strain sensors, Journal of Materials Chemistry B, 8 (2020) 3437-3459.

[17] X. Sun, F. Yao, J. Li, Nanocomposite hydrogel-based strain and pressure sensors: a review, Journal of Materials Chemistry A, 8 (2020) 18605-18623.

[18] Q. Zhang, L. Liu, C. Pan, D. Li, Review of recent achievements in self-healing conductive materials and their applications, Journal of Materials Science, 53 (2018) 27-46.

[19] B. Guo, Z. Ma, L. Pan, Y. Shi, Properties of conductive polymer hydrogels and their application in sensors, Journal of Polymer Science Part B: Polymer Physics, 57 (2019) 1606-1621.

[20] S. Jin, J. Qiu, M. Sun, H. Huang, E. Sakai, Strain‐Sensitive Performance of a Tough and Ink‐Writable Polyacrylic Acid Ionic Gel Crosslinked by Carboxymethyl Cellulose, Macromolecular rapid communications, 40 (2019) 1900329.

[21] H. Zhou, Z. Wang, W. Zhao, X. Tong, X. Jin, X. Zhang, Y. Yu, H. Liu, Y. Ma, S. Li, Robust and sensitive pressure/strain sensors from solution processable composite hydrogels enhanced by hollow-structured conducting polymers, Chemical Engineering Journal, 403 (2021) 126307.

[22] F. Pinelli, L. Magagnin, F. Rossi, Progress in hydrogels for sensing applications: a review, Materials Today Chemistry, 17 (2020) 100317.

[23] Z. Chen, Y. Chen, M.S. Hedenqvist, C. Chen, C. Cai, H. Li, H. Liu, J. Fu, Multifunctional conductive hydrogels and their applications as smart wearable devices, Journal of Materials Chemistry B, 9 (2021) 2561-2583.

[24] C. Cui, Q. Fu, L. Meng, S. Hao, R. Dai, J. Yang, Recent progress in natural biopolymers conductive hydrogels for flexible wearable sensors and energy devices: materials, structures, and performance, ACS Applied Bio Materials, 4 (2020) 85-121.

[25] Z. Wang, H. Zhou, J. Lai, B. Yan, H. Liu, X. Jin, A. Ma, G. Zhang, W. Zhao, W. Chen, Extremely stretchable and electrically conductive hydrogels with dually synergistic networks for wearable strain sensors, Journal of Materials Chemistry C, 6 (2018) 9200-9207.

[26] L. Guan, S. Yan, X. Liu, X. Li, G. Gao, Wearable strain sensors based on casein-driven tough, adhesive and anti-freezing hydrogels for monitoring human-motion, Journal of Materials Chemistry B, 7 (2019) 5230-5236.

[27] E. Scarpa, V. Mastronardi, F. Guido, L. Algieri, A. Qualtieri, R. Fiammengo, F. Rizzi, M. De Vittorio, Wearable piezoelectric mass sensor based on pH sensitive hydrogels for sweat pH monitoring, Scientific reports, 10 (2020) 1-10.

[28] Q. Wang, J. Guo, X. Lu, X. Ma, S. Cao, X. Pan, Y. Ni, Wearable lignin-based hydrogel electronics: A mini-review, International Journal of Biological Macromolecules, (2021).

[29] A.B. Imran, K. Esaki, H. Gotoh, T. Seki, K. Ito, Y. Sakai, Y. Takeoka, Extremely stretchable thermosensitive hydrogels by introducing slide-ring polyrotaxane cross-linkers and ionic groups into the polymer network, Nature communications, 5 (2014) 1-8.

[30] Y. Okumura, K. Ito, The polyrotaxane gel: A topological gel by figure‐of‐eight cross‐links, Advanced materials, 13 (2001) 485-487.

[31] K. Ito, Novel entropic elasticity of polymeric materials: why is slide-ring gel so soft?, Polymer journal, 44 (2012) 38-41.

[32] K. Kato, H. Komatsu, K. Ito, A versatile synthesis of diverse polyrotaxanes with a dual role of cyclodextrin as both the cyclic and capping components, Macromolecules, 43 (2010) 8799-8804.

[33] K. Kato, K. Inoue, M. Kidowaki, K. Ito, Organic−inorganic hybrid slide-ring gels: polyrotaxanes consisting of poly (dimethylsiloxane) and γ-cyclodextrin and subsequent topological cross-linking, Macromolecules, 42 (2009) 7129-7136.

[34] Z.-H. Chen, S.-T. Fan, Z.-J. Qiu, Z.-J. Nie, S.-X. Zhang, S. Zhang, B.-J. Li, Y. Cao, Tough double-network elastomers with slip-rings, Polymer Chemistry, 12 (2021) 3142-3152.

[35] J. Chen, X. Xu, M. Liu, Y. Li, D. Yu, Y. Lu, M. Xiong, I. Wyman, X. Xu, X. Wu, Topological cyclodextrin nanoparticles as crosslinkers for self-healing tough hydrogels as strain sensors, Carbohydrate Polymers, 264 (2021) 117978.

[36] C.W. Peak, J.J. Wilker, G. Schmidt, A review on tough and sticky hydrogels, Colloid and Polymer Science, 291 (2013) 2031-2047.

[37] M. Mihajlovic, M. Staropoli, M.-S. Appavou, H.M. Wyss, W. Pyckhout-Hintzen, R.P. Sijbesma, Tough supramolecular hydrogel based on strong hydrophobic interactions in a multiblock segmented copolymer, Macromolecules, 50 (2017) 3333-3346.

[38] X. Liang, H. Ding, Q. Wang, G. Sun, Tough physical hydrogels reinforced by hydrophobic association with remarkable mechanical property, rapid stimuli-responsiveness and fast self-recovery capability, European Polymer Journal, 120 (2019) 109278.

[39] G. Jiang, C. Liu, X. Liu, Q. Chen, G. Zhang, M. Yang, F. Liu, Network structure and compositional effects on tensile mechanical properties of hydrophobic association hydrogels with high mechanical strength, Polymer, 51 (2010) 1507-1515.

[40] D.C. Tuncaboylu, M. Sari, W. Oppermann, O. Okay, Tough and self-healing hydrogels formed via hydrophobic interactions, Macromolecules, 44 (2011) 4997-5005.

[41] J.K. Oh, R. Drumright, D.J. Siegwart, K. Matyjaszewski, The development of microgels/nanogels for drug delivery applications, Progress in Polymer Science, 33 (2008) 448-477.

[42] S.V. Vinogradov, Colloidal microgels in drug delivery applications, Current pharmaceutical design, 12 (2006) 4703-4712.

[43] M. Malmsten, H. Bysell, P. Hansson, Biomacromolecules in microgels—Opportunities and challenges for drug delivery, Current Opinion in Colloid & Interface Science, 15 (2010) 435-444.

[44] T. Huang, H. Xu, K. Jiao, L. Zhu, H.R. Brown, H. Wang, A novel hydrogel with high mechanical strength: a macromolecular microsphere composite hydrogel, Advanced Materials, 19 (2007) 1622-1626.

[45] T. Sakai, Gelation mechanism and mechanical properties of Tetra-PEG gel, Reactive and Functional Polymers, 73 (2013) 898-903.

[46] T. Sakai, T. Matsunaga, Y. Yamamoto, C. Ito, R. Yoshida, S. Suzuki, N. Sasaki, M. Shibayama, U.-i. Chung, Design and fabrication of a high-strength hydrogel with ideally homogeneous network structure from tetrahedron-like macromonomers, Macromolecules, 41 (2008) 5379-5384.

[47] K. Haraguchi, T. Takehisa, Nanocomposite hydrogels: A unique organic–inorganic network structure with extraordinary mechanical, optical, and swelling/de‑swelling properties, Advanced materials, 14 (2002) 1120-1124.

[48] C. Wang, M. Vázquez‑González, M. Fadeev, Y.S. Sohn, R. Nechushtai, I. Willner, Thermoplasmonic‑Triggered Release of Loads from DNA‑Modified Hydrogel Microcapsules Functionalized with Au Nanoparticles or Au Nanorods, Small, 16 (2020) 2000880.

[49] K. Haraguchi, Synthesis and properties of soft nanocomposite materials with novel organic/inorganic network structures, Polymer journal, 43 (2011) 223-241.

[50] M. Kokabi, M. Sirousazar, Z.M. Hassan, PVA–clay nanocomposite hydrogels for wound dressing, European polymer journal, 43 (2007) 773-781.

[51] R. Esmaeely Neisiany, M.S. Enayati, P. Sajkiewicz, Z. Pahlevanneshan, S. Ramakrishna, Insight into the current directions in functionalized nanocomposite hydrogels, Frontiers in materials, 7 (2020) 25.

[52] K. Madhumathi, P.S. Kumar, K. Kavya, T. Furuike, H. Tamura, S. Nair, R. Jayakumar, Novel chitin/nanosilica composite scaffolds for bone tissue engineering applications, International journal of biological macromolecules, 45 (2009) 289-292.

[53] C. Yao, Z. Liu, C. Yang, W. Wang, X.-J. Ju, R. Xie, L.-Y. Chu, Smart hydrogels with inhomogeneous structures assembled using nanoclay-cross-linked hydrogel subunits as building blocks, ACS applied materials & interfaces, 8 (2016) 21721-21730.

[54] W. Kangwansupamonkon, N. Klaikaew, S. Kiatkamjornwong, Green synthesis of titanium dioxide/acrylamide-based hydrogel composite, self degradation and environmental applications, European Polymer Journal, 107 (2018) 118-131.

[55] H. Li, D.Q. Wang, H.L. Chen, B.L. Liu, L.Z. Gao, A novel gelatin–carbon nanotubes hybrid hydrogel, Macromolecular Bioscience, 3 (2003) 720-724.

[56] Y. Xu, Z. Lin, X. Huang, Y. Wang, Y. Huang, X. Duan, Functionalized graphene hydrogel‐based high‐performance supercapacitors, Advanced materials, 25 (2013) 5779-5784.

[57] S.A. Hutchens, R.S. Benson, B.R. Evans, H.M. O'Neill, C.J. Rawn, Biomimetic synthesis of calcium-deficient hydroxyapatite in a natural hydrogel, Biomaterials, 27 (2006) 4661-4670.

[58] K.J. De France, T. Hoare, E.D. Cranston, Review of hydrogels and aerogels containing nanocellulose, Chemistry of Materials, 29 (2017) 4609-4631.

[59] D. Hu, Y. Cui, K. Mo, J. Wang, Y. Huang, X. Miao, J. Lin, C. Chang, Ultrahigh strength nanocomposite hydrogels designed by locking oriented tunicate cellulose nanocrystals in polymeric networks, Composites Part B: Engineering, 197 (2020) 108118.

[60] J.P. Gong, Materials both tough and soft, Science, 344 (2014) 161-162.

[61] A. Nakayama, A. Kakugo, J.P. Gong, Y. Osada, M. Takai, T. Erata, S. Kawano, High mechanical strength double‐network hydrogel with bacterial cellulose, Advanced Functional Materials, 14 (2004) 1124-1128.

[62] M.A. Haque, T. Kurokawa, J.P. Gong, Super tough double network hydrogels and their application as biomaterials, Polymer, 53 (2012) 1805-1822.

[63] Y. Hagiwara, A. Putra, A. Kakugo, H. Furukawa, J.P. Gong, Ligament-like tough double-network hydrogel based on bacterial cellulose, Cellulose, 17 (2010) 93-101.

[64] S.S. Jang, W.A. Goddard, M.Y.S. Kalani, Mechanical and transport properties of the poly (ethylene oxide)− poly (acrylic acid) double network hydrogel from molecular dynamic simulations, The Journal of Physical Chemistry B, 111 (2007) 1729-1737.

[65] F. Fu, J. Wang, H. Zeng, J. Yu, Functional conductive hydrogels for bioelectronics, ACS Materials Letters, 2 (2020) 1287-1301.

[66] A. Sinha, P.K. Kalambate, S.M. Mugo, P. Kamau, J. Chen, R. Jain, Polymer hydrogel interfaces in electrochemical sensing strategies: A review, TrAC Trends in Analytical Chemistry, 118 (2019) 488-501.

[67] T. Cheng, Y.Z. Zhang, S. Wang, Y.L. Chen, S.Y. Gao, F. Wang, W.Y. Lai, W. Huang, Conductive Hydrogel‐Based Electrodes and Electrolytes for Stretchable and Self‐Healable Supercapacitors, Advanced Functional Materials, (2021) 2101303.

[68] T. Distler, A.R. Boccaccini, 3D printing of electrically conductive hydrogels for tissue engineering and biosensors–A review, Acta biomaterialia, 101 (2020) 1-13.

[69] V.R. Feig, H. Tran, M. Lee, K. Liu, Z. Huang, L. Beker, D.G. Mackanic, Z. Bao, An electrochemical gelation method for patterning conductive PEDOT: PSS hydrogels, Advanced Materials, 31 (2019) 1902869.

[70] D. Pattavarakorn, P. Youngta, S. Jaesrichai, S. Thongbor, P. Chaimongkol, Electroactive performances of conductive polythiophene/hydrogel hybrid artificial muscle, Energy Procedia, 34 (2013) 673-681.

[71] A. Youssef, M. Abdel-Aziz, E. El-Sayed, M. Abdel-Aziz, A. Abd El-Hakim, S. Kamel, G. Turky, Morphological, electrical & antibacterial properties of trilayered

Cs/PAA/PPy bionanocomposites hydrogel based on Fe3O4-NPs, Carbohydrate polymers, 196 (2018) 483-493.

[72] V. Guarino, M.A. Alvarez‑Perez, A. Borriello, T. Napolitano, L. Ambrosio, Conductive PANi/PEGDA macroporous hydrogels for nerve regeneration, Advanced healthcare materials, 2 (2013) 218-227.

[73] A. Vashist, A. Kaushik, A. Vashist, V. Sagar, A. Ghosal, Y. Gupta, S. Ahmad, M. Nair, Advances in carbon nanotubes–hydrogel hybrids in nanomedicine for therapeutics, Advanced healthcare materials, 7 (2018) 1701213.

[74] Y. Ahn, H. Lee, D. Lee, Y. Lee, Highly conductive and flexible silver nanowire-based microelectrodes on biocompatible hydrogel, ACS applied materials & interfaces, 6 (2014) 18401-18407.

[75] D. Mawad, A. Lauto, G.G. Wallace, Conductive polymer hydrogels, Polymeric hydrogels as smart biomaterials, Springer2016, pp. 19-44.

[76] S. Mondal, S. Das, A.K. Nandi, A review on recent advances in polymer and peptide hydrogels, Soft Matter, 16 (2020) 1404-1454.

[77] S. Naficy, J.M. Razal, G.M. Spinks, G.G. Wallace, P.G. Whitten, Electrically conductive, tough hydrogels with pH sensitivity, Chemistry of Materials, 24 (2012) 3425-3433.

[78] C.-J. Lee, H. Wu, Y. Hu, M. Young, H. Wang, D. Lynch, F. Xu, H. Cong, G. Cheng, Ionic conductivity of polyelectrolyte hydrogels, ACS applied materials & interfaces, 10 (2018) 5845-5852.

[79] S. Hao, C. Shao, L. Meng, C. Cui, F. Xu, J. Yang, Tannic Acid–Silver Dual Catalysis Induced Rapid Polymerization of Conductive Hydrogel Sensors with Excellent Stretchability, Self-Adhesion, and Strain-Sensitivity Properties, ACS Applied Materials & Interfaces, 12 (2020) 56509-56521.

[80] C. Dispenza, C.L. Presti, C. Belfiore, G. Spadaro, S. Piazza, Electrically conductive hydrogel composites made of polyaniline nanoparticles and poly (N-vinyl-2-pyrrolidone), Polymer, 47 (2006) 961-971.

[81] X.F. Zhang, X. Ma, T. Hou, K. Guo, J. Yin, Z. Wang, L. Shu, M. He, J. Yao, Inorganic salts induce thermally reversible and anti‑freezing cellulose hydrogels, Angewandte Chemie International Edition, 58 (2019) 7366-7370.

[82] L. Tang, S. Wu, J. Qu, L. Gong, J. Tang, A Review of Conductive Hydrogel Used in Flexible Strain Sensor, Materials, 13 (2020) 3947.

[83] H. Liu, X. Wang, Y. Cao, Y. Yang, Y. Yang, Y. Gao, Z. Ma, J. Wang, W. Wang, D. Wu, Freezing-tolerant, highly sensitive strain and pressure sensors assembled from ionic conductive hydrogels with dynamic cross-links, ACS Applied Materials & Interfaces, 12 (2020) 25334-25344.

[84] Q. Lin, H. Li, N. Ji, L. Dai, L. Xiong, Q. Sun, Self-healing, stretchable, and freezing-resistant hydroxypropyl starch-based double-network hydrogels, Carbohydrate Polymers, 251 (2021) 116982.

[85] X. Li, D. Lou, H. Wang, X. Sun, J. Li, Y.N. Liu, Flexible Supercapacitor Based on Organohydrogel Electrolyte with Long‑Term Anti‑Freezing and Anti‑Drying Property, Advanced Functional Materials, 30 (2020) 2007291.

[86] J. Le Bideau, L. Viau, A. Vioux, Ionogels, ionic liquid based hybrid materials, Chemical Society Reviews, 40 (2011) 907-925.

[87] A. Vioux, L. Viau, S. Volland, J. Le Bideau, Use of ionic liquids in sol-gel; ionogels and applications, Comptes Rendus Chimie, 13 (2010) 242-255.

[88] Y. Ding, J. Zhang, L. Chang, X. Zhang, H. Liu, L. Jiang, Preparation of high‑performance ionogels with excellent transparency, good mechanical strength, and high conductivity, Advanced Materials, 29 (2017) 1704253.

[89] Y. Ren, J. Guo, Z. Liu, Z. Sun, Y. Wu, L. Liu, F. Yan, Ionic liquid–based click-ionogels, Science advances, 5 (2019) eaax0648.

[90] L. Zhang, D. Jiang, T. Dong, R. Das, D. Pan, C. Sun, Z. Wu, Q. Zhang, C. Liu, Z. Guo, Overview of ionogels in flexible electronics, The Chemical Record, 20 (2020) 948-967.

[91] S.A.M. Noor, P. Bayley, M. Forsyth, D.R. Macfarlane, Ionogels based on ionic liquids as potential highly conductive solid state electrolytes, Electrochimica acta, 91 (2013) 219-226.

[92] W. Ge, S. Cao, Y. Yang, O.J. Rojas, X. Wang, Nanocellulose/LiCl systems enable conductive and stretchable electrolyte hydrogels with tolerance to dehydration and extreme cold conditions, Chemical Engineering Journal, 408 (2021) 127306.

[93] C. Ghobril, M. Grinstaff, The chemistry and engineering of polymeric hydrogel adhesives for wound closure: a tutorial, Chemical Society Reviews, 44 (2015) 1820-1835.

[94] A.H. Gowda, Y. Bu, O. Kudina, K.V. Krishna, R.A. Bohara, D. Eglin, A. Pandit, Design of tunable gelatin-dopamine based bioadhesives, International Journal of Biological Macromolecules, 164 (2020) 1384-1391.

[95] B.J. Kim, D.X. Oh, S. Kim, J.H. Seo, D.S. Hwang, A. Masic, D.K. Han, H.J. Cha, Mussel-mimetic protein-based adhesive hydrogel, Biomacromolecules, 15 (2014) 1579-1585.

[96] J. Duan, X. Liang, K. Zhu, J. Guo, L. Zhang, Bilayer hydrogel actuators with tight interfacial adhesion fully constructed from natural polysaccharides, Soft Matter, 13 (2017) 345-354.

[97] Y. Fu, P. Ren, F. Wang, M. Liang, W. Hu, N. Zhou, Z. Lu, T. Zhang, Mussel-inspired hybrid network hydrogel for continuous adhesion in water, Journal of Materials Chemistry B, 8 (2020) 2148-2154.

[98] C. Cha, E. Antoniadou, M. Lee, J.H. Jeong, W.W. Ahmed, T.A. Saif, S.A. Boppart, H. Kong, Tailoring hydrogel adhesion to polydimethylsiloxane substrates using polysaccharide glue, Angewandte Chemie International Edition, 52 (2013) 6949-6952.

[99] P. Chakraborty, T. Guterman, N. Adadi, M. Yadid, T. Brosh, L. Adler-Abramovich, T. Dvir, E. Gazit, A self-healing, all-organic, conducting, composite peptide hydrogel as pressure sensor and electrogenic cell soft substrate, ACS nano, 13 (2018) 163-175.

[100] D.L. Taylor, M. in het Panhuis, Self‑healing hydrogels, Advanced Materials, 28 (2016) 9060-9093.

[101] A. Zhang, Y. Liu, D. Qin, M. Sun, T. Wang, X. Chen, Research status of self-healing hydrogel for wound management: A review, International Journal of Biological Macromolecules, (2020).

[102] V.K. Thakur, M.R. Kessler, Self-healing polymer nanocomposite materials: A review, Polymer, 69 (2015) 369-383.

[103] M.-M. Song, Y.-M. Wang, X.-Y. Liang, X.-Q. Zhang, S. Zhang, B.-J. Li, Functional materials with self-healing properties: a review, Soft Matter, 15 (2019) 6615-6625.

Chapter 2 Materials, Experiment and Characterizations

2.1 Materials

2.1.1 Phytic acid (PA)

Phytic acid (PA) is a six-fold dihydrogen phosphate ester of inositol (specifically, of the myo isomer), also called inositol hexakisphosphate (IP6) or inositol polyphosphate (Fig. 2.1). It is a natural plant compound with a unique structure that is responsible for its characteristic properties. PA holds plenty of hydroxyl groups, which could ionize a considerable number of hydrogen ions to display good conductivity. PA is also a crosslinker that could form physical crosslinking networks with polymers via hydrogen bonds. It is mainly found in the seeds, roots, and stems of plants, especially in the seeds of legumes, bran and germ of cereals.
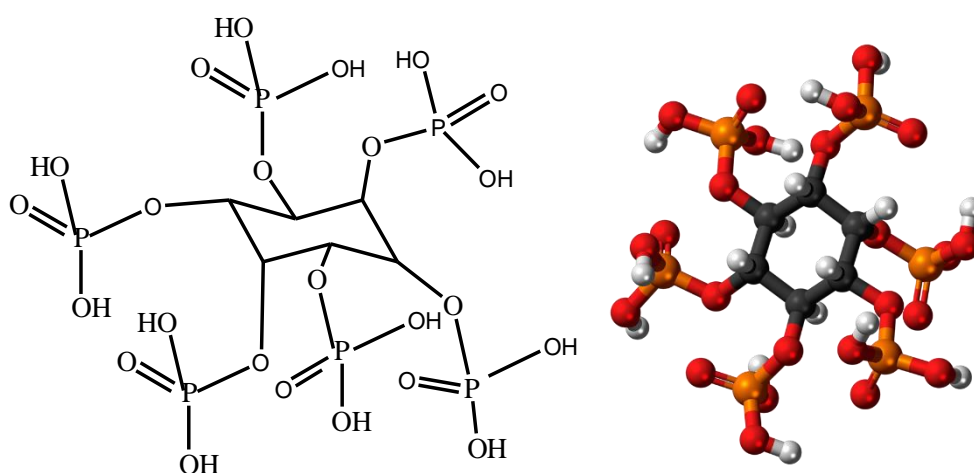
Fig. 2.1 Chemical structure of phytic acid.

2.1.2 Carboxymethyl cellulose (CMC)

CMC is a kind of cellulose ether obtained by carboxymethylation of natural cellulose. (Fig. 2.2). It is a negatively charged polyelectrolyte, prepared by the reaction of hydroxyl groups on alkali cellulose with monochloroacetic acid. It is the most productive, versatile and convenient product among cellulose ethers. Because of its high availability as well as its thickening and swelling properties, CMC is widely used in numerous industries. [1-3] As CMC is derived from natural cellulose, it exhibits gradual biodegradability and can be incinerated after use, making it a very environmentally friendly material.

$$R=H \text{ or } CH_2CO_2H$$
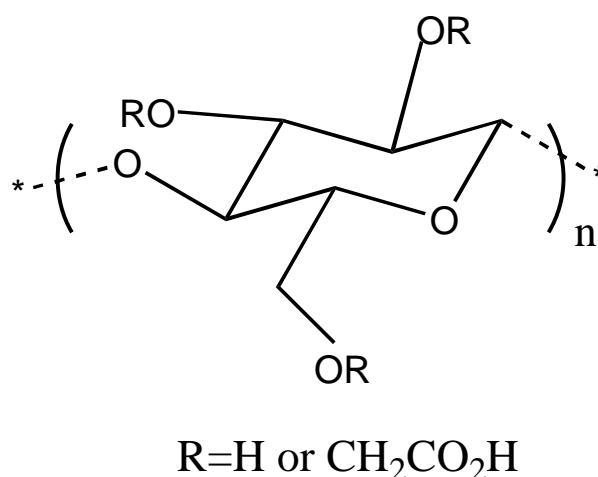
Fig. 2.2 Chemical structure of carboxymethyl cellulose.

2.1.3 Ice structuring proteins (ISPs)

Ice structure proteins (ISPs), also known as antifreeze proteins (AFPs), are a class of peptides produced by certain animals, plants, fungi and bacteria that allow them to survive below the freezing point of water. ISPs are important for the survival of organisms in cold environments. The protective function of ISPs is due to their properties, including ice plane affinity [4], thermal hysteresis [5], ice recrystallization inhibition [6], and transiently binding an organism to ice [7]. Different properties produce different antifreeze effects. Although an ISP can usually detect more than one

antifreeze property, its antifreeze effect is mainly based on one property. In general, all these properties or effects arise from the ability of ISPs to combine with small ice crystals to inhibit the growth and recrystallization of ice (Fig. 2.3). [8, 9]
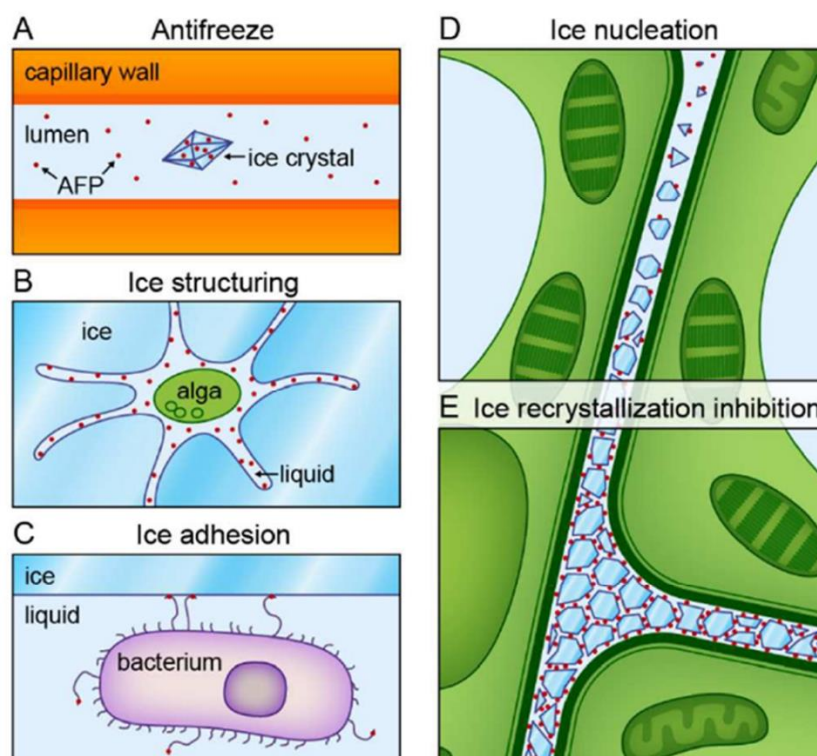
Fig. 2.3 Biological functions of structure proteins. [9]

2.1.4 Polyvinylpyrrolidone (PVP)

Polyvinylpyrrolidone (PVP) (Fig. 2.4) is a kind of Nonionic polymer compound, which is obtained from vinyl pyrrolidone (NVP) by bulk polymerization or solution polymerization. [10] It is divided into four grades according to its average molecular weight, which is usually expressed by K value, and different K values represent the corresponding average molecular weight range of PVP. K value is actually the eigenvalue related to the relative viscosity of PVP aqueous solution, and viscosity is the physical quantity related to the molecular weight of polymer, so K value can be used to characterize the average molecular weight of PVP. In general, the higher the K value, the greater the viscosity and the stronger the adhesion. As a synthetic water-soluble

polymer, PVP has unique physical and chemical properties, such as film formation, adhesion, hygroscopicity, solubilization, or condensation, which makes it useful in many pharmaceutical formulations, food, cosmetics and bath products, as well as industrial applications. [11-14]
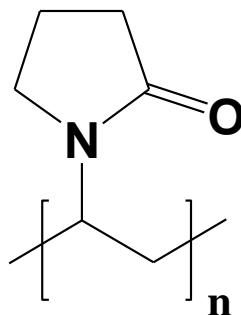
Fig. 2.4 Chemical structure of polyvinylpyrrolidone.

2.1.5   Other chemical reagents

In this research acrylic acid (AA)，ammonium persulfate (APS), calcium chloride (CaCl$_2$), and iron chloride hexahydrate (FeCl$_3$·6H$_2$O) were purchased from Nacalai Tesque, Inc. All reagents were used as received without further purification. All aqueous solutions were prepared with deionized water.

2.2 Experiment method

All the hydrogels were synthesized by a one-step radical polymerization. The hydrogel precursor solution was prepared under stirring followed by ultrasonic treatment for 10 minutes to remove the bubbles. Afterwards, the homogeneous hydrogel precursor was transferred into a custom mold (2 mm × 100 mm × 100 mm) and placed in an oven at 60 °C for 6 h to initiate the polymerization of acrylic acid and produce a hydrogel. The mechanism of free radical polymerization of acrylic acid is shown in Fig. 2.5.
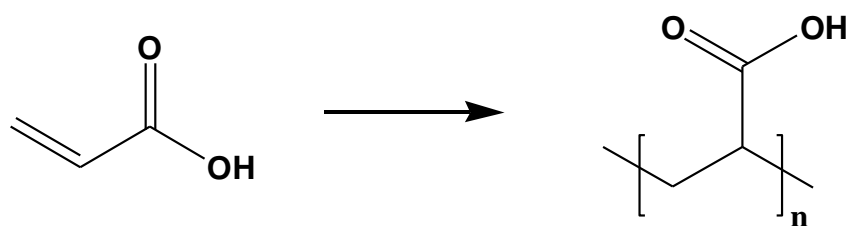
Fig. 2.5 Mechanism of radical polymerization of AA.

2.3 Instruments and Characteristics

2.3.1   Mechanical performance tests

The tensile tests at room temperature were tested by a universal testing machine (Instron, 3385, extra 50 N load cell, Instron Co., Ltd., Canton, USA) in accordance with standard JIS K6251. For the cyclic tensile test, loading–unloading measurements were performed at constant velocity of 100 mm/min.

The compressive tests were carried out by a universal testing machine (Instron, 3385, extra 50 N load cell, Instron Co., Ltd., Canton, USA) at a crosshead speed of 1 mm/min^{-1}.

2.3.2   Fourier Transform Infrared Spectrometer (FT-IR)

The FTIR spectra of the hydrogels were characterized by a Thermo Scientific Nicolet iN 10 infrared spectrometer.

2.3.3   Microstructure Characterizations

The microstructures of the hydrogels were observed by scanning electron microscopy (SEM, S-4300 Hitachi, Ltd. Japan). The hydrogels were freeze dried and then sputtered with platinum by an ion sputtering apparatus prior for SEM imaging at 5 kV.

2.3.4   Antifreeze behavior and properties

The melting behaviors of hydrogels were analyzed by the differential scanning

calorimetry (DSC, SII X-DSC 7000, Hitachi). The samples were first cooled from 20°C to -65°C with a cooling rate of 5°C/min. After holding for 5 minutes, the samples were heated from -65°C to 10°C at a rate of 5°C/min.

The tensile tests at sub-zero temperatures were performed by universal mechanical tester with an Instron Temperature Controlled Chamber (Instron 3382, Instron Co., Ltd., Canton, USA). The low temperature environment was achieved by liquid nitrogen cooling.

2.3.5   Electrical Tests

The electrochemical impedance spectroscopy (EIS) results of the prepared hydrogels were obtained by an electrochemical workstation (CS2350H, CORRTEST, China) in the range of 10^6 to 10 Hz at room temperature. The hydrogel was cut into a disk shape and placed between two stainless steel plates for the EIS tests.

The signals of the hydrogel-based sensors expressed by the resistance variations were noted via a digital source meter (LCR-6100, GWInstek).

2.3.6   Adhesion Tests

The adhesion properties of hydrogels were determined by lap shear tests using a universal testing machine (Instron 3385, Instron Co., Ltd., Canton, USA). The sample (15 mm × 15 mm × 0.6 mm) was sandwiched between two glass slides with a bonded area of 2.25 cm^2. Hold the glass slides with a long-tailed clip for 10 minutes before testing to make good contact between the slides and the sample. All tests were performed at a crosshead speed of 2 mm/min at room temperature. Repeated lap shear tests were also performed to show the reproducibility of hydrogel adhesion. The adhesion strength was calculated by dividing the maximum load by the initial bonding area.

2.3.7   Self-Healing Tests

The self-healing ability of the mechanical properties of the hydrogels was tested at room temperature with a universal mechanical tester (Instron 3385, Instron Co., Ltd., Canton, USA) equipped with a 50 N load cell at room temperature. Rectangular specimens (40 mm in length, 4 mm in width, and 2 mm in depth) were cut into halves with scissor, then the two halves were brought into contact immediate and were stored in a sealed vessel to heal for testing. The microscopic self-healing behavior of damaged sample was observed by a digital microscope (VHX-6000, KEYENCE, America). The self-healing behavior in electrical properties was detected by a digital source meter (LCR-6100, GWInstek).

References

[1] C.G. Lopez, S.E. Rogers, R.H. Colby, P. Graham, J.T. Cabral, Structure of sodium carboxymethyl cellulose aqueous solutions: A SANS and rheology study, Journal of Polymer Science Part B: Polymer Physics, 53 (2015) 492-501.

[2] G. Joshi, S. Naithani, V. Varshney, S.S. Bisht, V. Rana, P. Gupta, Synthesis and characterization of carboxymethyl cellulose from office waste paper: a greener approach towards waste management, Waste Management, 38 (2015) 33-40.

[3] T. Heinze, A. Koschella, Carboxymethyl ethers of cellulose and starch–a review, Macromolecular Symposia, Wiley Online Library, 2005, pp. 13-40.

[4] K. Basu, C.P. Garnham, Y. Nishimiya, S. Tsuda, I. Braslavsky, P. Davies, Determining the ice-binding planes of antifreeze proteins by fluorescence-based ice plane affinity, Journal of visualized experiments: JoVE, (2014).

[5] A. Flores, J.C. Quon, A.F. Perez, Y. Ba, Mechanisms of antifreeze proteins investigated via the site-directed spin labeling technique, European Biophysics Journal, 47 (2018) 611-630.

[6] L.L. Olijve, K. Meister, A.L. DeVries, J.G. Duman, S. Guo, H.J. Bakker, I.K. Voets, Blocking rapid ice crystal growth through nonbasal plane adsorption of antifreeze proteins, Proceedings of the National Academy of Sciences, 113 (2016) 3740-3745.

[7] S. Guo, C.P. Garnham, J.C. Whitney, L.A. Graham, P.L. Davies, Re-evaluation of a bacterial antifreeze protein as an adhesin with ice-binding activity, PloS one, 7 (2012) e48805.

[8] D. Goodsell, Molecule of the month: antifreeze proteins, Worldwide Protein Data Bank, New Jersey, USA, (2009).

[9] I. Voets, From ice-binding proteins to bio-inspired antifreeze materials, Soft Matter, 13 (2017) 4808-4823.

[10] F. Haaf, A. Sanner, F. Straub, Polymers of N-vinylpyrrolidone: synthesis, characterization and uses, Polymer Journal, 17 (1985) 143-152.

[11] F. Fischer, S. Bauer, Polyvinylpyrrolidon (PVP): ein vielseitiges Spezialpolymer―Verwendung in der Keramik und als Metallabschreckmedium, Keramische Zeitschrift, 61 (2009) 382-385.

[12] A. Göthlich, S. Koltzenburg, G. Schornick, Funktionale Polymere im Alltag: Vielseitig, Chemie in unserer Zeit, 39 (2005) 262-273.

[13] M.S.B. Husain, A. Gupta, B.Y. Alashwal, S. Sharma, Synthesis of PVA/PVP based hydrogel for biomedical applications: a review, Energy Sources, Part A: Recovery, Utilization, and Environmental Effects, 40 (2018) 2388-2393.

[14] B.V. Robinson, F. Sullivan, J.F. Borzelleca, S. Schwartz, PVP: a critical review of the kinetics and toxicology of polyvinylpyrrolidone (povidone), CRC Press2018.

Chapter 3 Simple preparation of carboxymethyl cellulose-based ionic conductive hydrogels for highly sensitive, stable, and durable sensors

3.1 Introduction

The similarity of water content between hydrogels and natural soft tissues has inspired the application of conductive hydrogels in electrical fields such as soft wearable sensors [1, 2], artificial muscle [3, 4] and electronic skin [5, 6]. Since the conversion of human activities into electrical signals relies on the conductivity of conductive hydrogels, the conductivity of a hydrogel is a significant property. [7, 8] The traditional approach of introducing conductivity is to disperse conductive fillers, such as metals [9], carbon-based materials (e.g., carbon nanotubes [10] and graphene [11]), into the hydrogel or to use conductive polymers (e.g., polypyrrole [12] or PEDOT [13]). However, both the aggregation or random distribution of fillers and the stiffness of the conductive polymers will cause a decrease in stretchability, recovery and conductivity, which will limit the application of these conductive hydrogels in flexible and stretchable electronics. It is well known that the conductivity of organisms is achieved by the movement of electrolytes in body fluids. Therefore, ionic conductive hydrogels incorporated with electrolyte salts as conductive donors have been increasingly studied to replace conventional fillers. [7, 14-16] In ionic conductive hydrogels, the hydrogel network serves as a soft carrier, while electrolytes provide movable ions that act as conductive donors. Thus, ionic conductive hydrogels usually exhibit good flexibility, stretchability, recovery and conductivity, which lead to their human skin-like features. [14, 17-19]

Despite the merits and advancements of ionic conductive hydrogels, it is still a challenge to prepare a hydrogel with desirable mechanical properties (tensile strength, stretchability, toughness and resilience) and ionic conductivity. For example, poly(vinyl alcohol) (PVA)-based composite hydrogels exhibit a high conductivity of 2.41 S/m, but weak tensile strength and stretchability (361 kPa, 363%) [20]; a covalent cross-linked PVA and poly(vinylpyrrolidone) (PVP) hydrogel possesses outstanding tensile strength (2.1 MPa), high toughness (9.0 MJ/m^3) and high stretchability (830%) but low sensitivity (0.348) [21] ; and supramolecular nanofibrillar hydrogels display high mechanical strength (0.750 MPa), reliable stretchability (3120%), and robust toughness (4.77 MJ/m^3) but unsatisfactory conductivity (10^{-2} S/m). [18] The lack of comprehensive properties consequently results in undesirable shortcomings when used as sensors, such as insensitivity, instability, and poor durability.

Moreover, it is also a challenge to explore a simple, cost-efficient and easy-to-process method for preparing ionic conductive hydrogels. To date, there are two main steps for the preparation of ionic conductive hydrogels: (1) the preparation of traditional strong hydrogels to construct soft carriers, and (2) the loading of electrolytes in a hydrogel network by soaking in a highly concentrated salt solution to improve conductivity [19, 22, 23]. The complex preparation procedure incurs undesirable costs of equipment, energy and time, which can become a large of waste resources.

To date, there are many strategies that can meet the demands of the mechanical properties of hydrogels, such as double networks [24], nanocomposites [25], topological structures [26], and macromolecular cross-linking [27], and so on [28]. Formerly reported research has proven that the introduction of a double network is an effective way to build a performance-controlled hydrogel [29]. Carboxymethyl cellulose (CMC), as a kind of cellulose derivative, is widely used in many fields, such as the food, medicine, textile and paper industries, due to its low cost, non-toxicity and biocompatibility. Previous studies have successfully formed functional hydrogels with CMC as a crosslinker. [30, 31] Our previous work also reported that, as an initiator and crosslinker, CMC could significantly improve the mechanical properties of polyacrylic

acid (PAA) hydrogels [32]. In addition, phytic acid (PA), as a natural substance in the seeds, roots and stems of plants, has been used as a crosslinker due to its unique structure [33, 34]. The conductivity of PA has also been reported to enhance the ionic conductivity [35]. Therefore, it is expected that PA can promote not only the mechanical performance but also the conductivity of ionic conducting hydrogels.

Herein, a simple one-step thermal polymerization is applied to prepare a novel double-network polyacrylic acid (PAA) hydrogel with carboxymethyl cellulose (CMC) as the first cross linker, and phytic acid (PA) as the ion donor and second cross linker. A balance among the mechanical properties, resilience, recovery, conductivity and sensitivity are realized due to the unique design of the microstructure. Interestingly, the resilience of the hydrogel (93%) is similar to that of natural resilin (92%), which has rarely been mentioned in reported ionic conductive hydrogels. As a result, these ionic conductive hydrogels can be used as tension and compression sensors to precisely detect both very small and large human activities, such as speaking, pulse, finger, and knee activities, with outstanding durability, stability and sensing performance. Furthermore, the need for a complicated process has been avoided since there is only one step for the preparation of these ionic conductive hydrogels. The characteristics of these ionic conductive hydrogels give them high potential for use in healthcare monitoring sensors, wearable devices, and artificial intelligence applications.

3.2 Experimental Section

3.2.1 Materials

Carboxymethyl cellulose sodium salt (CMC, EP), acrylic acid (AA, EP), ammonium peroxydisulfate (APS, GR), and phytic acid solution (50 wt.% in water) were used. All the above mentioned materials were employed without any further purification. Deionized water was employed to prepare aqueous solutions throughout the whole work.

3.2.2 Fabrication of Hydrogels

The hydrogels were prepared by heating with water as the solvent. In the reaction system, the concentration of AA was fixed at 25% of the total solution weight, while the mass ratio of PA to PAA acted as the control parameter. As shown in Table 1, 40 mg APS, 4.00 g of AA and a certain amount of PA (the mass ratio of PA to PAA was 0, 0.34, 1.01, 1.69 and 2.36, respectively) were mixed with deionized water by magnetic stirring. After that, 0.32 g of CMC was gradually added to the mixture with strong magnetic stirring. The precursor mixture was dissolved for 1 h with stirring followed by an ultrasonic treatment for 10 min to remove bubbles. The viscous precursor hydrogels were then transferred into a tailored mold and placed in an oven at 60 ℃ for 6 h to generate hydrogels. For simplicity, the prepared hydrogels were denoted as PCP-n, in which n=0, 1, 2, 3, and 4, which represented that the mass ratios of PA to PAA were 0, 0.34, 1.01, 1.69 and 2.36, respectively.

Table 1.1 The composition and the mechanical properties of the hydrogels.

Hydrogel	AA (mL)	H$_2$O (mL)	CMC (g)	APS (mg)	PA (mL)	PA / PAA(g/g)
PCP-0	4	11.10	0.32	40	0	0
PCP-1	4	9.67	0.32	40	1	0.34
PCP-2	4	6.81	0.32	40	3	1.01
PCP-3	4	3.94	0.32	40	5	1.69
PCP-4	4	3.94	0.32	40	7	2.36

3.3 Characterizations

3.3.1 Mechanical Tests

The mechanical tests were conducted with a universal mechanical tester (Instron 3385, Instron Co., Ltd., Canton, USA) equipped with a 50 N load cell at room temperature. The hydrogel was coated with silicone oil to minimize water evaporation during the

mechanical tests. The hydrogels were cut into rectangular specimens (20 mm × 4 mm × 2 mm) to determine the tensile strength at a speed of 100 mm/min. The fracture energy (toughness) was calculated by the area below the stress−strain curve. The tensile cycle tests were carried out at a speed of 100 mm/min by the same universal mechanical tester. The dissipated energy (Ed) was obtained from the area between the loading−unloading curves, while the resilience was defined as the quotient of the area under the unloading stress-strain and the loading stress-strain. The recovery behavior of the hydrogel was characterized by the intermittent tension cycles carried out on one hydrogel at a fixed strain of 300% for different intervals. The compressive tests were carried out at a cross-head speed of 1 mm/min^{-1} and a strain of 70% on a disk shaped sample with a diameter of 9 mm and a height of 2 mm.

3.3.2 Microstructure Characterizations of Hydrogels

The FTIR spectra of pure PAA, CMC, the PAA/CMC hydrogel and the PAA/CMC/PA hydrogel were characterized by a Thermo Scientific Nicolet iN 10 infrared spectrometer. The microstructures of the hydrogels were observed by scanning electron microscopy (SEM, S-4300 Hitachi, Ltd. Japan). The hydrogels were freeze dried for 24 h after quick-freezing by liquid nitrogen and then the cross-section was sputtered with platinum for SEM imaging at 5 kV.

3.3.3 Electrical Test

The electrochemical impedance spectroscopy (EIS) results of the prepared hydrogels were obtained by an electrochemical workstation (CS2350H, CORRTEST, China) in the range of 10^6 to 10 Hz at room temperature. The hydrogel was cut into a disk shape and placed between two stainless steel plates for the EIS tests. The conductivity of the hydrogels was calculated based on $\sigma = L/RS$, in which L, R and S represented the thickness, the impedance and contact area of the hydrogel, respectively.

The signals of the sensors expressed by the resistance variations were noted via a digital

source meter (LCR-6100, GWInstek) at a voltage of 10 mV. $\Delta R/R_0$ (the relative resistance change value) was computed from the equation $(R- R_0)/R_0$, in which ΔR, R_0 and R represented the change in resistance, original resistance and dynamic resistance under different strains, respectively. The sensitivity of the tensile sensors was defined as the gauge factor (GF), which was the value of $(\Delta R_0/R)/\varepsilon$ (ε represented the strains when the resistance equalled R). The sensitivity of the compression sensors (S) was defined as the slope of the curve of the relative resistance change (absolute value) versus pressure.

3.4 Results and Discussion

3.4.1 Synthesis of hydrogel

A simple and feasible one-step method was developed to prepare the designed hydrogels. Fig. 3.1a illustrates the fabrication procedure of the ionic conductive hydrogels. In brief, a predetermined amount of AA (monomer), CMC (crosslinker), PA (cross-linker and ion donor) and APS (initiator) was dissolved in deionized water to form a viscous solution. The solution was heated to initiate the polymerization of PAA and to form ionic conductive hydrogels.

During the preparation process, APS decomposed to generate anionic radicals upon heating, and then abstracted hydrogen from the hydroxyl group of CMC to form macro-radicals which initiated the polymerization of the acrylic acid monomer [36-38]. Our previous work reported in detail that CMC acts as the first crosslinker, and has a positive influence on the properties of PAA hydrogels [32]. To further improve the properties of the hydrogel, PA was introduced to the system to assume two roles in this work. First, it is well known that as a six-fold dihydrogen phosphate ester of inositol, PA contains numerous hydroxyl groups that can ionize a considerable number of hydrogen ions. Therefore, the first role of PA is to act as an ion donor to improve the conductivity of the hydrogel. Second, the presence of abundant hydrogen ions can also inhibit the ionization of the carboxyl groups of PAA, which will correspondingly create an

48

abundance of active physical crosslinking points, finally resulting in the crosslinking of polymer chains.[39] Furthermore, PA is also a crosslinker that can form physical crosslinking networks with both CMC and PAA via hydrogen bonds.
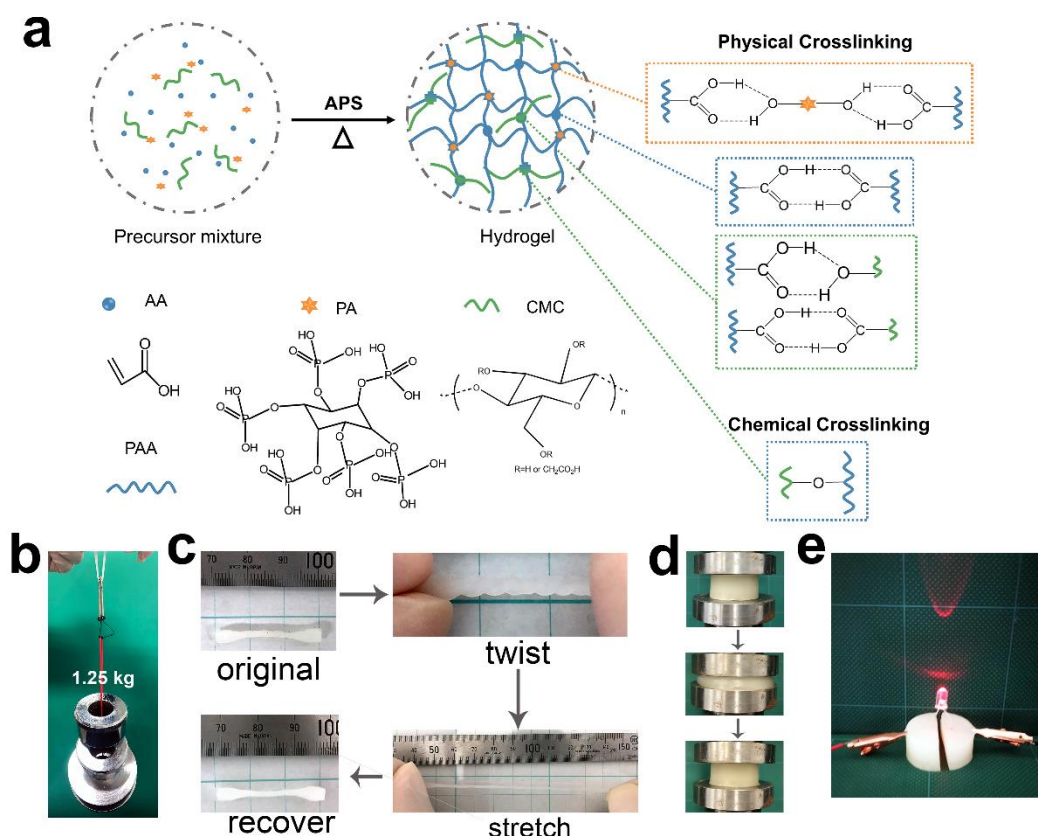

Fig. 3.1 Fabrication of the ionic conductive hydrogel and illustration of strength, stretchability, stretch recovery, compressive recovery and conductivity with digital photos. a) Illustration scheme of the formation and mechanism of the hydrogel. b) The hydrogel (width of 4 mm, thickness of 2 mm) is strong enough to lift a steel block with a weight of 1.25 kg. c) The hydrogel can be stretched and twisted and still recover to its original state without visible change. d) The hydrogel can bear large compression deformation with outstanding recovery. e) The conductivity of the hydrogel is good enough to light an LED bulb.

The interactions in the hydrogel were confirmed by FTIR spectroscopy (Fig. 3.2). As shown in FTIR spectra, absorption band of pure CMC at 3421 cm^{-1}, 1262 cm^{-1} and 899

cm^{-1} represented the stretching vibration of -OH, the in-plane bending vibration of –OH and the symmetric stretching vibration of C–O–C, respectively. After polymerization, the corresponding peaks were shifted to lower wave numbers at 3335 cm^{-1}, 1203 cm^{-1} and 895 cm^{-1} respectively in the hydrogel of PAA/CMC (Fig. 3.2c) when compared with pure CMC. Moreover, there was a new absorption at 1732 cm^{-1}, which ascribed to carboxyl groups of PAA in the spectrum of the hydrogel of PAA/CMC (Fig. 3.2c). Both of the carbonyl stretching from the carboxyl groups of PAA, and CMC were shifted after turning into PAA/CMC hydrogel. These results demonstrated that chemical network was formed under the crosslinking effect of CMC [36, 37]. The FTIR spectra has also been used to characterize the crosslinking effect of PA. It could be found that a new peak appeared at 2852 cm^{-1} in hydrogel PAA/CMC/PA (Fig. 3.2d) after adding PA. Meanwhile, the carbonyl stretching in the hydrogel PAA/CMC/PA shifted to higher wave numbers at 1745 cm^{-1} compared with the hydrogel of PAA/CMC, which confirmed that the physical crosslinking networks have been formed with the assistant of PA. In general, there were two kinds of crosslinking networks in the hydrogel. One was the chemical network formed between PAA and CMC by radical polymerization, which could improve the strength of the hydrogel via stress transfer at a large deformation. The other was multiple dynamic physical networks among CMC, PAA and PA, which could rapidly associate, dissociate and finally result in the improvement of the hydrogel recovery, resilience, and fatigue resistance.

As a result, the hydrogel possessed favorable mechanical properties to endure lifting, twisting, stretching and compression along with self-recovery performance (Fig. 3.1b-d). As shown in Fig. 3.1b, the hydrogel was mechanically sturdy enough to lift a steel block with a weight of 1.25 kg without any rupture. Besides, the self-recovery property of the hydrogel is excellent. A twisted dumbbell-shaped hydrogel could be stretched to 3 times its original length, and then returned to its original state immediately after removing the force (Fig. 3.1c). The hydrogel also possessed favourable compressive recovery as displayed in Fig. 3.1d. The cylinder-shaped hydrogel was compressed to 70% of its original height without fracture, and then as soon as the pressure was

removed, it immediately recovered to its original shape. Moreover, the conductivity of the hydrogel enabled it to light up an LED bulb (Fig. 3.1e). This method is expected to be used in large-scale manufacturing since there is simply blending and heating during the preparation process, which is the most widely utilized processes in industry.
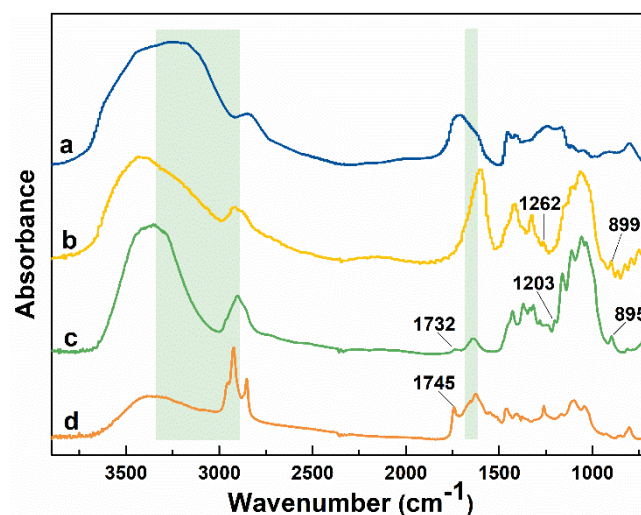

Fig. 3.2 FTIR spectra of a) PAA, b) CMC, c) the hydrogel of PAA/CMC and d) the hydrogel of PAA/CMC/PA.

3.4.2 Structural and mechanical properties

A series of hydrogels with various ratios of PA were prepared and compared with a hydrogel without PA (Table 1.1). The hydrogels gradually became opaque with an increasing content of PA (Fig. 3.3a), which may be explained by a change in the microstructure. As the SEM images of the hydrogel cross-sections show (Fig. 3.3b-f), the hydrogels possessed a three-dimensional (3D) porous structure with pore sizes in the range of 5-50 μm. The pore size of the hydrogel without PA was the largest, while with the introduction of PA, the crosslinking points of the hydrogels increased, and the pore sizes decreased accordingly. The more PA that was added, the denser the hydrogel structure became, which finally resulted in an opaque hydrogel appearance. Since the mechanical performance of 3D crosslinked network hydrogels is extremely dependent

51

on the crosslinking density [40], the increase in hydrogel cross-linking density resulting from the introduction of PA may enhance mechanical properties.
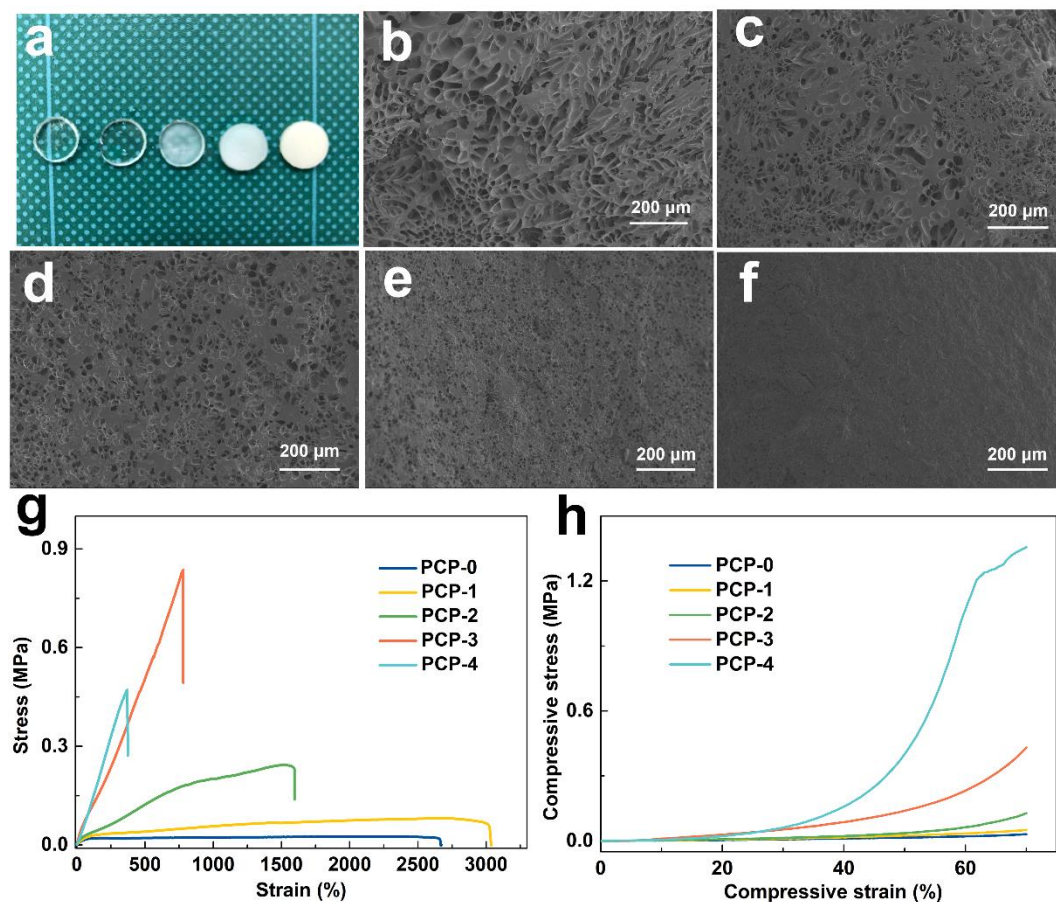

Fig. 3.3 Structural and mechanical performances of the hydrogel. a) Digital photos displaying the appearance of PCP-0, PCP-1, PCP-2, PCP-3 and PCP-4 (from left to right). b-f) Microstructure of the hydrogels (PCP-0, PCP-1, PCP-2, PCP-3 and PCP-4, successively) as characterized by SEM. g) Tensile stress-strain curves of the hydrogels. h) Compressive stress-strain of the hydrogels.

The mechanical properties of the hydrogels (PCP-0 to PCP-4) were further studied to verify the effect of PA. As the stress-strain curves of the hydrogel displayed in Fig. 3.3g, all hydrogels prepared were elastic. PA could increase the tensile strength of the hydrogel as expected while compromising the stretchability. The hydrogel without PA exhibited a tensile strength of 0.022 MPa and 2600% elongation at break. When the

mass ratio of PA to PAA was up to 1.69, the tensile strength reached 0.836 MPa (PCP-3), which was approximately 38 times that of the hydrogel without PA (PCP-0, 0.022 MPa). However, when the ratio was further increased to 2.36, the tensile strength decreased to 0.471 MPa, which may be caused by the uneven stress distribution resulting from aggregates in the hydrogel [41]. Moreover, the elongation at break showed a gradual downward trend with the introduction of PA, which was a common phenomenon for double crosslinking hydrogels [42]. However, the elongation at break of PCP-3 still exhibited a value of 779%, indicating the satisfactory elastic performance of the hydrogel. Interestingly, both the stretchability and tensile strength of PCP-1 (3000%, 0.065 MPa) were improved compared to the hydrogel without PA (PCP-0, 2600%, 0.022 MPa), which indicated that the addition of PA significantly improved not only the strength but also the toughness of the hydrogel. In addition, the toughness values of the hydrogels were calculated to further indicate their ability to withstand both high stresses and high strains (Fig. 3.4a). The toughness greatly increased with an increasing PA content from 0.61 MJ/m^3 (PCP-0, PA/PAA=0) to 3.11 MJ/m^3 (PCP-3, PA/PAA=1.69), and the improvement was achieved 5 times. However, the toughness decreased to 0.89 MJ/m^3 (PCP-4) as the PA content further increased (PA/PAA=2.36) due to the decrease in both the tensile strength and stretchability. In addition to tensile strength, the addition of PA also influenced the compression performance (Fig. 3.3h and Fig. 3.4b). The compression strength of the hydrogel without PA (PCP-0) was 0.03 MPa. With the addition of PA, the compressive strength showed an increasing trend, which went along with the structural changes. Notably, the compression strength of PCP-4 increased to 1.34 MPa, which was approximately 45 times that of the hydrogel without PA (PCP-0, 0.03 MPa). However, after compression to over 60% strain, PCP-4 showed an irregular trend, which may be caused by damage to the internal structure under large stresses [43]. PCP-3, possessing the highest toughness (3.11 MJ/m^3) and satisfactory tensile strength (0.836 MPa), stretchability (779%) and compression strength (0.43 MPa) was used for the subsequent research unless otherwise mentioned for comprehensive consideration.
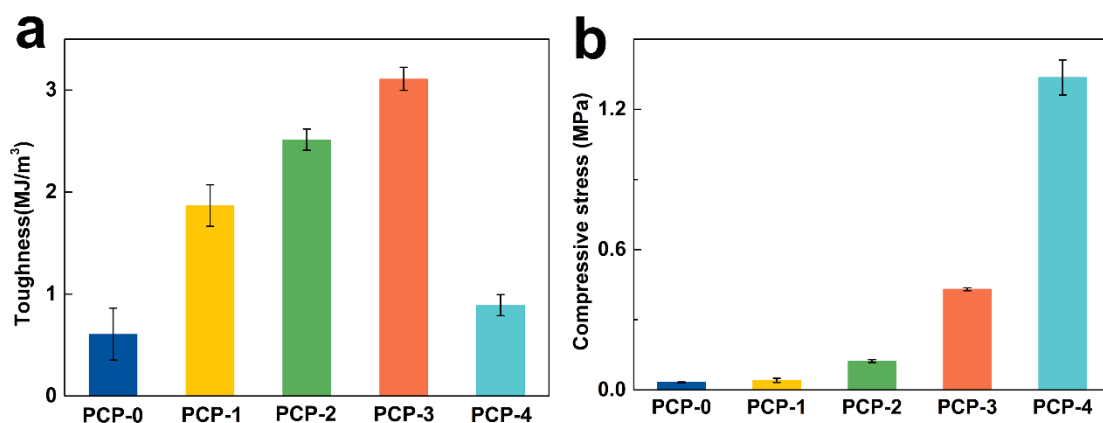
Fig. 3.4 a) Toughness of the hydrogels, b) Compression strength of the hydrogels.

3.4.3 Resilience, recovery, fatigue resistance

Stable mechanical properties such as recovery, resilience and fatigue resistance are also of great importance in the application of soft wearable sensors, artificial muscle and electronic skin due to the requirement of reliable performance [44]. The fatigue resistance properties of the produced hydrogel were studied via 20 successive loading-unloading tensile tests at a strain of 125% (Fig. 3.5a). There was a hysteresis loop in the 1st cycle, which was defined as "structure stabilization" resulting from microstructure changes, such as the untying of the physical crosslinked network, the drifting of polymer chains and the fracture of the network [45]. After that, the rest of the cycles showed similar loading–unloading curves with slight hysteresis. The energy dissipation (Ed) was calculated to further discuss this phenomenon. As shown in Fig. 3.5b, Ed decreased from 15.95 kJ/m^3(1st cycle) to 6.98 kJ/m^3 (3rd cycle) and then hardly changed in the remaining cycles. Accordingly, the resilience and residual strain achieved almost stable values at 93% and 6.7% after the first two cycles. The hydrogel resilience was similar to the resilience of natural resilin (92%) [46]. It is expected that the produced hydrogel could be used to mimic natural resilin, which plays an important role in dictating the movement and sound production of animals [47]. Since resilience is the ability of a material to absorb and release energy upon loading-unloading, the

remarkable resilience of the hydrogel suggests that it exhibits excellent and rapid recovery characteristics and fatigue resistance through energy dissipation after the structure is stabilized. Figures 3c and S1 also indicate the outstanding recovery of the hydrogel since it could recover to its original condition in 20 min after 7 cycles at a strain of 300%. All the above results demonstrated the outstanding recovery and fatigue resistance of our hydrogel when stretched.
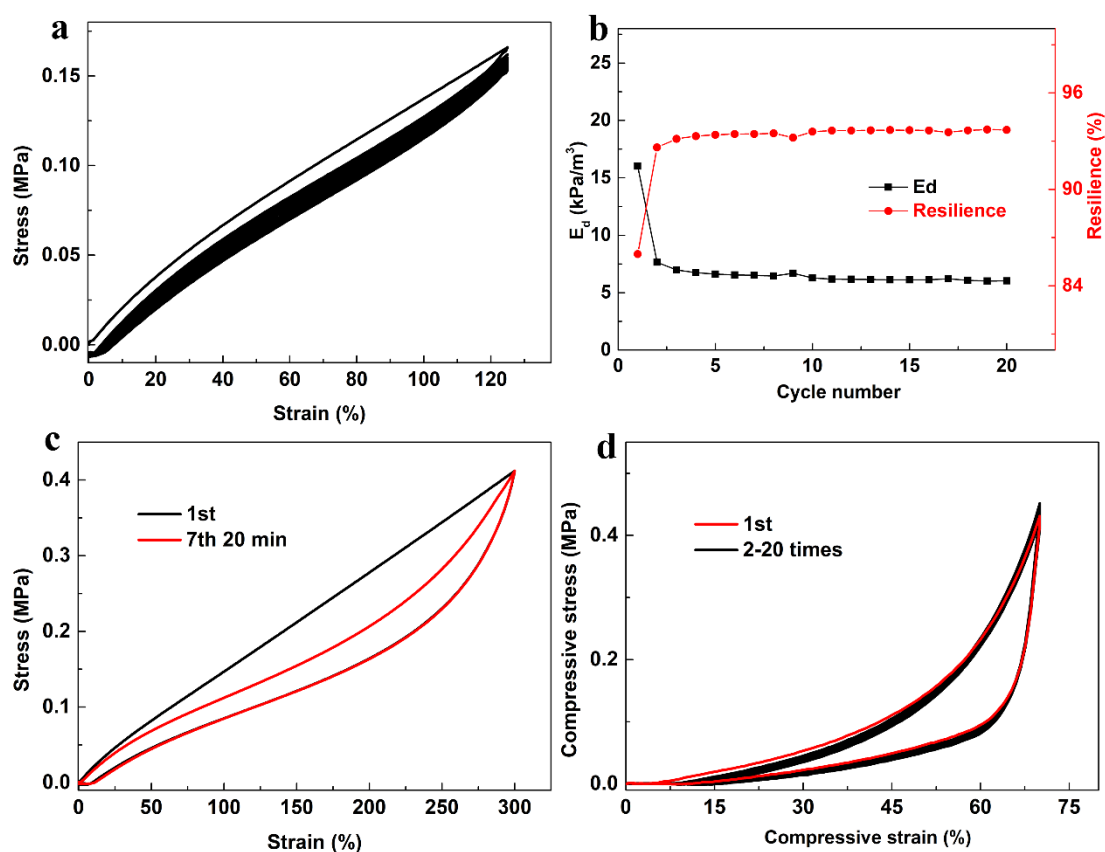
Fig. 3.5 a) Successive loading–unloading tensile tests for 20 cycles at a strain of 125%. b) Energy dissipation and resilience calculated from the loading-unloading curves at a strain of 125% during 20 successive loading-unloading cycles. c) The recovery of the hydrogel was displayed by the stress recovery after 7 cycles at a strain of 300% (recovered to its original condition after storing the hydrogel for 20 min at room temperature). d) Successive compressive tests of the hydrogel at 70% strain for 20 cycles.

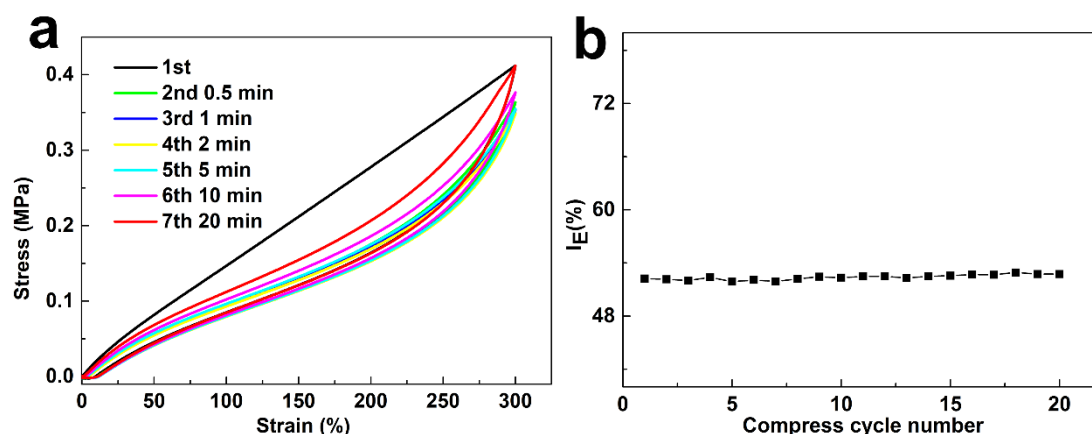Fig. 3.6 a) Recovery state of the hydrogel was displayed by stress recovery after storing for different time intervals at strain 300%. 1st, 2nd, 3rd, 4th, 5th, 6th, 7th represent the loading-unloading tensile cycles on the same hydrogel for the first time, the second time, the third time, the fourth time, the fifth time, the sixth time and the seventh time, respectively. b) The energy loss coefficient (IE) during successive compressive tests of the hydrogel at 70% strain for 20 cycles.

The recovery and fatigue resistance were further tested by applying a successive compression force for 20 cycles at 70% compressive strain on the hydrogel. Interestingly, there was no obvious change in the maximum compressive stress, and the energy loss coefficient (I_E) also showed little change during the compression cycles (Fig. 3.5d, Fig. 3.6). The hydrogel could quickly recover to its original state after removing the stress, which was due to the effective energy dissipation from the rapid tying and untying of the physical crosslinked network. The results indicated that the hydrogel was resilient with excellent shape recovery performance and fatigue resistance under compression.

3.4.4 Ionic conductivity

The conductivity of the hydrogel can also be improved due to the doping effect of PA [20, 35]. Electrochemical impedance spectroscopy (EIS) was introduced to characterize the conductivity of the hydrogels with varying PA contents (Fig. 3.7a). The linear trend

in all the EIS curves indicated the non-Faradaic process of the hydrogels, in which charge was gradually stored instead of moved across the electrode [19]. The intersection point between the curve and X-axis could be regarded as the impedance of the hydrogel. The conductivity of the hydrogel with various PA ratios was calculated and presented in Fig. 3.7b. With an increasing PA ratio, the conductivity shifted to a higher value, which indicated the effect of PA on the improvement in ionic conductivity. The highest conductivity (6.0 S/m) was achieved when the value of PA/PAA was 1.69 (PCP-3), which was 13 times that of the hydrogel without the addition of PA (PCP-0, 0.53 S/m). However, the conductivity of PCP-4 showed a slight decrease, which may result from the diminished pores.
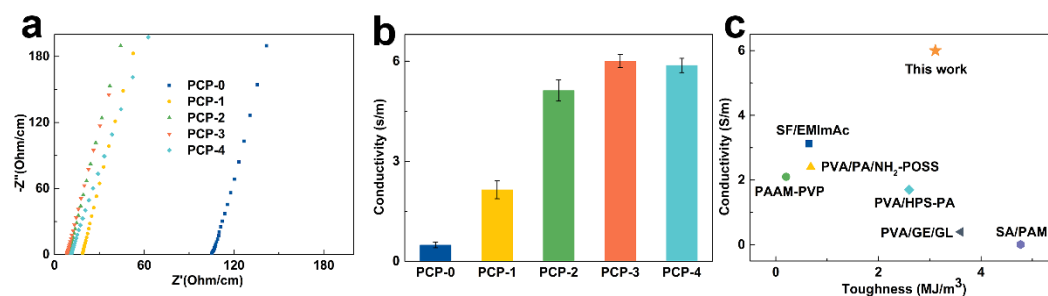

Fig. 3.7 Ionic conductivity of the hydrogels. a) EIS Nyquist plot of the hydrogels. b) Ionic conductivity of the hydrogels. c) Ashby plot of ionic conductivity versus toughness for comparison with formerly reported ionic conductive hydrogels. [18, 20, 48-51]

As a result, the hydrogel achieved a combination of favourable mechanical properties (tensile strength of 0.836 MPa, elongation at break of 779%, toughness of 3.11 MJ/m3, and resilience of 93%) and a conductivity of 6.0 S/m. The Ashby plot of toughness and conductivity is shown in Fig. 3.7c to compare the performance between PCP-3 and formerly reported hydrogels. This comparison demonstrated that the hydrogel designed in this work not only realized the integration of mechanical properties and conductivity but was also outstanding compared to former works.
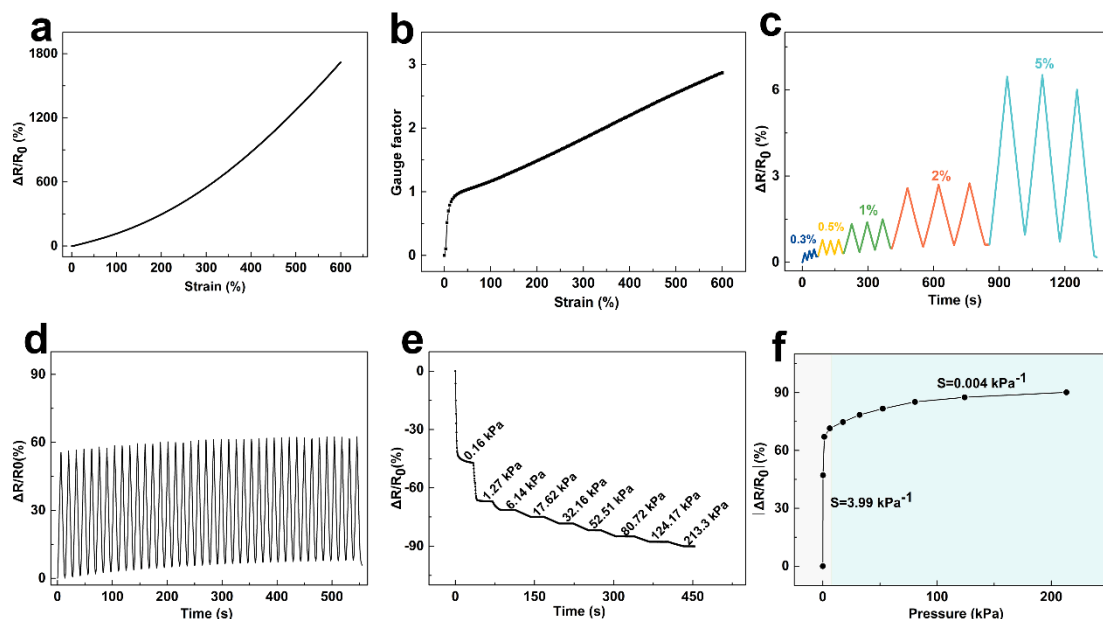
3.4.5 Sensing performance

Fig. 3.8 Sensing performance of the hydrogel-based sensor. a) Relative resistance variations of the hydrogel-based sensors under different tensile strains. b) The gauge factor (reflecting the strain sensitivity of sensors) increases with an increasing tensile strain. c) Repeatable and reversible $\Delta R/R_0$ under small tensile strain (0.3%-5%) in successive tests. d) Relative resistance variations of the hydrogel-based sensors under a cyclic uniaxial force at a tensile strain of 50% for 40 cycles. e) Relative resistance variations of the sensor with pressure. f) Absolute value of $\Delta R/R_0$ and the compression sensitivity (S) of the sensor.

The unique combination of mechanical performance and ionic conductivity in this hydrogel suggests that it could potentially be used in soft sensors. To investigate the potential sensing performance of the hydrogel, it was assembled into a resistive sensor. The tensile strain sensing ability was first evaluated by monitoring the variation in the resistance signal upon uniaxial stretching at a constant voltage of 10 mV. As displayed in Fig. 3.8a, the relative resistance change ($\Delta R/R_0$) increased with an increasing tensile strain from 0% to 600%, which illustrated the broad tensile strain sensing range of the sensor. The gauge factor (GF) is defined as the relative resistance change against tensile

58

strain ((ΔR/R0)/ε), which is an important parameter reflecting the tensile strain sensitivity of sensors. The GF of the sensor showed two trends with an increasing tensile strain (Fig. 3.8b). When the tensile strain was below 20%, the GF increased sharply to 0.95; then, when the tensile strain was further increased to 600%, the GF increased linearly to 2.86. The high GF enabled it to be sensitive enough to detect both small and large deformations. The repeatable and reversible ΔR/R$_0$ under small tensile strain (0.3%-5%) and large tensile strain (50%-300%) in successive tests (Fig. 3.8c and Fig. 3.9) also demonstrated the large-scale tensile strain sensing ability and stability of the sensor. The sensor was stretched at a tensile strain of 50% for 40 cycles to further reveal its good sensing stability under tensile stress (Fig. 3.8d).
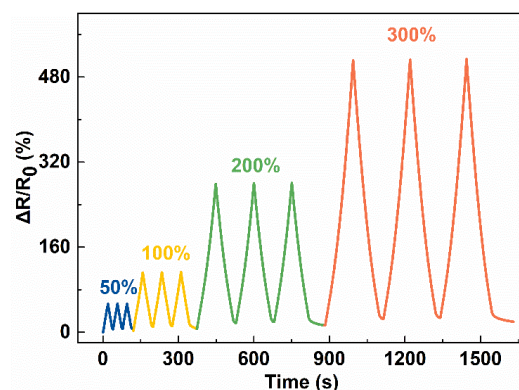

Fig. 3.9 The repeatable and reversible ΔR/R$_0$ under large tensile strain (50%-300%) in successive tests.

In addition to tensile strain sensing performance, the hydrogel also exhibited excellent compression sensing performance. The compression sensing ability of the sensor was evaluated by monitoring the resistance signal variation after compression at a constant voltage of 10 mV. The resistance of the sensor decreased rapidly when the pressure progressively increased from 0.16 kPa to 213.3 kPa, as shown in Fig. 3.8e. According to the formula R=ρL/S, the resistance is related to the resistivity (ρ), length (L) and cross-sectional area (S). As ρ of the prepared hydrogel is constant, the change in L/S would cause the variation in R. When pressure was applied to the sensor, the

deformation of the sensor decreased the value of L/S, which further reduced the resistance. The compression sensitivity S is defined as the slope of the curve of the relative resistance change (absolute value) versus pressure. As displayed in Fig. 3.8f, the sensitivity was divided into more than one region, which was similar to most previous research [18, 20]. The sensitivity was 0.004 kPa^{-1} when the applied pressure was within the range of 6.14-213.3 kPa, while the sensitivity was 3.99 kPa^{-1} when the applied pressure was less than 6.14 kPa. Both the tensile strain and compression sensing performance were prominent compared to previous works. The sensitivity was 0.004 kPa^{-1} when the applied pressure was within the ranges of 6.14-213.3 kPa, while the sensitivity was 3.99 kPa^{-1} when the applied pressure was less than 6.14 kPa. Both the tensile strain and compression sensing performance were prominent to previous works.[19, 52, 53]

3.4.6　Wearable sensor

Due to the outstanding sensing performance over a large scale of strains resulting from the integration of a favorable ionic conductivity and fine mechanical properties and recovery, the hydrogel shows high potential for use in wearable devices. The hydrogel was fabricated into wearable sensors and assembled into various human body parts to monitor the change in resistance during human activities (Fig. 3.10).

Fig. 3.10a illustrates the folding and unfolding process of the index finger detected by the sensor during consecutive cycles. $\Delta R/R_0$ increased rapidly along with the bending of the finger, while it returned to the original value when the finger was straightened. The whole process could be distinguished clearly, and the signals of each cycle were almost without any hysteresis, which was due to the reliability and sensitivity of the sensor. Moreover, as shown in Fig. 3.10b, when the index finger bent from 0° to 90° and returned to 0° step by step, $\Delta R/R_0$ changed to a correspondingly precise value and remained constant at a certain angle until the next action occurred. As a result, the whole process accurately presented terraced variation. These accurate records were also

attributed to the high sensitivity of the wearable sensor. The movements of the knee were also detected to illustrate the application of the wearable sensor for detecting large actions (Fig. 3.10c).

In addition, the sensor was also sensitive enough to detect subtle and complicated activities, such as the vibration of the throat during speaking. When a volunteer expressed greetings in three languages (English "hello", Chinese "nihao" and Japanese "konnichiwa", respectively), the phonation could be clearly recognized due to their differences in syllables (Fig. 3.10d). The characteristic peaks and valleys were similar when the words were repeated six times, which indicated the reliability of the sensor. The ability of the sensor for voice detection promotes its potential application in the field of phonation recognition and voice control switches, which is beneficial for people who have difficulties speaking or for human/machine interfaces [54]. When attached to the wrist, the highly sensitive sensor was able to monitor the blood flow of a volunteer (Fig. 3.10e). According to the pulse signal shown in Fig. 3.10e, the pulse frequency was calculated to be 65 beats/min with an ordinary and repeatable pulse shape, which was within the pulse range of a normal human body.

Moreover, the sensor was utilized as a pressure sensor to detect a gentle finger touch (Fig. 3.10f). A sharp increase in $\Delta R/R_0$ was recorded when the finger touched the surface of the sensor, while $\Delta R/R_0$ rapidly recovered to 0 when the finger pressure disappeared. It only took 0.3 s for one contact period, which demonstrated the sensitivity and recovery of the sensor once again. The ability of the sensor for finger touch detection makes it possible for it to be assembled into tactile panels to fabricate smart wearable keyboards.

As discussed above, the sensor could be used to monitor both large human activities, such as joint motions, and very small activities, such as phonation recognition and heart pulse detection. Furthermore, the sensing signals were not only stable and durable but also sensitive. Therefore, the sensor shows high potential for use in personal healthcare, wearable devices, and artificial intelligence applications.
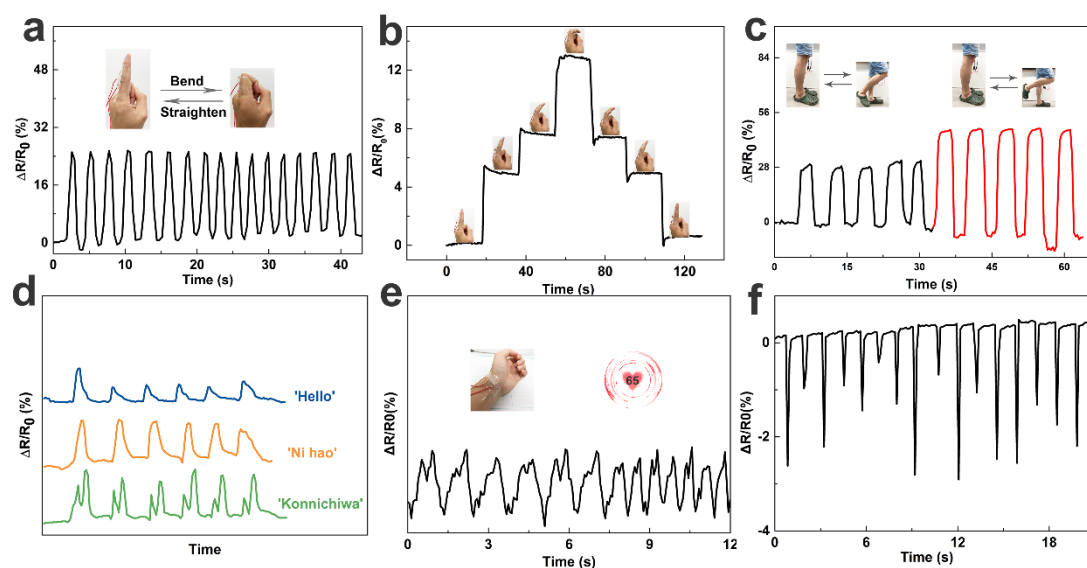
Fig. 3.10 Hydrogel-based wearable sensors for the real-time detection of human activities. a) Signals express the folding and unfolding process of an index finger during consecutive cycles. b) Response to a finger bending step by step. c) Response to the movements of the knee at different angles for consecutive cycles. d) Recognition of phonation via the sensor. e) Precisely monitored heart pulse signal. f) Recording of a gentle finger touch by the pressure sensor.

3.5 Conclusions

In summary, a novel ionic conductive poly(acrylic acid)/carboxymethyl cellulose/phytic acid hydrogel with outstanding comprehensive performance was fabricated via a simple and economical method. The high mechanical performance, good resilience and recovery and favorable fatigue resistance of the hydrogel were attributed to its unique microstructure resulting from the synergistic effects of the double crosslinked network. The outstanding conductivity (6.0 S/m) combined with the unique microstructure endowed a hydrogel-based sensor with excellent sensitivity when used as both a tension and compression sensor. Based on the outstanding comprehensive performances, the prepared hydrogel could be used as a wearable sensor to precisely record human activities (such as knee and finger motion and heart pulse

detection) over a broad strain window with excellent sensitivity, stability, and durability. In general, this research provides a new way to facilely and effectively prepare ionic conductive hydrogels with outstanding comprehensive performance. In addition, hydrogel-based sensors with high sensitivity, stability and durability exhibit high potential to be widely applied in sensing and flexible devices, such as health-recording sensors, wearable devices, and artificial intelligence.

References

[1] Y. Zhao, Z. Li, S. Song, K. Yang, H. Liu, Z. Yang, J. Wang, B. Yang, Q. Lin, Skin‑inspired antibacterial conductive hydrogels for epidermal sensors and diabetic foot wound dressings, Advanced Functional Materials, 29 (2019) 1901474.

[2] Z. Wang, Y. Cong, J. Fu, Stretchable and tough conductive hydrogels for flexible pressure and strain sensors, Journal of Materials Chemistry B, 8 (2020) 3437-3459.

[3] T. Distler, A.R. Boccaccini, 3D printing of electrically conductive hydrogels for tissue engineering and biosensors–A review, Acta Biomaterialia, 101 (2020) 1-13.

[4] J. Yang, J. Yao, S. Guan, Enhanced electroresponsive and electrochemical properties of the biological gel artificial muscle prepared by sodium alginate and carboxylated chitosan, Sensors and Actuators B: Chemical, (2020) 128526.

[5] B. Ryplida, K.D. Lee, I. In, S.Y. Park, Light‑Induced Swelling‑Responsive Conductive, Adhesive, and Stretchable Wireless Film Hydrogel as Electronic Artificial Skin, Advanced Functional Materials, 29 (2019) 1903209.

[6] Z. Zhang, Z. Chen, Y. Wang, Y. Zhao, Bioinspired conductive cellulose liquid-crystal hydrogels as multifunctional electrical skins, Proceedings of the National Academy of Sciences, 117 (2020) 18310-18316.

[7] X. Sui, H. Guo, P. Chen, Y. Zhu, C. Wen, Y. Gao, J. Yang, X. Zhang, L. Zhang, Zwitterionic Osmolyte‑Based Hydrogels with Antifreezing Property, High Conductivity, and Stable Flexibility at Subzero Temperature, Advanced Functional Materials, 30 (2020) 1907986.

[8] B. Zhang, J. He, M. Shi, Y. Liang, B. Guo, Injectable self-healing supramolecular hydrogels with conductivity and photo-thermal antibacterial activity to enhance complete skin regeneration, Chemical Engineering Journal, 400 (2020) 125994.

[9] L. Wang, W.A. Daoud, Hybrid conductive hydrogels for washable human motion energy harvester and self-powered temperature-stress dual sensor, Nano Energy, 66 (2019) 104080.

[10] L.-Y. Hsiao, L. Jing, K. Li, H. Yang, Y. Li, P.-Y. Chen, Carbon nanotube-integrated conductive hydrogels as multifunctional robotic skin, Carbon, 161 (2020) 784-793.

[11] C. Zheng, Y. Yue, L. Gan, X. Xu, C. Mei, J. Han, Highly stretchable and self-healing strain sensors based on nanocellulose-supported graphene dispersed in electro-conductive hydrogels, Nanomaterials, 9 (2019) 937.

[12] K. Ren, Y. Cheng, C. Huang, R. Chen, Z. Wang, J. Wei, Self-healing conductive hydrogels based on alginate, gelatin and polypyrrole serve as a repairable circuit and a mechanical sensor, Journal of Materials Chemistry B, 7 (2019) 5704-5712.

[13] L.V. Kayser, D.J. Lipomi, Stretchable conductive polymers and composites based on PEDOT and PEDOT: PSS, Advanced Materials, 31 (2019) 1806133.

[14] Y. Zhou, C. Wan, Y. Yang, H. Yang, S. Wang, Z. Dai, K. Ji, H. Jiang, X. Chen, Y. Long, Highly stretchable, elastic, and ionic conductive hydrogel for artificial soft electronics, Advanced Functional Materials, 29 (2019) 1806220.

[15] H. Wang, C.N. Zhu, H. Zeng, X. Ji, T. Xie, X. Yan, Z.L. Wu, F. Huang, Reversible Ion‐Conducting Switch in a Novel Single‐Ion Supramolecular Hydrogel Enabled by Photoresponsive Host–Guest Molecular Recognition, Advanced Materials, 31 (2019) 1807328.

[16] Y. Wang, L. Zhang, A. Lu, Transparent, antifreezing, ionic conductive cellulose hydrogel with stable sensitivity at subzero temperature, ACS applied materials & interfaces, 11 (2019) 41710-41716.

[17] Q. Zhang, X. Liu, L. Duan, G. Gao, Nucleotide-driven skin-attachable hydrogels toward visual human–machine interfaces, Journal of Materials Chemistry A, 8 (2020) 4515-4523.

[18] X. Zhang, N. Sheng, L. Wang, Y. Tan, C. Liu, Y. Xia, Z. Nie, K. Sui, Supramolecular nanofibrillar hydrogels as highly stretchable, elastic and sensitive ionic sensors, Materials Horizons, 6 (2019) 326-333.

[19] Y. Ye, Y. Zhang, Y. Chen, X. Han, F. Jiang, Cellulose Nanofibrils Enhanced, Strong, Stretchable, Freezing‐Tolerant Ionic Conductive Organohydrogel for Multi‐Functional Sensors, Advanced Functional Materials, 30 (2020) 2003430.

[20] L. Shao, Y. Li, Z. Ma, Y. Bai, J. Wang, P. Zeng, P. Gong, F. Shi, Z. Ji, Y. Qiao, A Highly Sensitive Strain Sensor Based on Stretchable and Conductive Poly (vinyl alcohol)/Phytic Acid/NH2-POSS Hydrogel with a 3D Microporous Structure, ACS Applied Materials & Interfaces, (2020).

[21] Y.-J. Liu, W.-T. Cao, M.-G. Ma, P. Wan, Ultrasensitive wearable soft strain sensors of conductive, self-healing, and elastic hydrogels with synergistic "soft and hard" hybrid networks, ACS applied materials & interfaces, 9 (2017) 25559-25570.

[22] S. Pan, M. Xia, H. Li, X. Jiang, P. He, Z. Sun, Y. Zhang, Transparent, high-strength, stretchable, sensitive and anti-freezing poly (vinyl alcohol) ionic hydrogel strain sensors for human motion monitoring, Journal of Materials Chemistry C, 8 (2020) 2827-2837.

[23] S. Li, H. Pan, Y. Wang, J. Sun, Polyelectrolyte complex-based self-healing, fatigue-resistant and anti-freezing hydrogels as highly sensitive ionic skins, Journal of Materials Chemistry A, 8 (2020) 3667-3675.

[24] G. Chen, J. Huang, J. Gu, S. Peng, X. Xiang, K. Chen, X. Yang, L. Guan, X. Jiang, L. Hou, Highly tough supramolecular double network hydrogel electrolytes for an artificial flexible and low-temperature tolerant sensor, Journal of Materials Chemistry A, 8 (2020) 6776-6784.

[25] Z.-K. Cui, S. Kim, J.J. Baljon, B.M. Wu, T. Aghaloo, M. Lee, Microporous methacrylated glycol chitosan-montmorillonite nanocomposite hydrogel for bone tissue engineering, Nature communications, 10 (2019) 1-10.

[26] B. Kong, Y. Chen, R. Liu, X. Liu, C. Liu, Z. Shao, L. Xiong, X. Liu, W. Sun, S. Mi, Fiber reinforced GelMA hydrogel to induce the regeneration of corneal stroma, Nature communications, 11 (2020) 1-12.

[27] Y. Liu, X. Huang, K. Han, Y. Dai, X. Zhang, Y. Zhao, High-performance lignin-based water-soluble macromolecular photoinitiator for the fabrication of hybrid hydrogel, ACS Sustainable Chemistry & Engineering, 7 (2019) 4004-4011.

[28] A.K. Means, M.A. Grunlan, Modern strategies to achieve tissue-mimetic, mechanically robust hydrogels, ACS Publications, 2019.

[29] S. Liu, K. Li, I. Hussain, O. Oderinde, F. Yao, J. Zhang, G. Fu, A Conductive Self‐Healing Double Network Hydrogel with Toughness and Force Sensitivity, Chemistry‐A European Journal, 24 (2018) 6632-6638.

[30] H. Zhang, X. Wu, Z. Qin, X. Sun, H. Zhang, Q. Yu, M. Yao, S. He, X. Dong, F. Yao, Dual physically cross-linked carboxymethyl cellulose-based hydrogel with high stretchability and toughness as sensitive strain sensors, Cellulose, (2020) 1-15.

[31] P. Heidarian, A.Z. Kouzani, A. Kaynak, M. Paulino, B. Nasri-Nasrabadi, R. Varley, Double dynamic cellulose nanocomposite hydrogels with environmentally adaptive self-healing and pH-tuning properties, Cellulose, 27 (2020) 1407-1422.

[32] L. Zhu, J. Qiu, E. Sakai, K. Ito, Rapid recovery double cross-linking hydrogel with stable mechanical properties and high resilience triggered by visible light, ACS applied materials & interfaces, 9 (2017) 13593-13601.

[33] Z. Sang, J. Qian, J. Han, X. Deng, J. Shen, G. Li, Y. Xie, Comparison of three water-soluble polyphosphate tripolyphosphate, phytic acid, and sodium hexametaphosphate as crosslinking agents in chitosan nanoparticle formulation, Carbohydrate Polymers, 230 (2020) 115577.

[34] X. Wang, K. Wen, X. Yang, L. Li, X. Yu, Biocompatibility and anti-calcification of a biological artery immobilized with naturally-occurring phytic acid as the crosslinking agent, Journal of Materials Chemistry B, 5 (2017) 8115-8124.

[35] S. Zhang, Y. Zhang, B. Li, P. Zhang, L. Kan, G. Wang, H. Wei, X. Zhang, N. Ma, One-Step Preparation of a Highly Stretchable, Conductive, and Transparent Poly (vinyl alcohol)–Phytic Acid Hydrogel for Casual Writing Circuits, ACS applied materials & interfaces, 11 (2019) 32441-32448.

[36] Z.E.-S. Mohamed, A. Amr, D. Knittel, E. Schollmeyer, Synthesis and application of new sizing and finishing additives based on carboxymethyl cellulose, Carbohydrate polymers, 81 (2010) 769-774.

[37] Y. Liu, W. Wang, A. Wang, Adsorption of lead ions from aqueous solution by using carboxymethyl cellulose-g-poly (acrylic acid)/attapulgite hydrogel composites, Desalination, 259 (2010) 258-264.

[38] T. Anirudhan, A. Tharun, S. Rejeena, Investigation on poly (methacrylic acid)-grafted cellulose/bentonite superabsorbent composite: synthesis, characterization, and adsorption characteristics of bovine serum albumin, Industrial & engineering chemistry research, 50 (2011) 1866-1874.

[39] M.X. Wang, Y.M. Chen, Y. Gao, C. Hu, J. Hu, L. Tan, Z. Yang, Rapid self-recoverable hydrogels with high toughness and excellent conductivity, ACS applied materials & interfaces, 10 (2018) 26610-26617.

[40] L. Bian, C. Hou, E. Tous, R. Rai, R.L. Mauck, J.A. Burdick, The influence of hyaluronic acid hydrogel crosslinking density and macromolecular diffusivity on human MSC chondrogenesis and hypertrophy, Biomaterials, 34 (2013) 413-421.

[41] L. Zhang, H. Lu, J. Yu, Y. Fan, J. Ma, Z. Wang, Contribution of lignin to the microstructure and physical performance of three-dimensional lignocellulose hydrogels, Cellulose, 26 (2019) 2375-2388.

[42] D. Jeong, C. Kim, Y. Kim, S. Jung, Dual crosslinked carboxymethyl cellulose/polyacrylamide interpenetrating hydrogels with highly enhanced mechanical strength and superabsorbent properties, European Polymer Journal, (2020) 109586.

[43] X. Zhu, C. Yang, P. Wu, Z. Ma, Y. Shang, G. Bai, X. Liu, G. Chang, N. Li, J. Dai, Precise control of versatile microstructure and properties of graphene aerogel via freezing manipulation, Nanoscale, 12 (2020) 4882-4894.

[44] G. Ge, Y. Zhang, J. Shao, W. Wang, W. Si, W. Huang, X. Dong, Stretchable, Transparent, and Self‐Patterned Hydrogel‐Based Pressure Sensor for Human Motions Detection, Advanced Functional Materials, 28 (2018) 1802576.

[45] P. Lin, S. Ma, X. Wang, F. Zhou, Molecularly engineered dual‐crosslinked hydrogel with ultrahigh mechanical strength, toughness, and good self‐recovery, Advanced Materials, 27 (2015) 2054-2059.

[46] Z. Wang, L. Yuan, F. Jiang, Y. Zhang, Z. Wang, C. Tang, Bioinspired high resilient elastomers to mimic resilin, ACS Macro Letters, 5 (2016) 220-223.

[47] A.S. Tatham, P.R. Shewry, Comparative structures and properties of elastic proteins, Philosophical Transactions of the Royal Society of London. Series B: Biological Sciences, 357 (2002) 229-234.

[48] H. Zhang, W. Niu, S. Zhang, Extremely stretchable, sticky and conductive double-network ionic hydrogel for ultra-stretchable and compressible supercapacitors, Chemical Engineering Journal, 387 (2020) 124105.

[49] W. Wang, Y. Liu, S. Wang, X. Fu, T. Zhao, X. Chen, Z. Shao, Physically Cross-Linked Silk Fibroin-Based Tough Hydrogel Electrolyte with Exceptional Water Retention and Freezing Tolerance, ACS Applied Materials & Interfaces, 12 (2020) 25353-25362.

[50] H. Zhou, Z. Wang, W. Zhao, X. Tong, X. Jin, X. Zhang, Y. Yu, H. Liu, Y. Ma, S. Li, Robust and Sensitive Pressure/Strain Sensors from Solution Processable Composite Hydrogels Enhanced by Hollow-Structured Conducting Polymers, Chemical Engineering Journal, (2020) 126307.

[51] H. Chen, X. Ren, G. Gao, Skin-Inspired Gels with Toughness, Antifreezing, Conductivity, and Remoldability, ACS applied materials & interfaces, 11 (2019) 28336-28344.

[52] Z. Wang, H. Zhou, J. Lai, B. Yan, H. Liu, X. Jin, A. Ma, G. Zhang, W. Zhao, W. Chen, Extremely stretchable and electrically conductive hydrogels with dually synergistic networks for wearable strain sensors, Journal of Materials Chemistry C, 6 (2018) 9200-9207.

[53] J. Song, S. Chen, L. Sun, Y. Guo, L. Zhang, S. Wang, H. Xuan, Q. Guan, Z. You, Mechanically and Electronically Robust Transparent Organohydrogel Fibers, Advanced Materials, 32 (2020) 1906994.

[54] X. Wang, Y. Gu, Z. Xiong, Z. Cui, T. Zhang, Silk‑molded flexible, ultrasensitive, and highly stable electronic skin for monitoring human physiological signals, Advanced materials, 26 (2014) 1336-1342.

Chapter 4 Low-temperature adaptive conductive hydrogel based on ice structuring proteins/CaCl₂ anti-freeze system as wearable strain and temperature sensor

4.1 Introduction

Conductive hydrogels have recently become a research hopot due to their wide applications in sensing and flexible devices [1-4]. However, when an ionic conductive hydrogel is used below sub-zero temperatures, it will lose its original performances [5-8]. It is well known that the most abundant component in an ionic conductive hydrogel is water. When temperature drops below 0 °C, the hydrogel will be frozen without external intervention, inevitably causing it to lose flexibility, conductivity, resilience and so on [9, 10]. Therefore, to extend the application of ionic conductive hydrogels below sub-zero temperatures, it's necessary to prevent the freezing behavior of the water in the hydrogel below 0 °C.

To depress the freeze point of the water in a hydrogel is an effective way to prepare antifreeze hydrogels or organohydrogels [10-13]. There are two main ways to depress the freeze point. One is to introduce binary water/organic solvent systems into hydrogels by immersing a hydrogel in an organic solvent or by directly polymerizing in a binary solvent system [14, 15]. For example, the participation of H_2O/ ethylene glycol as a binary solvent made PVA organohydrogels exhibited stable flexibility and strain sensitivity even at -55.0°C [16]. However, the introduction of organic solvents will hinder the migration of ions, thus resulting poor conductivity of ionic conductive hydrogel [17]. In addition, some organic solvents may case safety risks that will narrow

the applications of ionic conductive hydrogels [18]. The other way to depress the freeze point of an ionic conductive hydrogel is to add inorganic salts in the hydrogel [9, 11, 19]. Yang et al. reported that melting temperatures of the hydrogels decreased with the increasing of salt concentration [9]. When the salt concentration was high enough, melting peak was not even found in the calorimetric map of the hydrogel in the temperature range of -80-50°C. Nevertheless, high concentration of inorganic salts may lead to salting-out effects, which in turn destroys the stability of ionic conductive hydrogel network [20].

Certain organisms can survive below the freezing point of water because they have ice structuring proteins (ISPs) in their body fluids [21-23]. Researches have found that ISPs can bind to the surface of small ice crystals to inhibit the growth and recrystallization of ice [24-26]. Inspired by this mechanism, antifreeze protein has been used to construct anti-icing hydrogel sensors with low temperature adhesion and toughness [20]. It is expected that antifreeze proteins can also play a role in the hydrogel network.

Despite the recent rapid developments of antifreeze hydrogels, most of them have focused on a single aspect of antifreeze. It is well known that water freezing includes two processes, ice nucleation and growth. The development of an anti-freeze system that can inhibit both ice nucleation and growth is expected to effectively improve the anti-freeze properties of hydrogels. Motivated by water freezing processes and existing researches, in this work, a novel antifreeze system was designed to inhibit both ice nucleation and growth in ionic conductive hydrogel. The hydrogels are prepared by one-pot in situ polymerization of acrylic acid (AA) in the presence of $CaCl_2$ and ISPs. Ca^{2+}, as an indispensable ion for all physiological activities of the organism, is used to lower the freezing point of water, thus preventing ice nuclei from forming. The Ca^{2+} also plays an important role in the mechanical properties of the hydrogel via ionic bonds [27]. ISPs, refer to a class of polypeptides produced by certain organisms, are introduced to inhibit ice growth and recrystallization. With the dual effect of inhibiting both ice nuclei formation and ice growth, the stretchability and conductivity can be maintained at sub-zero temperatures. The hydrogels achieve good conductivity of 0.50

71

S/m even at −20 °C. The ioic conductive hydrogel can also be stretched to a strain of 890% at -20°C. When used in wearable sensors, the hydrogels can be used as strain and temperature sensor, demonstrating good stability and durability at both room temperature and -20°C.

4.2 Experimental Section

4.2.1 Materials

Acrylic acid (AA, EP), ammonium peroxydisulfate (APS, GR), calcium chloride (CaCl$_2$, EP). Ice structuring proteins (ISPs) were supplied by Shanghai Ruifeng Industrial Co., Ltd, China, and were extracted from plants. All reagents were used as received without further purification. All aqueous solutions were prepared with deionized water.

4.2.2 Preparation of Hydrogels

Table 2.1 The raw materials amount of hydrogels.

Hydrogel	ISPs (0.8% aq)/g	AA/g	H$_2$O/g	CaCl$_2$ (40% aq)/g	APS/g
PAA/ISP$_1$-Ca$_1$	6	6	6	2	0.1
PAA/ISP$_1$-Ca$_2$	6	6	4	4	0.1
PAA/ISP$_1$-Ca$_3$	6	6	2	6	0.1
PAA/ISP$_1$-Ca$_4$	6	6	0	8	0.1
PAA/ISP$_1$	6	6	8	0	0.1
PAA	0	6	14	0	0.1
PAA-Ca$_3$	0	6	8	6	0.1
PAA/ISP$_2$-Ca$_3$	8	6	0	6	0.1

The hydrogels were prepared by one-step method. 6 g AA, a certain amount of CaCl$_2$ (40% aqueous solution) and deionized water were mixed under stirring. After that a

certain quantity of ISPs (0.8% aqueous solution) was slowly added to above solution under strong stirring, followed by adding 0.1g APS. The weight ratio of AA was fixed at 30% of the total solution weight. The precursor solution was dissolved under stirring for 2 h, followed by a 10 min ultrasonic treatment to remove air bubbles. The hydrogel precursors were then transferred to a custom mold and placed in an oven at 60°C for 6 h to produce a hydrogel. The hydrogels were abbreviated as PAA/ISP$_m$-Ca$_n$, the corresponding recipes were shown in Table 2.1. For comparison, PAA hydrogel and PAA-Ca$_3$ hydrogel were also fabricated under the same condition without ISPs.

4.2.3　Characterizations

(1)　DSC analysis

The melting behaviors of hydrogels were analyzed by the differential scanning calorimetry (DSC, SII X-DSC 7000, Hitachi). The samples were first cooled from 20°C to -65°C with a cooling rate of 5°C/min. After holding for 5 minutes, the samples were heated from -65°C to 10°C at a rate of 5°C/min. The frozen water amount (W_f) was calculated from the melting peaks. $W_f = \triangle H / \triangle H_0 \times 100\%$, where $\triangle H$ was the enthalpy of hydrogel melting peak obtained by integration and $\triangle H_0$ was the enthalpy of pure water (334 J/g).

(2)　Microstructure Characterizations

Scanning electron microscope (SEM, Hitachi, Ltd S-4300, Japan) was used to observe the microstructure of the hydrogels. Samples were rapidly frozen in liquid nitrogen and then freeze-dried for 24 hours for testing.

(3)　Mechanical Tests

Mechanical performance at room temperature were tested by universal mechanical tester (Instron 3385, Instron Co., Ltd., Canton, USA), while mechanical performance at sub-zero temperatures were performed by universal mechanical tester with an Instron

Temperature Controlled Chamber (Instron 3382, Instron Co., Ltd., Canton, USA). The low temperature environment was achieved by liquid nitrogen cooling. Rectangular samples (20 mm × 4 mm × 2 mm) were used to determine the mechanical performance at a speed of 100 mm/min. The tensile strength was tested more than 3 times. To do the low temperature test, the samples were cooled at -20°C for 30 minutes, then clamped to the fixture and held at -20°C for another 5 minutes before testing. Dissipated energy (Ed) was obtained from the area between the loading−unloading curves. Resilience was defined as the area quotient under unloading stress-strain and the loading stress-strain.

(4) Electrical Test

The resistance was measured by a digital source meter (LCR-6100, GWInstek). The disc-shaped sample was sandwiched between two stainless steel discs for measurement. The ionic conductivity of the hydrogels was calculated according to $\sigma = L/RS$. L, R and S represented the thickness of hydrogel, the resistance and the contact area, respectively. The relative resistance change $\Delta R/R_0$ was calculated from $(R - R_0)/R_0 \times 100\%$, where ΔR, R_0 and R represented the amount of resistance change, the initial resistance and the real-time resistance.

4.3 Results and Discussion

4.3.1 Design and fabrication of Hydrogel

A one-step radical polymerization method was employed for the synthesis of PAA/ISP-Ca hydrogel. The production process was illustrated in Fig. 4.1a. Briefly, AA, $CaCl_2$ aqueous solution, ISPs aqueous solution and APS were mixed to form a pre-solution under stirring. The pre-solution was heated to initiate the polymerization of AA and form target PAA/ISP-Ca hydrogel. A novel ice structuring proteins/$CaCl_2$ (ISPs/$CaCl_2$) anti-freeze system was introduced into the hydrogel to improve the adaptability of hydrogels at sub-zero temperatures. The $CaCl_2$ were used to reinforce the hydrogel and

inhibit ice formation, while ISPs were added to inhibit growth and recrystallization of ice crystals. It is well known that when dissolve in water, $CaCl_2$ salts ionizes into Ca^{2+} and Cl^-. The ions have a strong influence on the colligative property of water in the hydrogel, leading to the inhibition of ice crystal formation at sub-zero temperature conditions [28]. On the other hand, ISPs, which ensures that organisms survive in subzero environments, are shown to prevent ice crystallization and crystal growth by binding to small ice crystals [24]. Thus, the $ISPs/CaCl_2$ anti-freeze system was expected to not only inhibit the formation of ice crystal but also prevent crystal growth. The anti-freeze mechanism and properties would be discussed in detail later.
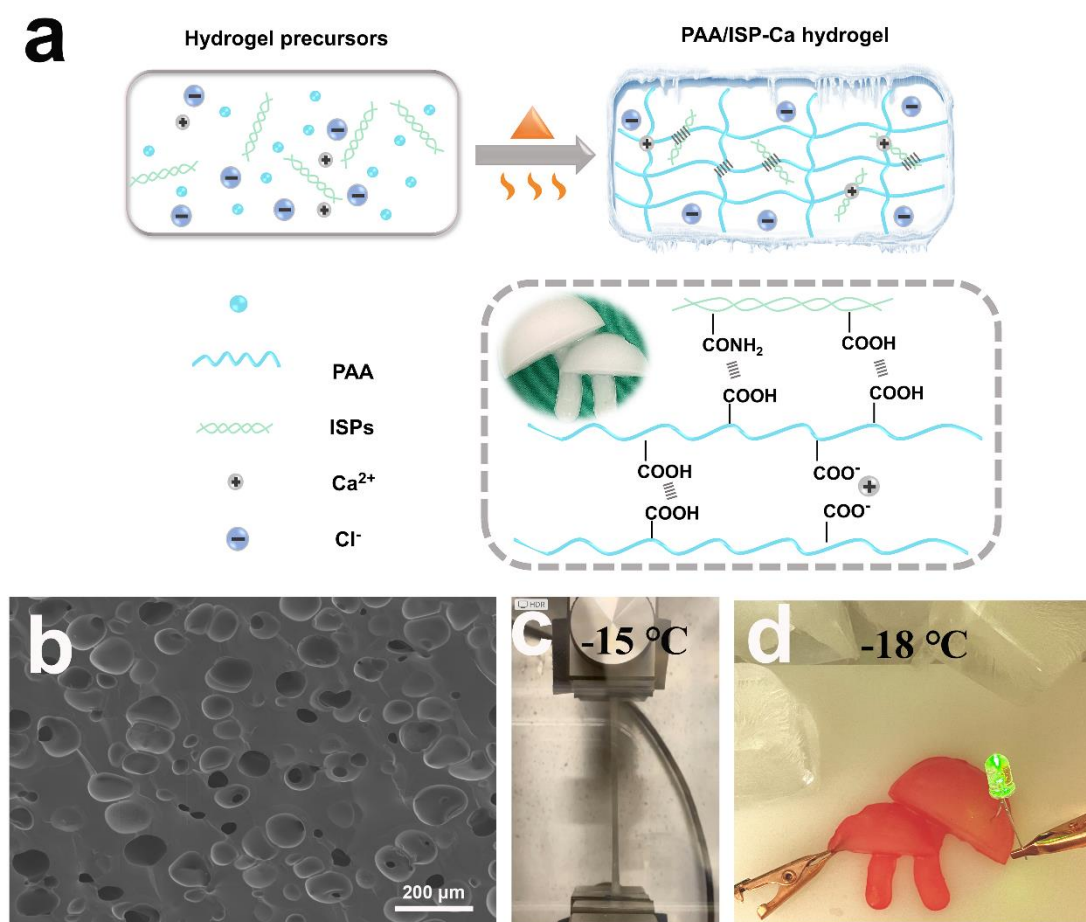
Fig. 4.1 a) Schematic diagram of the preparation process and mechanism of PAA/ISP-Ca hydrogel. b) Microstructure of PAA/ISP-Ca hydrogel. c) PAA/ISP-Ca hydrogel can be stretched at sub-zero temperature. d) PAA/ISP-Ca hydrogel can light an LED bulb at sub-zero temperature.

A circular porous structure was obtained by dynamic cross-linking networks (Fig. 4.1b). The dynamic cross-linking networks of PAA/ISP-Ca hydrogels were built by two kinds of physical networks. One was ionic crosslinking between Ca^{2+} and $-COO^-$, the other was hydrogen bond between $-COOH$ and $-NH_2$. The physical cross-linked networks were used to provide support for structure, flexibility and mechanical strength of the hydrogels. The anti-freeze system was used to ensure that these properties could be maintained at low temperatures. As a result, the hydrogel obtained good flexibility and conductivity even at low temperatures. (Fig. 4.1c, 4.1d; Fig. 4.2)
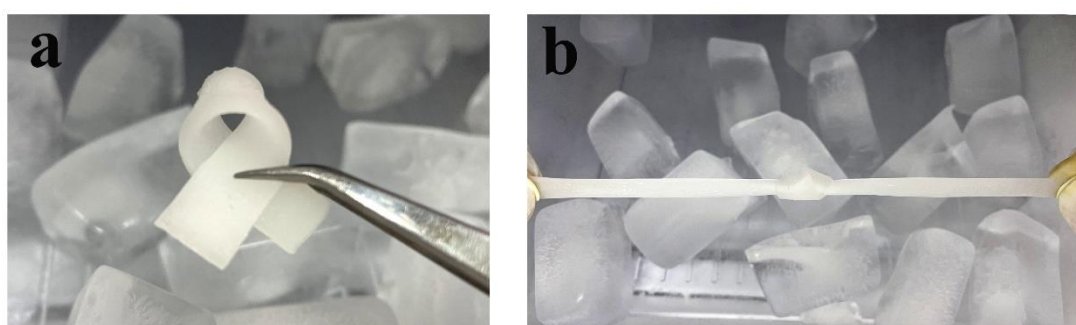
Fig. 4.2 a) PAA/ISP-Ca hydrogel can be bent at sub-zero temperature. b) PAA/ISP-Ca hydrogel can be stretched after knotting at sub-zero temperature.

4.3.2 Anti-freezing mechanism

Due to the large amount of water stored in the cross-linked network of hydrogels, they are generally prone to freezing in sub-zero temperatures. The frozen hydrogels are stiff and friable, resulting in poor flexibility and conductivity. Therefore, to improve the low-temperature resistance of hydrogels is to prevent formation of ice nuclei and the growth of ice crystal. It is generally believed that there are three different states of water in the hydrogel: non-bound water, frozen bound water and non-frozen bound water [29, 30]. Non-bound water participates in neither hydrogen bonding nor hydration, and exhibits a similar icing temperature to that of bulk water. Frozen bound water is the water that interacts weakly with the ions or hydrogel network, while non-frozen bound water strongly bounds to the hydrogel network. The state of water in hydrogels was studied by DSC to show the effect of ISP/$CaCl_2$ antifreeze system on the low-temperature
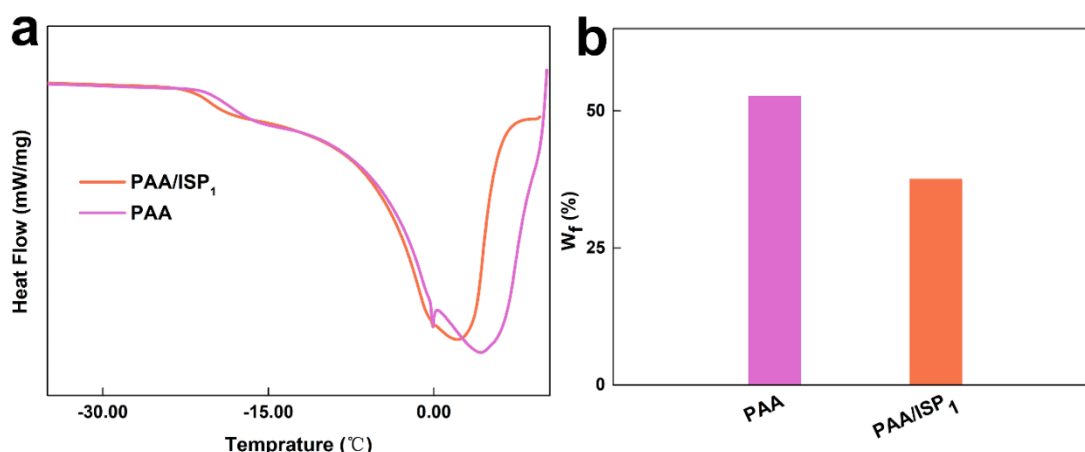
adaptation of the hydrogel.

Fig. 4.3 a) DSC curves for heating PAA and PAA/ISP$_1$ hydrogel from -65°C to 10°C. b) W$_f$ of the PAA and PAA/ISP$_1$ hydrogels.

Certain species can produce ISPs to allow them to survive in sub-zero temperatures. When freezing of the body fluids of these species occurs, ISPs can bind to small ice crystals, thereby inhibiting the ice crystals from further binding to each other into large ice crystals [31]. The effects of ISPs on the water behavior of the hydrogels at low temperatures were investigated by DSC. As could be seen from Fig. 4.3a, due to the addition of ISPs, the melting point of ice in the PAA/ISP$_1$ hydrogel was reduced by 2°C compared to PAA hydrogel. Furthermore, the amounts of frozen water (non-bound water and frozen bound water) can be calculated from the DSC melting peaks [32, 33]. The addition of ISPs also lowered the frozen water amount (W$_f$) from 52.6% (PAA/ISP$_1$ hydrogel) to 37.5% (PAA hydrogel) (Fig. 4.3b), which meant ISPs caused less frozen water in the hydrogel system. Moreover, a decrease in melting point and W$_f$ could also be found in PAA/ISP-Ca hydrogel. As shown in Fig. 4.4a, 4.4b, both the melting point and W$_f$ of the hydrogel containing ISPs (PAA/ISP$_1$-Ca$_3$ hydrogel) were decreased compared to the corresponding hydrogel without ISPs (PAA-Ca$_3$ hydrogel). In general, the addition of ISPs to the hydrogel system could not only effectively reduce the W$_f$, but also lower the melting point, suggesting that ISPs played a role in the anti-freeze system. The possible reason for the effects was that ISPs could bind to ice surfaces as

long as ice crystals were formed in the hydrogel, thereby inhibiting the ice crystal growth and recrystallization of the hydrogel. However, a further increase in ISPs (PAA/ISP$_2$-Ca$_3$) did not reveal a significant change in melting point, but a further decrease in W$_f$. This result was consistent with previous researches that ISPs had non-colligative properties [24, 34].
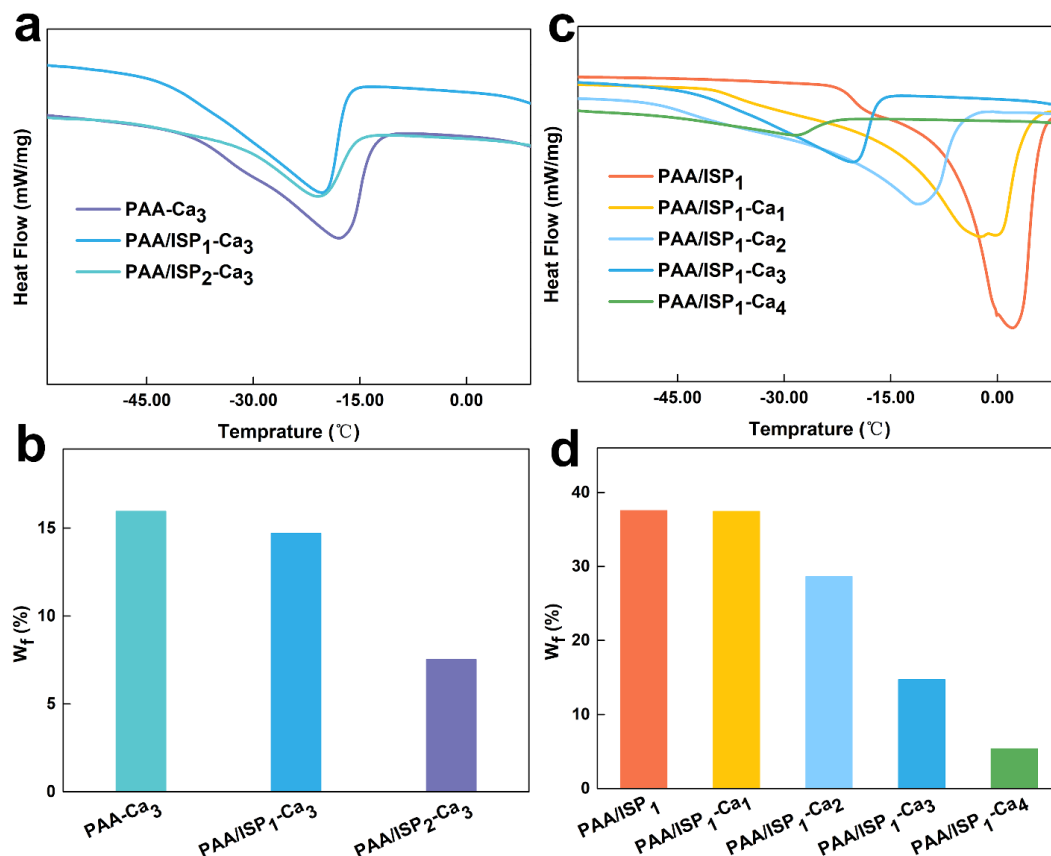

Fig. 4.4 a) DSC curves for heating the PAA/ISP$_1$, PAA/ISP$_1$-Ca$_1$, PAA/ISP$_1$-Ca$_2$, PAA/ISP$_1$-Ca$_3$ and PAA/ISP$_1$-Ca$_4$ hydrogel from -65°C to 10°C. b) DSC curves for heating PAA-Ca$_3$, PAA/ISP$_1$-Ca$_3$ and PAA/ISP$_2$-Ca$_3$ hydrogel from -65°C to 10°C. c) Frozen water amount (W$_f$) of the PAA/ISP$_1$, PAA/ISP$_1$-Ca$_1$, PAA/ISP$_1$-Ca$_2$, PAA/ISP$_1$-Ca$_3$ and PAA/ISP$_1$-Ca$_4$ hydrogels. d) W$_f$ of the PAA-Ca$_3$, PAA/ISP$_1$-Ca$_3$ and PAA/ISP$_2$-Ca$_3$ hydrogels.

The role of CaCl$_2$ in the anti-freeze system has also been studied (Fig. 4.4c, 4.4d). With the introduction of CaCl$_2$, the melting peaks of the PAA/ISP-Ca hydrogels started to shift toward sub-zero temperatures (Fig. 4.4c). The decrease in the melting point of

PAA/ISP-Ca hydrogels suggested that the added $CaCl_2$ not only interacted with the hydrogel network but also affected the structure of the water in the hydrogel. In addition to melting point, W_f of PAA/ISP hydrogel also gradually decreased from 37.5% to 5.4% with the introduction of $CaCl_2$ (Fig. 4.4d). The results showed that the change of melting point was related to the amount of $CaCl_2$ added to the hydrogel, which implied that the effect of $CaCl_2$ on the melting point in the hydrogel had a collegiality.

Based on the above-mentioned results, we propose that the synergistic effect of ISPs/$CaCl_2$ anti-freeze system play a significant role in simultaneously inhibiting the formation of ice nuclei and ice crystal growth and recrystallization. PAA/ISP-Ca hydrogels were expected to have good sub-zero temperature tolerance.

4.3.3 Structure and mechanical properties

Mechanical properties are essential for conductive hydrogels to withstand mechanical deformation and to convert the deformation into electrical signals. In this work, dynamic physical crosslinking was used to ensure the mechanical properties of the hydrogel.

Internal structures of the hydrogels were observed by SEM. The PAA hydrogels possessed a three-dimensional (3D) porous structure (Fig. 4.5a). After adding $CaCl_2$, the porous structure became denser and turned into a circular porous structure (PAA/ISP$_1$-Ca$_3$, Fig. 4.5b).

The denser structure further influenced mechanical properties of PAA/ISP-Ca hydrogels. As shown in Fig. 4.5c, tensile strength of the hydrogels was significantly increased with the introducing of $CaCl_2$, proving that the crosslinking effect of $CaCl_2$. Meanwhile, the elongation at break showed a gradual downward trend as the introducing of $CaCl_2$. However, the elongation at break of PAA/ISP$_1$-Ca$_3$ still exhibited a value of 920%, indicating good flexibility of the hydrogel. For comprehensive consideration, PAA/ISP$_1$-Ca$_3$ was selected for the follow-up study.
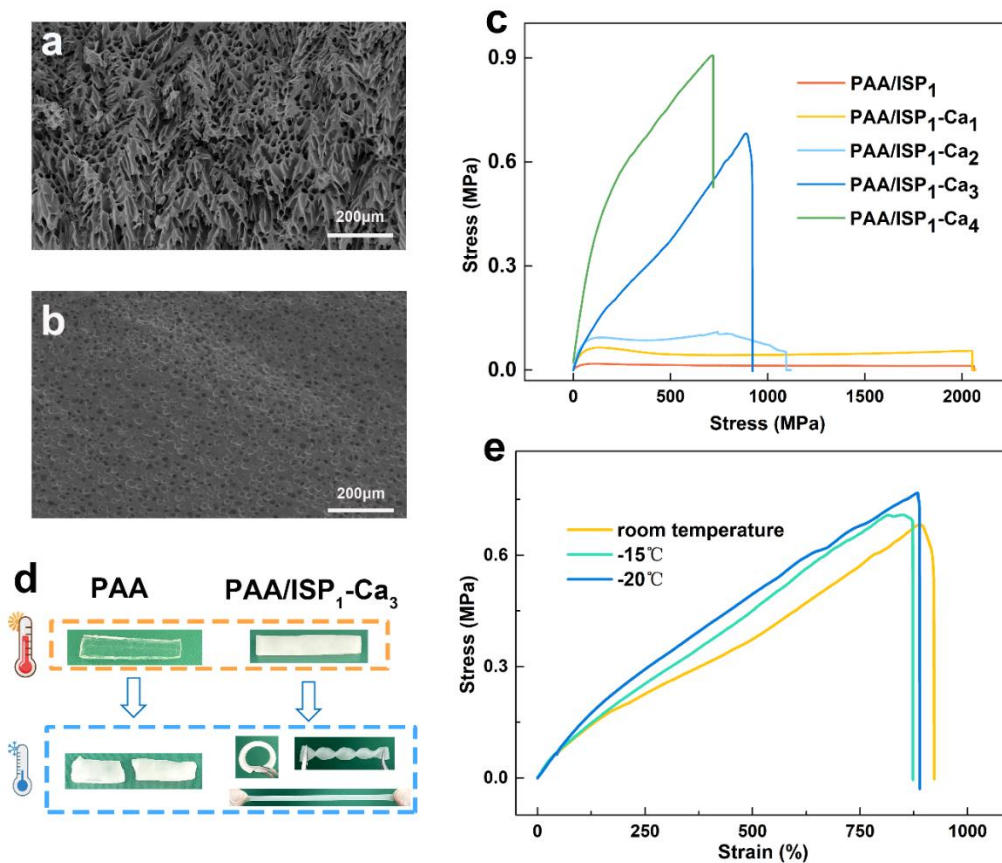
Fig. 4.5 a-b) Microstructure of the PAA (a) and PAA/ISP$_1$-Ca$_3$ (b) hydrogels as characterized by SEM. c) Tensile stress-strain curves of the hydrogels. d) the PAA and PAA/ISP$_1$-Ca$_3$ hydrogels reveal different low-temperature adaptability. e) Tensile stress-strain curves of the PAA/ISP$_1$-Ca$_3$ hydrogel at room temperature, -15°C and -20°C.
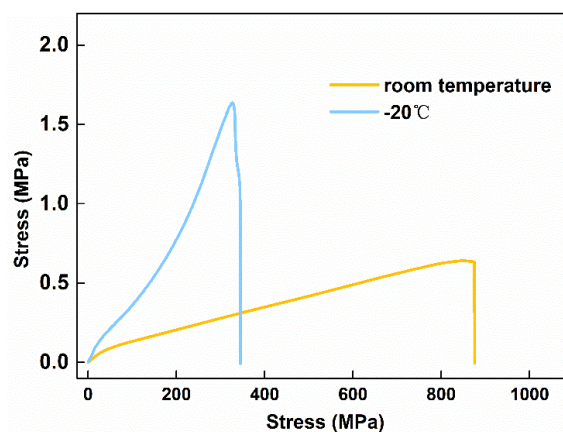

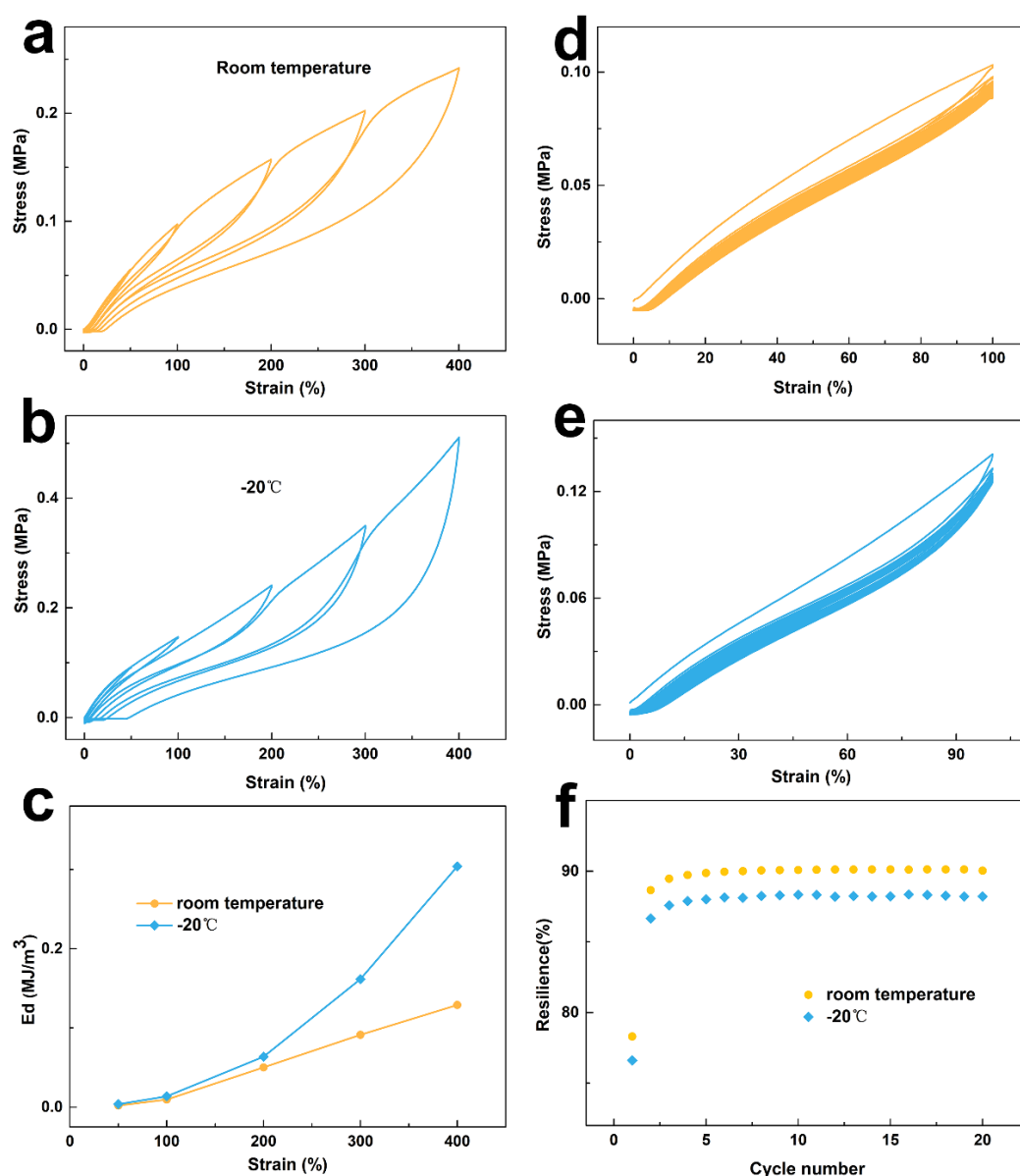Fig. 4.6 Tensile stress-strain curves of the PAA -Ca$_3$ hydrogel at room temperature and -20°C.

Fig. 4.7 a-b) Continuous loading-unloading tests at different maximum strains of PAA/ISP$_1$-Ca$_3$ hydrogel at room temperature and -20°C. c) The comparation of calculated energy dissipation (Ed) of PAA/ISP$_1$-Ca$_3$ hydrogel at room temperature and -20°C. d-e) Continuous loading-unloading tests of the PAA/ISP$_1$-Ca$_3$ hydrogel for 20 cycles at a strain of 100% at room temperature and -20°C. f) The comparation of resilience of PAA/ISP$_1$-Ca$_3$ hydrogel at room temperature and -20°C.

Conventional hydrogels containing large amounts of water are highly susceptible to freezing at low temperatures, resulting in loss of stretchability. Here, because of the introduction of novel ISPs/CaCl$_2$ anti-freeze system, the hydrogel exhibited a good

flexibility and could withstand deformation in curling, twisting and stretching (Fig. 4.5d) after holding at -18°C for 24 h. In contrast, PAA hydrogel became a hard, ice-like solid and was brittle under bending (Fig. 4.5d). The tensile stress-strain curves of the PAA/ISP$_1$-Ca$_3$ hydrogels showed slight variations at room temperature, -15°C and -20°C (Fig. 4.5e), which implied good performance even at extreme low temperatures. Notably, the elongation of PAA-Ca$_3$ hydrogel was significantly reduced at -20°C (Fig. 4.6), indicating that ISPs in the anti-freeze system is necessary to maintain the low temperature flexibility of the hydrogel. In general, the ISPs/CaCl$_2$ anti-freeze system enabled the PAA/ISP-Ca hydrogel with good flexibility even at -20°C.

In order to further investigate the mechanical properties of the hydrogel, loading-unloading tests at different maximum strains were performed. PAA/ISP$_1$-Ca$_3$ hydrogels were constructed by reversible non-covalent interactions, which could be dissociated to dissipate energy during stretching. Fig. 4.7a-b showed the loading−unloading curves of PAA/ISP$_1$-Ca$_3$ hydrogel at room temperature and -20°C. Similarly, the hydrogels exhibited significant hysteresis loops at both room temperature and -20°C, which became larger with increasing maximum strain. The calculated energy dissipation also showed that the energy dissipation increased with increasing strain at room temperature and -20°C (Fig. 4.7c). These results indicated that the physical interactions (ionic coordination and hydrogen bonds) in the hydrogel network were readily dissociated during the deformation process to dissipate force for toughening the hydrogels. As the strain increased, more physically cross-linked interactions were dissociated to dissipate energy. The physical interactions could also dissociate at -20°C, indicating that the mechanical properties of the hydrogel could adapt to low-temperature environments.

The hydrogel also had good recovery ability, since the broken non-covalent interactions can be recovered automatically. Herein, 20 successive cyclic loading-unloading tensile tests were performed at a maximum strain of 100% to investigate the recovery ability of the hydrogel at room temperature and -20°C (Fig. 4.7d-e). To better investigate the ability of the hydrogel to deform reversibly without loss of energy, resilience was calculated as shown in Fig. 4.7f. The hydrogel had good resilience, which was stable at

90% and 88% with increasing number of cycles at room temperature and -20°C, respectively. These results indicated that the hydrogel had good recovery ability and that its recovery ability can be maintained at sub-zero temperature, which further confirmed its outstanding mechanical property stability and freezing tolerance at subzero temperature.

4.3.4 Conductivity

After connecting the hydrogel to circuit, bulb in this circuit could be lit (Fig. 4.8a), which indicated that the hydrogel had good ionic conductivity. There was not much difference in the brightness at room temperature and sub-zero temperature, which meant that the hydrogel maintained good conductivity even at sub-zero temperature. Fig. 4.8b showed the conductivity of PAA/ISP$_1$-Ca$_3$ hydrogel at different temperatures. The conductivity at 20°C was 1.86 s/m. As temperature decreased the conductivity tended to decrease, which was likely due to the slower ion migration rate at low temperatures. Although the conductivity decreased with temperature, it still had a conductivity of 0.50 s/m at -20°C. Interestingly, linear relationship between ionic conductivity and temperature (range of 20°C to -20°C) was revealed.
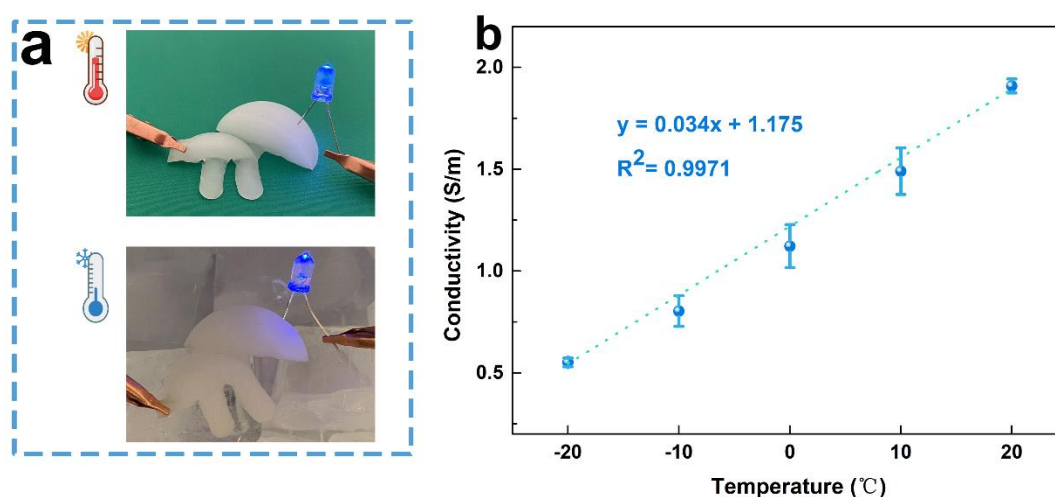

Fig. 4.8 a) The bulb in circuit with the PAA/ISP$_1$-Ca$_3$ hydrogel can be lit at room temperature and -18°C. b) The conductivity of PAA/ISP$_1$-Ca$_3$ hydrogel at different temperatures.

Furthermore, both resistance (R) of the PAA/ISP$_1$-Ca$_3$ hydrogel and the PAA-Ca$_3$ hydrogel increased at -20°C and -30°C (Fig. 4.9). The resistance of PAA-Ca$_3$ hydrogel increased more drastically, which implied a more decrease in conductivity. It was well known that ion migration rate, which directly affected the resistance and conductivity, was influenced by temperature and ion migration channels. When temperature decreased, in addition to the effect of low temperature, the reduction of ion migration channels due to icing also would increase resistance. Therefore, the sharp increase in resistance at -30°C of both the PAA/ISP$_1$-Ca$_3$ hydrogel and PAA-Ca$_3$ hydrogel may mainly be caused by icing below the freezing point. The more growth in resistance of PAA-Ca$_3$ hydrogel compared to the PAA/ISP$_1$-Ca$_3$ hydrogel was probably due to more ice crystal growth and recrystallization. The resistance of the PAA-Ca$_3$ hydrogel also revealed a much more increase than the PAA/ISP$_1$-Ca$_3$ hydrogel at -20°C. Since -20°C was a temperature below the freezing point of the PAA-Ca$_3$ hydrogel and above the freezing point of the PAA/ISP$_1$-Ca$_3$ hydrogel, the increased resistance of the PAA/ISP$_1$-Ca$_3$ hydrogel was more like caused by the decrease of temperature, and differently, both the decrease of temperature and icing may be the reasons of the increase in resistance of the PAA -Ca$_3$ hydrogel. Thus, ISPs also played a role in the anti-freeze system for the improvement of the conductivity of hydrogel at low temperature.

In general, the novel anti-freeze system enabled the PAA/ISP-Ca hydrogel with good conductivity even at sub-zero temperature.
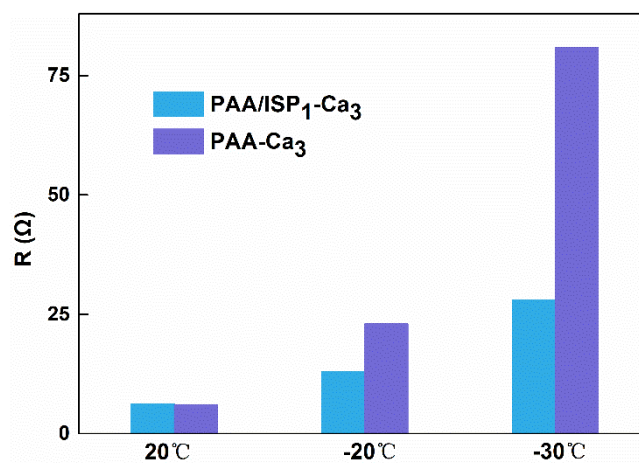

Fig. 4.9 The resistance of PAA -Ca$_3$ and PAA/ISP$_1$-Ca$_3$ hydrogel at 20°C, -20°C and -30°C.
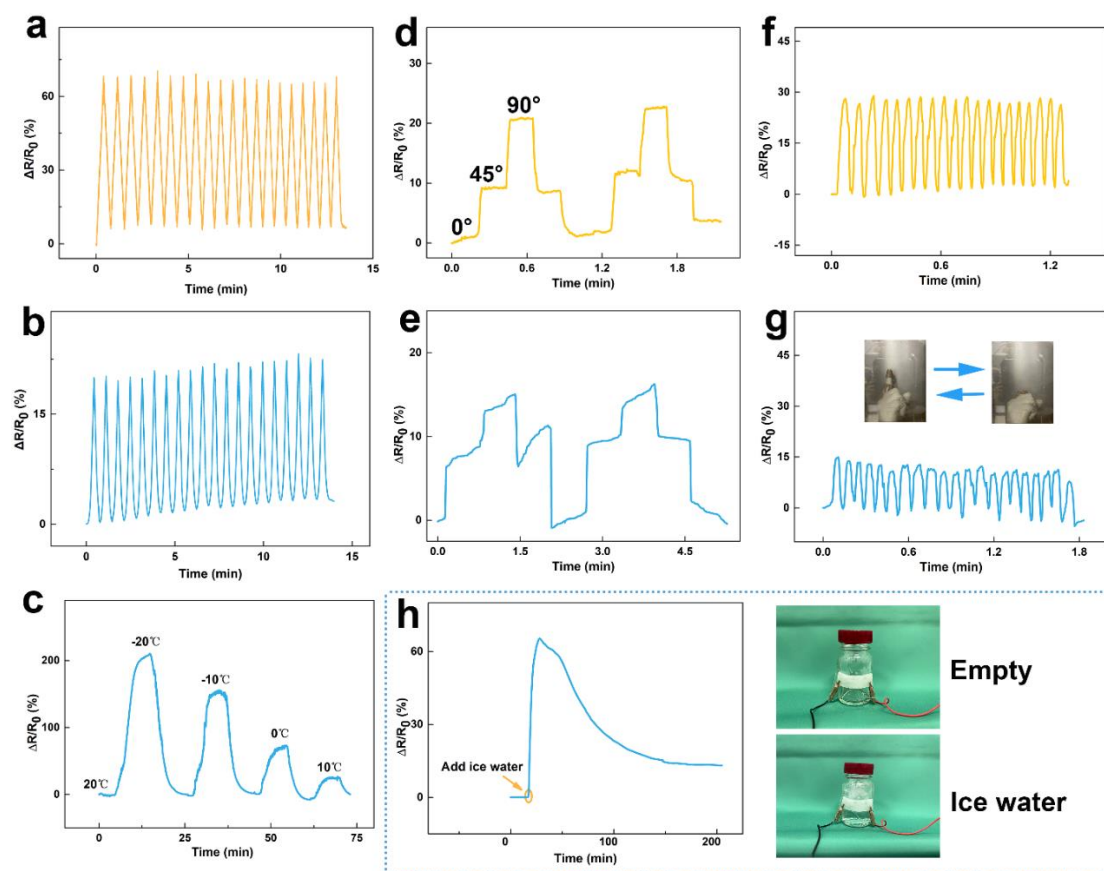
4.3.5 Application in sensors

Fig. 4.10 a-b) Relative resistance change ($\Delta R/R_0$) signals of strain sensor during continuous loading-unloading tensile tests at room temperature and -20°C. c) $\Delta R/R_0$ signals of temperature sensor during the temperature change. d-g) A wearable sensor to detect the finger activities at room temperature and -20°C. h) The temperature sensor to monitor the temperature change process of an empty bottle and after the addition of ice water.

The good ionic conductivity, as well as flexibility, mechanical strength and self-recovery ability of the hydrogel at sub-zero temperature indicated its potential for use in cold conditions. Here, we demonstrated ion sensors that took advantage of these properties.

(1) Strain sensor

First, strain sensor was assembled to record the strain sensing performance of the hydrogel. Relative resistance change ($\Delta R/R_0$) signals during successive loading-unloading tensile tests were shown in Fig. 4.10a. The $\Delta R/R_0$ of the sensor increased as the tensile strain increased, while as the strain gradually decreased to the original strain, the $\Delta R/R_0$ decreased accordingly, which was attributed to the strain sensing ability of the sensor. Further, there was no significant loss of electrical signal during 20 cycles at strain of 50%, indicating remarkable stability and repeatability of the strain sensor. Strain sensing tests were also performed at -20°C at the same strain of 50% (Fig. 4.10b). As expected, the strain sensor exhibited a similar pattern of signal changes during 20 cycles at strain of 50% at -20°C, which revealed its low-temperature adaptability. Signal stability together with low-temperature adaptability under strain enabled its application as a strain sensor at sub-zero temperatures.

(2) Temperature sensor

The hydrogel was also expected to be used as temperature response sensor due to the variation in conductivity at different temperatures. Hydrogel sensor was placed in a temperature controller to detect its temperature response. The temperature responsiveness of the hydrogel, as shown in Fig. 4.10c, was expressed by the curve of $\Delta R/R_0$ of the sensor with temperature. It could be found that when temperature changed from 20°C to -20°C, $\Delta R/R_0$ of the hydrogel changed from 0% to 200%, and the $\Delta R/R_0$ could restore to 0% when the temperature returned to 20°C. Similarly, $\Delta R/R_0$ varied with temperature when cycling from 20°C to -10, 0, and 10°C, respectively. Even after several successive temperature cycles, $\Delta R/R_0$ could still recover to 0%, which was important for the application of the hydrogel as a temperature sensor with low-temperature adaptation.

(3) Practical applications of sensors

The sensor was assembled into a wearable sensor to detect the finger activities at room temperature and -20°C (Fig. 4.10d, 4.10e). When monitoring finger flexion-extension, the response increased monotonically with increasing bending angle and the signal remained constant when the bending angle was maintained. The signal could also return to its initial value at a certain angle when the finger angle decreased. The signal was the same for both flexion-extension cycles of the finger at room temperature and -20°C, indicating good accuracy and stability of the sensor. The stability of the sensor was further investigated by cyclically bending the finger at room temperature and -20°C (Fig. 4.10f, 4.10g).

In a practical application of temperature monitoring, the hydrogel was assembled into a simple temperature sensor to monitor the temperature change of a bottle containing ice water (Fig. 4.10h). Set the $\Delta R/R_0$ of an empty glass bottle at room temperature to 0%. When ice water was added to the bottle, $\Delta R/R_0$ increased rapidly to 60%. The glass bottle was then left at room temperature and $\Delta R/R_0$ gradually decreased with time, which was caused by heat absorption of bottle and water at room temperature.

4.4 Conclusions

In summary, a novel $ISPs/CaCl_2$ anti-freeze system was introduced to conductive hydrogel to improve its adaptability to low temperatures. Because the system could inhibit ice nucleation and ice growth, the stretchability, recovery and conductivity of the hydrogel were maintained at sub-zero temperatures. The hydrogels achieve good conductivity of 0.50 S/m at −20°C. The ionic conductive hydrogel can also be stretched to a strain of 890% at -20°C. The hydrogel had good resilience (88%) even at -20°C. Good features made it available for sensors. When used as strain and temperature sensors, the hydrogel demonstrated good stability and durability at both room temperature and -20°C.

References

[1] V. Amoli, J.S. Kim, S.Y. Kim, J. Koo, Y.S. Chung, H. Choi, D.H. Kim, Ionic tactile sensors for emerging human‑interactive technologies: a review of recent progress, Advanced Functional Materials, 30 (2020) 1904532.

[2] C. Lu, J. Qiu, M. Sun, Q. Liu, E. Sakai, G. Zhang, Simple preparation of carboxymethyl cellulose-based ionic conductive hydrogels for highly sensitive, stable and durable sensors, Cellulose, 28 (2021) 4253-4265.

[3] F. Lu, Y. Wang, C. Wang, S. Kuga, Y. Huang, M. Wu, Two-dimensional nanocellulose-enhanced high-strength, self-adhesive, and strain-sensitive poly (acrylic acid) hydrogels fabricated by a radical-induced strategy for a skin sensor, ACS Sustainable Chemistry & Engineering, 8 (2020) 3427-3436.

[4] Q. Wang, J. Guo, X. Lu, X. Ma, S. Cao, X. Pan, Y. Ni, Wearable lignin-based hydrogel electronics: A mini-review, International Journal of Biological Macromolecules, (2021).

[5] M. Zhu, X. Wang, H. Tang, J. Wang, Q. Hao, L. Liu, Y. Li, K. Zhang, O.G. Schmidt, Antifreezing hydrogel with high zinc reversibility for flexible and durable aqueous batteries by cooperative hydrated cations, Advanced Functional Materials, 30 (2020) 1907218.

[6] D. Bao, Z. Wen, J. Shi, L. Xie, H. Jiang, J. Jiang, Y. Yang, W. Liao, X. Sun, An anti-freezing hydrogel based stretchable triboelectric nanogenerator for biomechanical energy harvesting at sub-zero temperature, Journal of Materials Chemistry A, 8 (2020) 13787-13794.

[7] C. Lu, X. Chen, All-temperature flexible supercapacitors enabled by antifreezing and thermally stable hydrogel electrolyte, Nano letters, 20 (2020) 1907-1914.

[8] X. Sui, H. Guo, P. Chen, Y. Zhu, C. Wen, Y. Gao, J. Yang, X. Zhang, L. Zhang, Zwitterionic Osmolyte‑Based Hydrogels with Antifreezing Property, High Conductivity, and Stable Flexibility at Subzero Temperature, Advanced Functional Materials, 30 (2020) 1907986.

[9] J. Yang, Z. Xu, J. Wang, L. Gai, X. Ji, H. Jiang, L. Liu, Antifreezing Zwitterionic Hydrogel Electrolyte with High Conductivity of 12.6 mS cm− 1 at− 40° C through Hydrated Lithium Ion Hopping Migration, Advanced Functional Materials, 31 (2021) 2009438.

[10] X.P. Morelle, W.R. Illeperuma, K. Tian, R. Bai, Z. Suo, J.J. Vlassak, Highly stretchable and tough hydrogels below water freezing temperature, Advanced Materials, 30 (2018) 1801541.

[11] W. Ge, S. Cao, Y. Yang, O.J. Rojas, X. Wang, Nanocellulose/LiCl systems enable conductive and stretchable electrolyte hydrogels with tolerance to dehydration and extreme cold conditions, Chemical Engineering Journal, 408 (2021) 127306.

[12] H. Gao, Z. Zhao, Y. Cai, J. Zhou, W. Hua, L. Chen, L. Wang, J. Zhang, D. Han, M. Liu, Adaptive and freeze-tolerant heteronetwork organohydrogels with enhanced mechanical stability over a wide temperature range, Nature communications, 8 (2017) 1-8.

[13] Q. Wang, J. Lan, Z. Hua, X. Ma, L. Chen, X. Pan, Y. Li, S. Cao, Y. Ni, An oriented Fe3+-regulated lignin-based hydrogel with desired softness, conductivity, stretchability, and asymmetric adhesiveness towards anti-interference pressure sensors, International Journal of Biological Macromolecules, 184 (2021) 282-288.

[14] L. Wu, L. Li, M. Qu, H. Wang, Y. Bin, Mussel-inspired self-adhesive, antidrying, and antifreezing poly (acrylic acid)/bentonite/polydopamine hybrid glycerol-hydrogel and the sensing application, ACS Applied Polymer Materials, 2 (2020) 3094-3106.

[15] E. Feng, J. Li, G. Zheng, Z. Yan, X. Li, W. Gao, X. Ma, Z. Yang, Long-Term Anti-freezing Active Organohydrogel Based Superior Flexible Supercapacitor and Strain Sensor, ACS Sustainable Chemistry & Engineering, (2021).

[16] Q. Rong, W. Lei, L. Chen, Y. Yin, J. Zhou, M. Liu, Anti‐freezing, conductive self‐healing organohydrogels with stable strain‐sensitivity at subzero temperatures, Angewandte Chemie International Edition, 56 (2017) 14159-14163.

[17] Q. Rong, W. Lei, M. Liu, Conductive hydrogels as smart materials for flexible electronic devices, Chemistry–A European Journal, 24 (2018) 16930-16943.

[18] Y. Jian, S. Handschuh-Wang, J. Zhang, W. Lu, X. Zhou, T. Chen, Biomimetic anti-freezing polymeric hydrogels: keeping soft-wet materials active in cold environments, Materials Horizons, 8 (2021) 351-369.

[19] Y. Gao, S. Gu, F. Jia, Q. Wang, G. Gao, "All-in-one" hydrolyzed keratin protein-modified polyacrylamide composite hydrogel transducer, Chemical Engineering Journal, 398 (2020) 125555.

[20] J. Xu, R. Jing, X. Ren, G. Gao, Fish-inspired anti-icing hydrogel sensors with low-temperature adhesion and toughness, Journal of Materials Chemistry A, 8 (2020) 9373-9381.

[21] N.S. Ustun, S. Turhan, Antifreeze proteins in foods, Antifreeze Proteins Volume 2, Springer2020, pp. 231-260.

[22] D.S. Friis, H. Ramløv, Physicochemical Properties of Antifreeze Proteins, Antifreeze Proteins Volume 2, Springer2020, pp. 43-67.

[23] H. Xiang, X. Yang, L. Ke, Y. Hu, The properties, biotechnologies, and applications of antifreeze proteins, International journal of biological macromolecules, 153 (2020) 661-675.

[24] I. Voets, From ice-binding proteins to bio-inspired antifreeze materials, Soft Matter, 13 (2017) 4808-4823.

[25] A.P. Esser-Kahn, V. Trang, M.B. Francis, Incorporation of antifreeze proteins into polymer coatings using site-selective bioconjugation, Journal of the American Chemical Society, 132 (2010) 13264-13269.

[26] A. Jorov, B.S. Zhorov, D.S. Yang, Theoretical study of interaction of winter flounder antifreeze protein with ice, Protein Science, 13 (2004) 1524-1537.

[27] Z. Li, Y. Su, B. Xie, H. Wang, T. Wen, C. He, H. Shen, D. Wu, D. Wang, A tough hydrogel–hydroxyapatite bone-like composite fabricated in situ by the electrophoresis approach, Journal of Materials Chemistry B, 1 (2013) 1755-1764.

[28] J. Zhang, L. Zeng, Z. Qiao, J. Wang, X. Jiang, Y.S. Zhang, H. Yang, Functionalizing Double-Network Hydrogels for Applications in Remote Actuation and

in Low-Temperature Strain Sensing, ACS Applied Materials & Interfaces, 12 (2020) 30247-30258.

[29] I.D. Jones, R.A. Gortner, Free and bound water in elastic and non-elastic gels, The Journal of Physical Chemistry, 36 (2002) 387-436.

[30] K.R. Foster, H.A. Resing, A.N. Garroway, Bounds on" bound water": transverse nuclear magnetic resonance relaxation in barnacle muscle, Science, 194 (1976) 324-326.

[31] J.G. Duman, Antifreeze and ice nucleator proteins in terrestrial arthropods, Annual Review of Physiology, 63 (2001) 327-357.

[32] D.J. Lee, S.F. Lee, Measurement of bound water content in sludge: the use of differential scanning calorimetry (DSC), Journal of Chemical Technology & Biotechnology: International Research in Process, Environmental AND Clean Technology, 62 (1995) 359-365.

[33] I.N. Savina, V.M. Gun'Ko, V.V. Turov, M. Dainiak, G.J. Phillips, I.Y. Galaev, S.V. Mikhalovsky, Porous structure and water state in cross-linked polymer and protein cryo-hydrogels, Soft Matter, 7 (2011) 4276-4283.

[34] G.L. Fletcher, C.L. Hew, P.L. Davies, Antifreeze proteins of teleost fishes, Annual review of physiology, 63 (2001) 359-390.

Chapter 5 A tough hydrogel with fast self-healing and adhesive performance for wearable sensors

5.1 Introduction

In recent years, wearable sensors based on conductive hydrogels have attracted a lot of attention in the field of human motion detection due to their many advantages, such as flexibility, sensitivity and accuracy [1-5]. In these wearable sensors, the conductive hydrogel serves as a transducer for converting external deformations (e.g., stretch, compression, and bending) into electrical signals [6]. Much work has been done to improve the performance of hydrogels for better applications in wearable sensors [7-9]. Unfortunately, hydrogels usually face the challenge of being unable to strike a balance between mechanical properties, adhesion, and self-healing ability [10, 11]. Therefore, adhesive hydrogels are usually difficult to withstand repeated adhesion and reuse. Furthermore, in previous studies, the raw materials used for adhesive hydrogels were often specific and the production process was complex, which limited their widespread use.

A hydrogel without adhesive property needs to be combined with other adhesives to establish good contact with substrates, which brings some disadvantages (e.g., complicates the procedure, does not facilitate lightweighting of the device, and leads to undesired signal loss). Ultimately, there will be a waste of energy and a negative effect on the accuracy and real time of signal transmission. So far, many efforts have been made to improve the adhesion of hydrogels[12]. The adhesion of hydrogels is mainly achieved through chemical bonds and/or physical interactions between the functional groups of the hydrogel and other substrates [13]. Typically, chemical bonds with high energies are usually strong but irreversible. Physical interactions (such as hydrogen

bonding, hydrophobic interactions, metal complexation, π–π stacking, cation–π interactions [14-20]) are relatively weak but reversible and may be used for repeated adhesions. The adhesive hydrogel can establish reliable contact with the surface of the skin, which is favorable for wearable sensors. For instance, inspired by mussel foot proteins, the strong adhesion of hydrogels was achieved through a variety of interactions (covalent interactions, electrostatic attraction, π-π/cation-π bonds, hydrogen bonds, and hydrophobic interactions) [19]. Jin et al. [21] fabricated a new adhesive hydrogel with GO@DA nanofillers to make the hydrogel adhesive and physically and chemically crosslinked network to ensure that the hydrogel was stretchable and self-healing. Unfortunately, most of adhesive hydrogels usually suffer from weak mechanical properties (e.g., poor tensile strength, elongation, toughness), which are too weak to withstand repeated adhesions and reusability. For example, lv et al. [22] designed a mussel-inspired conductive hydrogel that showed excellent adhesion strength of 49.6 kPa but only 42.4 kPa of tensile toughness. An ionic hydrogel based on the mussel and zwitterionic adhesion mechanisms could robust adhere to tissues with a strength of 19.4 kPa, but the maximum tensile strength and fracture strain of the hydrogel were just 90 kPa and 900% [23]. The lack of mechanical properties will also affect the stability and reliability of hydrogels used in wearable sensors, thus hindering the development of hydrogels in practical applications. Therefore, it is of great interest to develop a hydrogel with both adhesion and good mechanical properties.

When used as a sensor, the hydrogel will inevitably undergo mechanical damage during long-term cyclic deformation, which will affect its signal stability, reliability and service life. Hydrogels with self-healable performances, which can repair their own damage, are widely used to solve this problem [24-28]. There are still some challenges with self-healing hydrogels, such as low healing efficiency, long self-healing time and the need for assistance (mechanical, thermal, optical, electrical or magnetic stimulation) in the healing process [27, 29, 30].

Polyvinylpyrrolidone (PVP) is a traditional industrial product that is often used as an adhesive for glue sticks, hot-melt adhesives, etc. because it can act as a hydrogen bond

acceptor to form strong interactions with a hydrogen bond donor. The biocompatibility and adhesion of PVP also enable it to be used as ingredients in the pharmaceutical field, such as pharmaceutical tablets, temporary skin coverings, and wound dressings. In previous studies, the use of PVP to improve the adhesion of hydrogels has hardly been mentioned. Herein, taking advantage of PVP, an adhesive hydrogel is prepared in this work by an easily accessible fabrication method. The hydrogel is constructed by strong hydrogen bonding interactions between polyacrylic acid (PAA) and PVP as well as ionic coordination between Fe^{3+} and PAA. Good adhesion and mechanical properties were achieved simultaneously in this hydrogel. The involvement of PVP provides the hydrogel with a robust adhesion (64 kPa). The good mechanical properties ensure that the adhesion can be reused. The hydrogel also has a rapid self-healing ability with high healing efficiency in terms of both mechanical properties and conductivity. Because of the combination of favorable adhesion, mechanical properties and self-healing ability, the hydrogel-based sensors to provide good stability, accuracy and reliability in real-time monitoring. In addition to the excellent performance, the raw materials used in this hydrogel are all mature products and the preparation process is simple, which is expected to be applied in large scale industrial production.

5.2 Experimental Section

5.2.1 Materials

Acrylic acid (AA, EP), polyvinylpyrrolidone (PVP K-30, EP), ammonium peroxydisulfate (APS, GR), iron chloride hexahydrate ($FeCl_3 \cdot 6H_2O$, EP). All the above materials were not subjected to any further purification. Deionized water was used to prepare the aqueous solution throughout the work.

5.2.2 Fabrication of Hydrogels

The hydrogels were prepared by one-step method. 10 g AA, a certain amount of

FeCl$_3$·6H$_2$O aqueous solution and deionized water were mixed followed by the adding of a certain quantity of PVP under stirring. After that 0.1 g APS was added to the solution. After fully dissolving, the above solution was treated by ultrasonic for 10 min to remove air bubbles. The hydrogel precursor was then poured into a custom mold to form the hydrogel in a 60°C oven for 6 h. The hydrogels were abbreviated as PAA/Fe/PVP-n, the corresponding recipes were shown in Table S1. For comparison, PAA/Fe hydrogel and PAA/PVP hydrogel were also fabricated under the same condition.

5.2.3 Characterization

(1) Microstructural Characterizations

The FTIR spectra of pure PVP, PAA/PVP, and PAA/Fe/PVP hydrogel were characterized by a Thermo Scientific Nicolet iN 10 infrared spectrometer. The microstructure of the PAA/Fe/PVP hydrogel was observed by scanning electron microscopy (SEM, S-4300 Hitachi, Ltd. Japan). The hydrogels were freeze dried for 24 h after quick-freezing by liquid nitrogen and then the cross-section was sputtered with platinum for SEM imaging at 5 kV.

(2) Mechanical Test

The mechanical tests were conducted with a universal mechanical tester (Instron 3385, Instron Co., Ltd., Canton, USA) equipped with a 50 N load cell at room temperature. Rectangular hydrogel strips (20 mm × 4 mm × 2 mm) were used for mechanical tests (tensile speed of 100 mm/min). The area of integration under the stress-strain curve was defined as the toughness.

(3) Adhesion Test

The adhesion properties of hydrogels were determined by lap shear tests using a universal testing machine (Instron 3385, Instron Co., Ltd., Canton, USA). The sample

(15 mm × 15 mm × 0.6 mm) was sandwiched between two glass slides with a bonded area of 2.25 cm^2. Hold the glass slides with a long-tailed clip for 10 minutes before testing to make good contact between the slides and the sample. All tests were performed at a crosshead speed of 2 mm/min at room temperature. Repeated lap shear tests were also performed to show the reproducibility of hydrogel adhesion. The adhesion strength was calculated by dividing the maximum load by the initial bonding area.

(4) Self-Healing Test

The self-healing ability of the mechanical properties of the hydrogels was tested at room temperature with a universal mechanical tester (Instron 3385, Instron Co., Ltd., Canton, USA) equipped with a 50 N load cell at room temperature. Rectangular specimens (40 mm in length, 4 mm in width, and 2 mm in depth) were cut into halves with scissor, then the two halves were brought into contact immediate and were stored in a sealed vessel to heal for testing. The healing efficiency (HE) was the ratio of tensile strength (HE of tensile strength) or tensile stress (HE of tensile stress) between the healed hydrogel and the original hydrogel. The microscopic self-healing behavior of damaged sample was observed by a digital microscope (VHX-6000, KEYENCE, America).

(5) Electrical Test

A digital source meter (LCR-6100, GWInstek) was used to monitor the resistance in real time. The relative resistance change $\triangle R/R_0$ was computed from $(R- R_0)/R_0 \times 100\%$, where R, R_0 and ΔR represented the real-time resistance, inherent resistance and the difference between R and R_0, respectively.

5.3 **Results**

5.3.1 **Synthesis of Hydrogels**
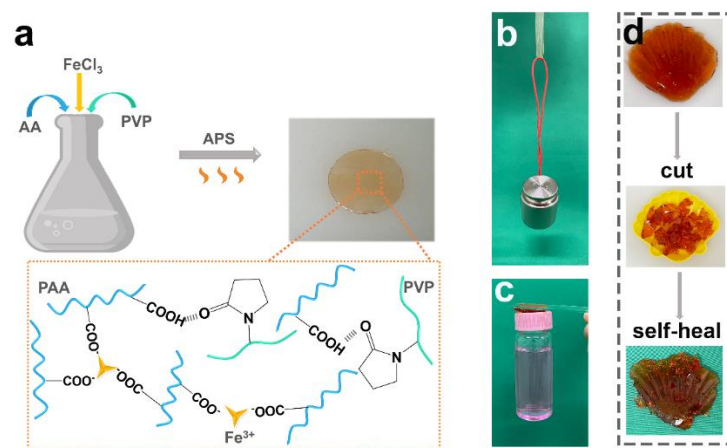
Fig. 5.1 a) Schematic diagram of the fabrication process and mechanism of PAA/Fe/PVP hydrogel. b). The hydrogel is strong enough to lift a weight of 200 g. c) Strong adhesion enables the PAA/ Fe/PVP hydrogel to withstand a heavy load of 80 g. d) The PAA/Fe/PVP hydrogel can self-heal to the original shape at room temperature.

PAA/Fe/PVP hydrogel was synthesized by a simple one-step radical polymerization method. The mechanism scheme of synthesis was shown in Fig. 5.1a. In brief, AA, $FeCl_3 \cdot 6H_2O$ aqueous solution, PVP and APS were mixed to form a pre-solution under stirring. The pre-solution was heated to initiate the polymerization of AA and form the target PAA/Fe/PVP hydrogel. PAA, as a hydrogen donor, formed strong hydrogen bond with the carbonyl group of PVP [31]. In fact, another type of hydrogen bond may exist between PAA and PVP, which was formed between the partially positively charged nitrogen atom of PVP and the carboxyl group of PAA. However, this type of hydrogen bonding was rare due to the spatial site resistance between the ring and the macromolecular chain [32]. There was also another kind of physical bond in the hydrogel. Fe^{3+}, as an ionic cross-linker, could form ionic coordinate bonds with -COO$^-$ of PAA[33, 34]. The hydrogen bonding and ion coordination built strong interactions

in the PAA/Fe/PVP hydrogel, giving the hydrogel good mechanical properties (Fig. 5.1b, the hydrogel could lift a weight of 200 g). Due to the involvement of PVP, the hydrogel also displayed strong adhesion and was able to withstand a heavy load of 80 g (Fig. 5.1c). The good self-healing performance allowed the sheared hydrogel fragments to heal to the original shape at room temperature (Fig. 5.1d). Furthermore, the raw materials used were all commonly used products and easily available. The preparation process was simple. The method in this work had the potential to enable large-area, low-cost manufacturing.

5.3.2 Mechanical properties
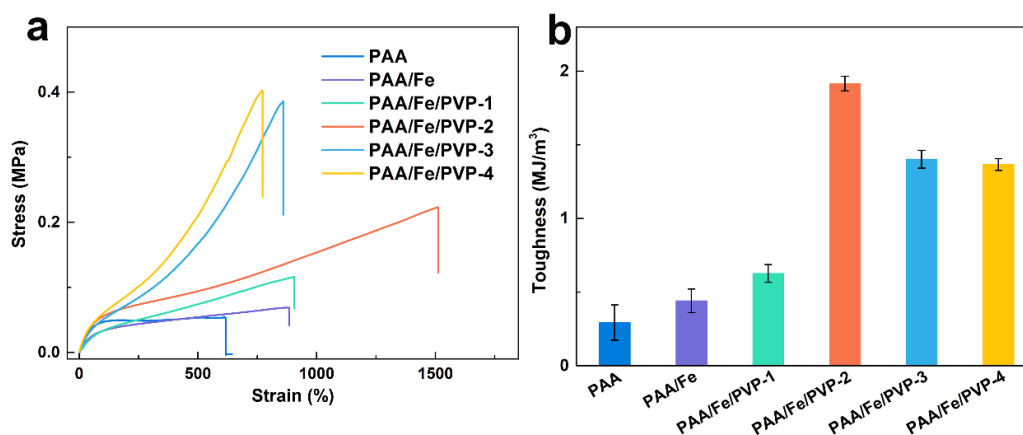
Fig. 5.2 a) Tensile stress-strain curves of the PAA//Fe/PVP hydrogel. b) Toughness of the PAA//Fe/PVP hydrogel.

The mechanical properties were further investigated by tensile stress-strain tests. Fig. 5.2a displayed the representative tensile stress-strain curves of the hydrogels. The presence of PVP had a positive effect on the mechanical properties as a result of strong hydrogen bonding interactions between carbonyl groups of PVP and carboxyl groups of PAA [35]. As the content of PVP increased, the tensile strength increased monotonically from 0.05 MPa (PAA hydrogel) to 0.40 MPa (PAA/Fe/PVP-4 hydrogel). Different from the tensile strength, the elongation increased to 1500% at first and then decreased. Tensile stress-strain curves of PAA hydrogel and PAA/Fe hydrogel indicated

that ionic coordinate bonds could also improve the mechanical properties. Toughness of the hydrogels were calculated to demonstrate the mechanical properties (Fig. 5.2b) more visually. The change in toughness further demonstrated the effect of hydrogen bonds and ionic coordinate bonds on improving the mechanical properties. PAA/Fe/PVP-2 hydrogel had a toughness of up to 1.91 MJ/m^3. For comprehensive considerations, PAA/Fe/PVP-2 hydrogel was used in the subsequent experiments unless otherwise stated.

5.3.3 Adhesion
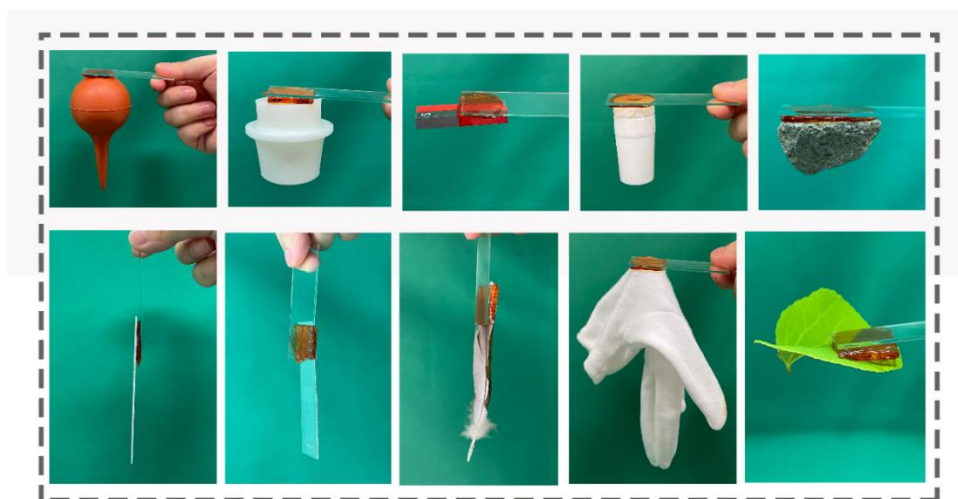
Fig. 5.3 The hydrogel demonstrates robust adhesion to various substrates.

PVP is widely used in various adhesive formulations because of its strong adhesion to the surfaces of the objects. The hydrogel also showed good adhesion due to the addition of PVP. As demonstrated in Fig. 5.3 the hydrogel could adhere to various substrate surfaces such as rubber, plastic, metal, and textiles. Adhesion strength was tested by lap shear tests (Fig. 5.4a). Representative adhesion strength-displacement curves of the PAA/Fe/PVP-2 hydrogel with glass, chicken skin and stainless steel as substrates were shown in Fig. 5.4b. The adhesive strength was 64 kPa, 36 kPa, and 59 kPa with glass, chicken skin, and stainless steel as substrates, respectively, which was higher than that of the previously reported adhesive hydrogels [21, 36, 37].
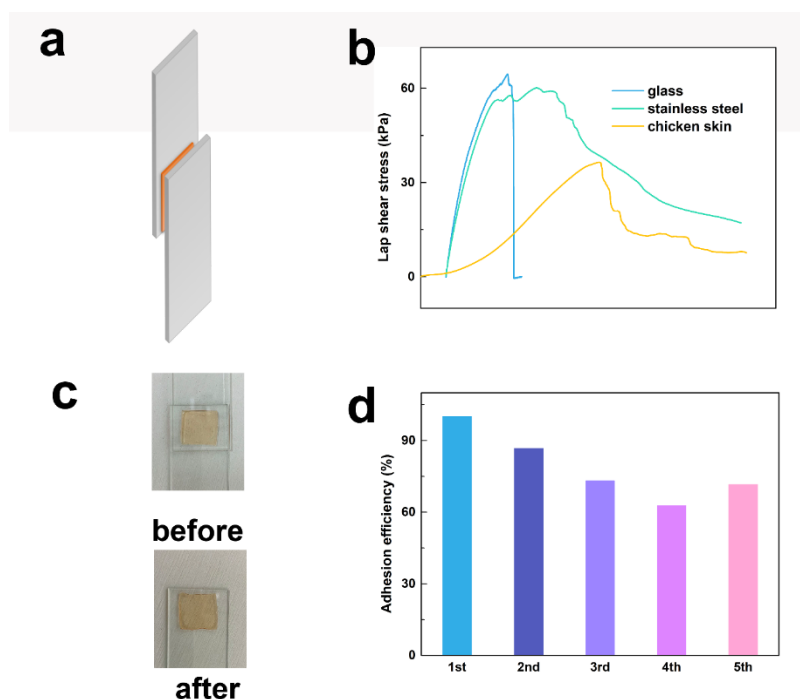
Fig. 5.4 a) Schematic diagram of lap shear test. b) Representative adhesion strength-displacement curves of the PAA/Fe/PVP-2 hydrogel with glass, chicken skin and stainless steel as substrates. c) The adhesion performance of the hydrogel could withstand multiple uses without breaking down. d) The adhesion efficiency of the PAA/Fe/PVP-2 hydrogel.

The effect of PVP on adhesive performance of the hydrogel was further studied. Representative adhesion strength-displacement curves were shown in Fig. 5.5a. The maximum strength was used as the interfacial adhesion strength of the hydrogel and results were shown in Fig. 5.5b. It was found that PVP had a significantly influence on the adhesive strength of the hydrogel. The adhesion strength of the hydrogel without PVP (PAA/Fe hydrogel) was about 18 kPa, which tended to increase with the addition of PVP and finally reached up to 64 kPa (PAA/Fe/PVP-2 hydrogel). With the further increase of the amount of PVP, the adhesion strength of the hydrogel (PAA/Fe/PVP-3, PAA/Fe/PVP-4 hydrogel) did not change much. From the adhesion strength of the

PAA/Fe hydrogel and PAA/PVP hydrogel, it could also be found that PVP had a more significant effect on the improvement of the hydrogel system. It is well known that PVP is a hydrogen bond acceptor with multiple hydrogel-acceptable sites. Since the vinylpyrrolidone unit in the PVP repeating unit can form hydrogen bonds with other functional groups, strong surface adsorption can be achieved between PVP and the substrate surfaces. Therefore, the substantial improvement in the adhesion performance of the hydrogel was considered to be caused by the hydrogen bonding originating from carbonyl group.
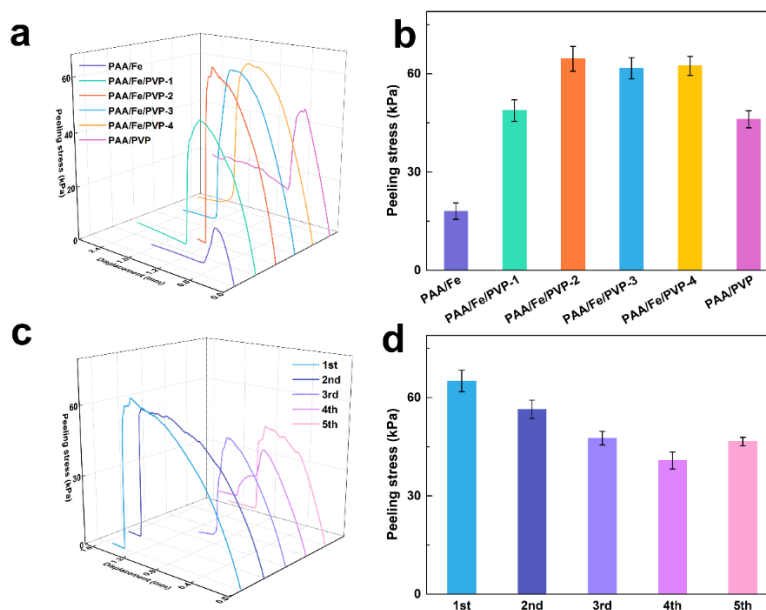
Fig. 5.5 a) Representative adhesion strength-displacement curves of the PAA/Fe hydrogel, PAA/Fe/PVP hydrogel and PAA/PVP hydrogel. b) Adhesion strength of the PAA/Fe hydrogel, PAA/Fe/PVP hydrogel and PAA/PVP hydrogel. c) Representative adhesion strength-displacement curves of the same PAA/Fe-2 hydrogel used 5 times. d) Adhesion strength of the same PAA/Fe-2 hydrogel used 5 times.

A lap shear test was also performed on the same sample to investigate the feasibility of reuse of the hydrogel. As expected, the adhesion performance of the hydrogel could withstand multiple uses without breaking down (Fig. 5.4c). As shown in Fig. 5.5c and Fig. 5.5d, the adhesion strength could be maintained after 5 repeated tests, and the minimum adhesion efficiency was over 60% for all 5 cycles (Fig. 5.4d). There are two

kinds of interactions when bonding hydrogel with substrates. One is surface adhesion, which decides the adhesion strength of the hydrogel. The other is cohesion, which determines the inner strength of the hydrogel. The hydrogel could achieve not only favorable adhesion strength but also be reused when adhesion and cohesion are balanced. Therefore, the high mechanical properties played an important role in the repeated bonding of the hydrogel, as it helped the hydrogel not to be broken during the bonding and stretching process.

5.3.4   Self-healing

A self-healing material is a substance that has the inherent ability to automatically repair its damage. The ability to self-heal is highly desired for materials, as it extends the life of the material. In order to study the self-healing performance of the PAA/Fe/PVP hydrogel, the hydrogel was artificially damaged, and a series of experiments were performed on the damaged samples.
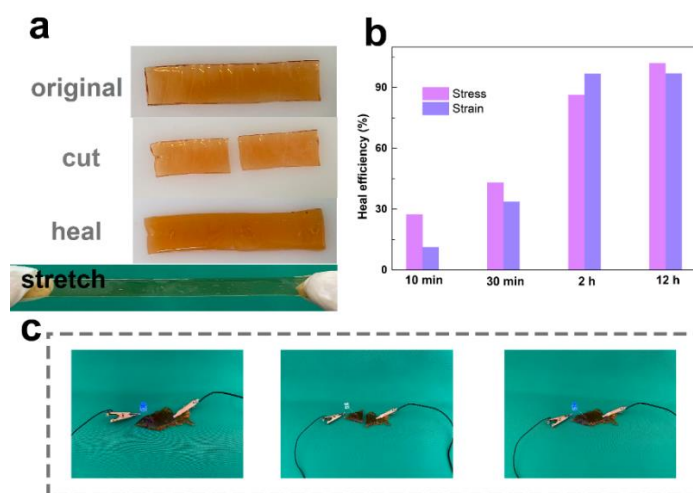
Fig. 5.6 a) The PAA/Fe/PVP hydrogel revealed good self-healing performance against mechanical damage. b) The self-healing efficiencies of tensile strength and elongation. c) The hydrogel is conductive to allow the LED bulb to be lit in the hydrogel-connected circuit. The LED bulb goes off and immediately come back on when the two parts are placed together again.

The PAA/Fe/PVP hydrogel revealed good self-healing performance against mechanical damage. When the two halves of the cut hydrogel were joined again, they healed automatically into one piece at room temperature with virtually no gaps. Besides, the healed piece could withstand stretching without being damaged (Fig. 5.6a). The microscopic process of hydrogel self-healing was further observed by optical microscopy (Fig. 5.7a). It could be noted that the self-healing ability of the hydrogel showed a time-dependent characteristics. As shown in Fig. 5.7a, the crack became smaller and smaller with time and finally almost disappear within 2 h, indicating that the hydrogel had fast and good self-healing properties. Further, the self-heal of the mechanical properties of the damaged hydrogel was studied. The hydrogel was cut into two pieces with scissors and re-contacted to heal itself without any external force. The tensile strength and elongation of the healed hydrogel showed significant enhancement with increasing healing time (Fig. 5.7b). The self-healing efficiencies of tensile strength and elongation were calculated to quantitatively represent the self-healing ability (Fig. 5.6b). After 2 h of healing, the healing efficiency reached 86% (tensile strength) and 96% (elongation), and after 12 h of autonomous healing, more than 95% of healing efficiency was obtained for both tensile strength and elongation. The results indicated that the PAA/Fe/PVP hydrogel showed good self-healing performance against mechanical damage.

In addition to mechanical performance, the self-healing performance of conductivity was further investigated. The hydrogel was conductive due to the involvement of $FeCl_3$ in the hydrogel, which allowed the LED bulb to be lit in the hydrogel-connected circuit (Fig. 5.6c). After the hydrogel was cut into two parts, the LED bulb went off and immediately came back on when the two parts were placed together again. The electrical signals during hydrogel cutting and healing were recorded to investigate the healing behavior of electrical conductivity. As displayed in Fig. 5.7c, once an open circuit was formed due to the hydrogel being cut, the resistance increased to an infinite value. When the two pieces came into contact again, the resistance dropped rapidly to close to its initial value. This process was repeated six times and the signal showed the

same trend. In addition, it can be seen from the detail plot (Fig. 5.7d) that the resistance was lower than the steady-state value at the instant of contact between the two pieces, which was the result of free ions transferred in the hydrogel[38]. It cost about 1.6 s for the resistance to recover to the steady-state value, demonstrating the rapid self-healing ability of conductivity.
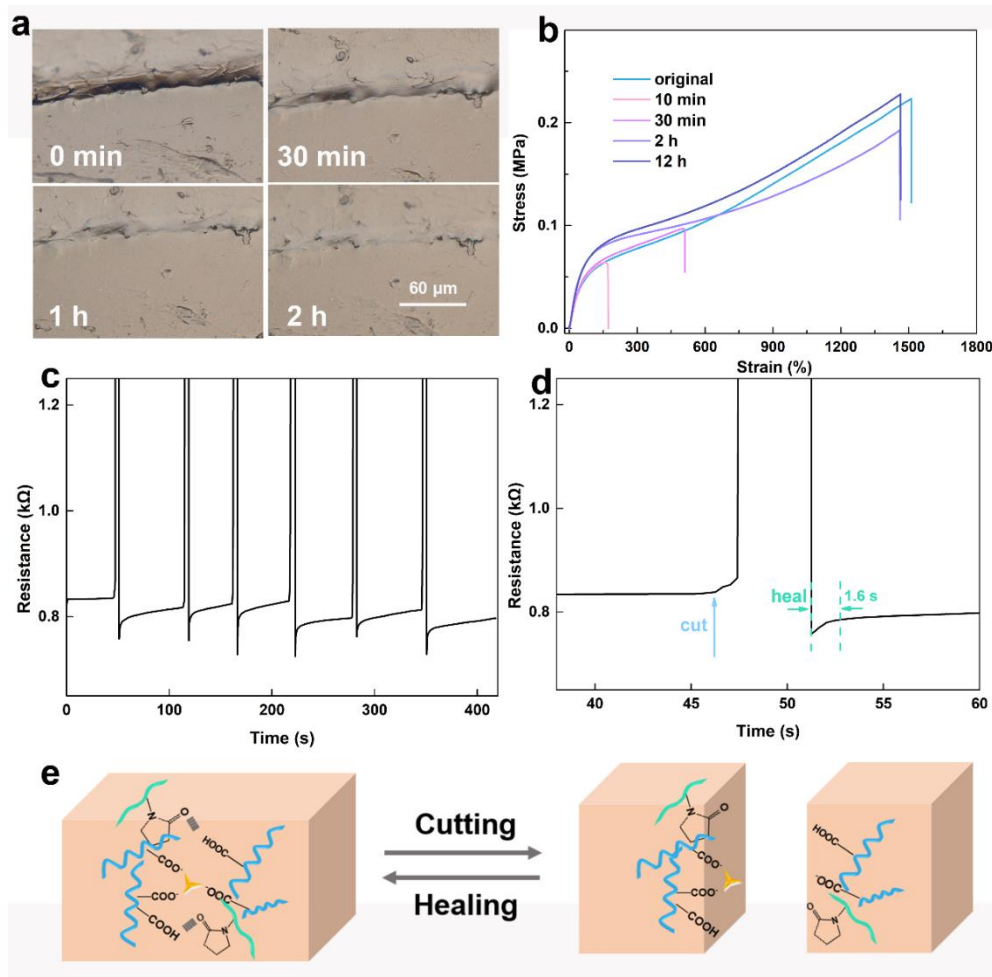

Fig. 5.7 a) The microscopic process of hydrogel self-healing observed by optical microscopy. b) Representative tensile stress-stress curves of PAA/Fe/PVP-2 hydrogel and self-healing samples at different time intervals. c) Resistance changes indicate the process of the PAA/Fe/PVP-2 hydrogel being cut and self-healing. d) Rapid self-healing speed of the PAA/Fe/PVP-2 hydrogel in conductivity. e) Self-healing mechanism illustrations of the hydrogel.

It is well known that hydrogen bonds and ionic coordination in hydrogels are reversible

and can be broken and recombined during the cutting and healing process [39, 40]. The mechanism of rapid and outstanding self-healing ability of the PAA/Fe/PVP hydrogel can probably be explained by the physical bonds in the hydrogel, as shown in Fig. 5.7e.

5.3.5 Sensor Applications
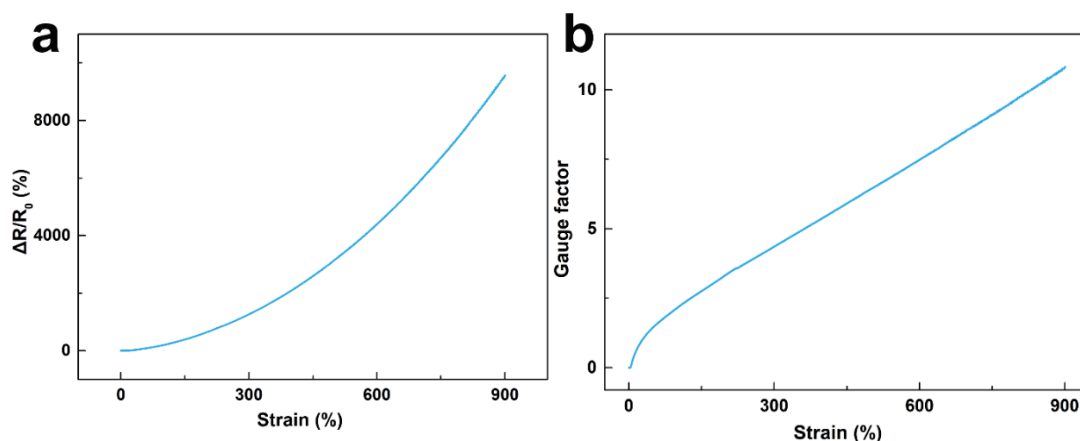
Fig. 5.8 a) The hydrogel-based sensor was sensitive to deformations. b) The gauge factor (GF) of the hydrogel-based sensor.

The hydrogel was assembled into strain sensors to investigate its application in sensing. As shown in Fig. 5.8a the hydrogel-based sensor was sensitive to deformations. The relative resistance change ($\Delta R/R_0$) increased with increasing tensile strain from 0% to 900%, indicating that the sensor had a wide strain sensing range. The gauge factor (GF) is defined as $\Delta R/R0/\varepsilon$, which reflects the tensile strain sensitivity of sensors. As shown in Fig. 5.8b, when the tensile strain was below 50%, the GF increased sharply to 1.5; then, when the tensile strain was further increased to 900%, the GF increased linearly to 10.8. The GF was compatible to previous research that had a similar purpose [41-43]. 20 consecutive load-unload tensile cycles were performed at a strain of 50%, and the relative resistance change ($\Delta R/R_0$) of the sensor increased and decreased correspondingly with the change in strain (Fig. 5.9a). In this process, the signals were stable and accurate, which stemmed from the good mechanical properties, conductivity

and self-heal ability.
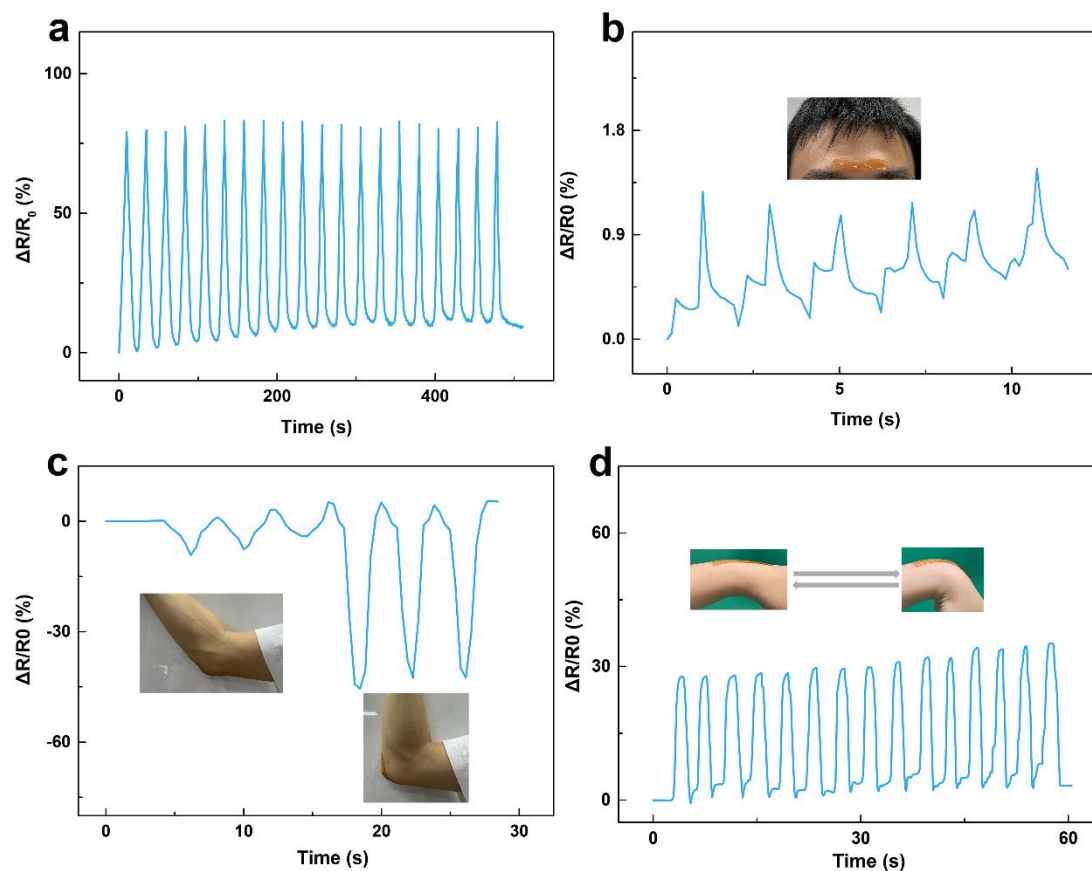
Fig. 5.9 a) Signal of the relative resistance ($\Delta R/R_0$) of the hydrogel-based sensor over time during 20 consecutive loading-unloading tensile tests. b) The $\Delta R/R0$ signal of a wearable hydrogel-based sensor represents a tiny frowning process. c-d) The real-time response signals of elbow and wrist flexion.

Further, sensors based on the hydrogel could be made into various shapes adapted to the human body for wearable applications. As shown in Fig. 5.9b, the hydrogel-based sensor was adhered to the forehead to sense facial micro-expressions. Tiny frowns were converted into electrical signals and recorded. Muscle contraction (frown) and muscle relaxation (frown relaxed) corresponded to the peaks in the waveform. Repeated peaks could be detected stably when the frown was repeated. The subtle frowns were steadily and repeatedly converted into electrical signals, indicating close contact between the hydrogel-based sensor and the forehead. In addition to tiny facial micro-expressions,

the hydrogel-based sensor could also be adhered to human joints to detect large movements. Fig. 5.9c, d displayed the real-time response signals of elbow and wrist flexion. When the elbow was bent to 45° and straightened, the electrical signals could steadily change to the corresponding value. And the peak value also responded to the angle changes, becoming larger when the bending was greater to 90° (Fig. 5.9c). Moreover, the process of 15 repetitive flexion and extension of the wrist was monitored precisely and stably (Fig. 5.9d). In short, the hydrogel exhibited good sensing performance as wearable sensors because of its good mechanical properties, strong adhesion, and self-healing ability.

5.4 Conclusions

In summary, a novel ionic conductive PAA/Fe/PVP hydrogel with good mechanical properties, robust adhesion and rapid self-healing ability was fabricated via a simple radical polymerization method. This work solves the problem of generally poor mechanical properties of adhesive hydrogels. The involvement of PVP provided the hydrogel with robust adhesion to a variety of substrates. The good mechanical properties supported by hydrogen and ionic bonding ensured that the adhesion of the hydrogel could withstand multiple uses. In addition, both mechanical properties and conductivity could rapidly repair themselves after damage without any assistance. Outstanding adhesion, mechanical properties and self-healing ability enabled hydrogel-based sensors to demonstrate stability, accuracy, and reliability in real-time monitoring. Moreover, the raw material and preparation process of this work are expected to be applied in large-scale industrial production.

References

[1] C. Yang, Z. Suo, Hydrogel ionotronics, Nature Reviews Materials, 3 (2018) 125-142.

[2] G. Ge, Y. Zhang, J. Shao, W. Wang, W. Si, W. Huang, X. Dong, Stretchable, transparent, and self‐patterned hydrogel‐based pressure sensor for human motions detection, Advanced Functional Materials, 28 (2018) 1802576.

[3] C. Lu, J. Qiu, M. Sun, Q. Liu, E. Sakai, G. Zhang, Simple preparation of carboxymethyl cellulose-based ionic conductive hydrogels for highly sensitive, stable and durable sensors, Cellulose, 28 (2021) 4253-4265.

[4] X. Sun, Z. Qin, L. Ye, H. Zhang, Q. Yu, X. Wu, J. Li, F. Yao, Carbon nanotubes reinforced hydrogel as flexible strain sensor with high stretchability and mechanically toughness, Chemical Engineering Journal, 382 (2020) 122832.

[5] M. Sun, J. Qiu, S. Jin, W. Liu, E. Sakai, Visible light induced synthesis of high toughness, self-healing ionic hydrogel and its application in strain sensing, Colloids and Surfaces A: Physicochemical and Engineering Aspects, 607 (2020) 125438.

[6] F. Sun, X. Huang, X. Wang, H. Liu, Y. Wu, F. Du, Y. Zhang, Highly Transparent, Adhesive, Stretchable and conductive PEDOT: PSS/Polyacrylamide hydrogels for Flexible Strain Sensors, Colloids and Surfaces A: Physicochemical and Engineering Aspects, (2021) 126897.

[7] Z. Lei, Q. Wang, P. Wu, A multifunctional skin-like sensor based on a 3D printed thermo-responsive hydrogel, Materials Horizons, 4 (2017) 694-700.

[8] C. Lu, J. Qiu, W. Zhao, E. Sakai, G. Zhang, R. Nobe, M. Kudo, T. Komiyama, Low-temperature adaptive conductive hydrogel based on ice structuring proteins/CaCl2 anti-freeze system as wearable strain and temperature sensor, International Journal of Biological Macromolecules, 188 (2021) 534-541.

[9] Y. Tai, M. Mulle, I.A. Ventura, G. Lubineau, A highly sensitive, low-cost, wearable pressure sensor based on conductive hydrogel spheres, Nanoscale, 7 (2015) 14766-14773.

[10] J. Yang, R. Bai, B. Chen, Z. Suo, Hydrogel adhesion: A supramolecular synergy of chemistry, topology, and mechanics, Advanced Functional Materials, 30 (2020) 1901693.

[11] J. Liu, S. Lin, X. Liu, Z. Qin, Y. Yang, J. Zang, X. Zhao, Fatigue-resistant adhesion of hydrogels, Nature communications, 11 (2020) 1-9.

[12] L. Zhang, M. Liu, Y. Zhang, R. Pei, Recent progress of highly adhesive hydrogels as wound dressings, Biomacromolecules, 21 (2020) 3966-3983.

[13] S. Li, Y. Cong, J. Fu, Tissue adhesive hydrogel bioelectronics, J Mater Chem B, 9 (2021) 4423-4443.

[14] L. Han, X. Lu, K. Liu, K. Wang, L. Fang, L.-T. Weng, H. Zhang, Y. Tang, F. Ren, C. Zhao, Mussel-inspired adhesive and tough hydrogel based on nanoclay confined dopamine polymerization, ACS nano, 11 (2017) 2561-2574.

[15] Z. Gao, L. Duan, Y. Yang, W. Hu, G. Gao, Mussel-inspired tough hydrogels with self-repairing and tissue adhesion, Applied Surface Science, 427 (2018) 74-82.

[16] Q. Zhao, D.W. Lee, B.K. Ahn, S. Seo, Y. Kaufman, J.N. Israelachvili, J.H. Waite, Underwater contact adhesion and microarchitecture in polyelectrolyte complexes actuated by solvent exchange, Nature materials, 15 (2016) 407-412.

[17] J. Chen, D. Wang, L.H. Wang, W. Liu, A. Chiu, K. Shariati, Q. Liu, X. Wang, Z. Zhong, J. Webb, An adhesive hydrogel with "Load‐Sharing" effect as tissue bandages for drug and cell delivery, Advanced Materials, 32 (2020) 2001628.

[18] Y. Liang, Z. Li, Y. Huang, R. Yu, B. Guo, Dual-dynamic-bond cross-linked antibacterial adhesive hydrogel sealants with on-demand removability for post-wound-closure and infected wound healing, ACS nano, 15 (2021) 7078-7093.

[19] X. Fan, Y. Fang, W. Zhou, L. Yan, Y. Xu, H. Zhu, H. Liu, Mussel foot protein inspired tough tissue-selective underwater adhesive hydrogel, Materials Horizons, 8 (2021) 997-1007.

[20] S. Lu, X. Zhang, Z. Tang, H. Xiao, M. Zhang, K. Liu, L. Chen, L. Huang, Y. Ni, H. Wu, Mussel-inspired blue-light-activated cellulose-based adhesive hydrogel with

fast gelation, rapid haemostasis and antibacterial property for wound healing, Chemical Engineering Journal, 417 (2021) 129329.

[21] X. Jin, H. Jiang, Z. Zhang, Y. Yao, X. Bao, Q. Hu, Ultrastretchable, self-adhesive, strain-sensitive and self-healing GO@ DA/Alginate/P (AAc-co-AAm) multifunctional hydrogels via mussel-inspired chemistry, Carbohydrate Polymers, 254 (2021) 117316.

[22] R. Lv, Z. Bei, Y. Huang, Y. Chen, Z. Zheng, Q. You, C. Zhu, Y. Cao, Mussel‐Inspired Flexible, Wearable, and Self‐Adhesive Conductive Hydrogels for Strain Sensors, Macromolecular rapid communications, 41 (2020) 1900450.

[23] X. Pei, H. Zhang, Y. Zhou, L. Zhou, J. Fu, Stretchable, self-healing and tissue-adhesive zwitterionic hydrogels as strain sensors for wireless monitoring of organ motions, Materials Horizons, 7 (2020) 1872-1882.

[24] Y. Li, L. Li, Z. Zhang, J. Cheng, Y. Fei, L. Lu, An all-natural strategy for versatile interpenetrating network hydrogels with self-healing, super-adhesion and high sensitivity, Chemical Engineering Journal, 420 (2021) 129736.

[25] F.B. Kadumudi, M. Hasany, M.K. Pierchala, M. Jahanshahi, N. Taebnia, M. Mehrali, C.F. Mitu, M.A. Shahbazi, T.G. Zsurzsan, A. Knott, The Manufacture of Unbreakable Bionics via Multifunctional and Self‐Healing Silk‐Graphene Hydrogels, Advanced Materials, (2021) 2100047.

[26] A. Zhang, Y. Liu, D. Qin, M. Sun, T. Wang, X. Chen, Research status of self-healing hydrogel for wound management: A review, International Journal of Biological Macromolecules, 164 (2020) 2108-2123.

[27] Z. Deng, H. Wang, P.X. Ma, B. Guo, Self-healing conductive hydrogels: preparation, properties and applications, Nanoscale, 12 (2020) 1224-1246.

[28] X. Yu, Y. Zheng, H. Zhang, Y. Wang, X. Fan, T. Liu, Fast-Recoverable, Self-Healable, and Adhesive Nanocomposite Hydrogel Consisting of Hybrid Nanoparticles for Ultrasensitive Strain and Pressure Sensing, Chemistry of Materials, 33 (2021) 6146-6157.

[29] X. Wang, Y. Qiu, G. Chen, Z. Chu, A. Shadike, C. Chen, C. Chen, Z. Zhu, Self-healable poly (vinyl alcohol) photonic crystal hydrogel, ACS Applied Polymer Materials, 2 (2020) 2086-2092.

[30] R. Zhang, H. Ruan, Q. Fu, X. Zhu, Y. Yao, A high strain, adhesive, self-healable poly (acrylic acid) hydrogel with temperature sensitivity as an epidermal sensor, Materials Advances, 1 (2020) 329-333.

[31] J. Dong, Y. Ozaki, K. Nakashima, Infrared, Raman, and near-infrared spectroscopic evidence for the coexistence of various hydrogen-bond forms in poly (acrylic acid), Macromolecules, 30 (1997) 1111-1117.

[32] H. Kaczmarek, A. Szalla, A. Kamińska, Study of poly (acrylic acid)–poly (vinylpyrrolidone) complexes and their photostability, Polymer, 42 (2001) 6057-6069.

[33] J.-N. Zhang, H. Zhu, T. Liu, Y. Chen, C. Jiao, C. He, H. Wang, Strong adhesion of hydrogels by polyelectrolyte adhesives, Polymer, 206 (2020) 122845.

[34] H. Zhang, X. Wu, Z. Qin, X. Sun, H. Zhang, Q. Yu, M. Yao, S. He, X. Dong, F. Yao, Dual physically cross-linked carboxymethyl cellulose-based hydrogel with high stretchability and toughness as sensitive strain sensors, Cellulose, 27 (2020) 9975-9989.

[35] N. An, X. Wang, Y. Li, L. Zhang, Z. Lu, J. Sun, Healable and mechanically super‑strong polymeric composites derived from hydrogen‑bonded polymeric complexes, Advanced Materials, 31 (2019) 1904882.

[36] Z. Deng, T. Hu, Q. Lei, J. He, P.X. Ma, B. Guo, Stimuli-responsive conductive nanocomposite hydrogels with high stretchability, self-healing, adhesiveness, and 3D printability for human motion sensing, ACS applied materials & interfaces, 11 (2019) 6796-6808.

[37] J. Yin, S. Pan, L. Wu, L. Tan, D. Chen, S. Huang, Y. Zhang, P. He, A self-adhesive wearable strain sensor based on a highly stretchable, tough, self-healing and ultra-sensitive ionic hydrogel, Journal of Materials Chemistry C, 8 (2020) 17349-17364.

[38] G. Cai, J. Wang, K. Qian, J. Chen, S. Li, P.S. Lee, Extremely stretchable strain sensors based on conductive self‑healing dynamic cross‑links hydrogels for human‑motion detection, Advanced Science, 4 (2017) 1600190.

[39] Z. Deng, Y. Guo, X. Zhao, P.X. Ma, B. Guo, Multifunctional stimuli-responsive hydrogels with self-healing, high conductivity, and rapid recovery through host–guest interactions, Chemistry of Materials, 30 (2018) 1729-1742.

[40] C.H. Li, J.L. Zuo, Self‑healing polymers based on coordination bonds, Advanced Materials, 32 (2020) 1903762.

[41] T. Zhu, Y. Cheng, C. Cao, J. Mao, L. Li, J. Huang, S. Gao, X. Dong, Z. Chen, Y. Lai, A semi-interpenetrating network ionic hydrogel for strain sensing with high sensitivity, large strain range, and stable cycle performance, Chemical Engineering Journal, 385 (2020) 123912.

[42] H. Zhou, Z. Jin, Y. Yuan, G. Zhang, W. Zhao, X. Jin, A. Ma, H. Liu, W. Chen, Self-repairing flexible strain sensors based on nanocomposite hydrogels for whole-body monitoring, Colloids and Surfaces A: Physicochemical and Engineering Aspects, 592 (2020) 124587.

[43] J. Zhang, W. Xue, Y. Dai, L. Wu, B. Liao, W. Zeng, X. Tao, Double Network Hydrogel Sensors with High Sensitivity in Large Strain Range, Macromolecular Materials and Engineering, (2021) 2100486.

Chapter 6 Conclusion

Based on the needs of hydrogel-based flexible devices for signal stability, durability, and low-temperature adaptability, functionalities have been introduced to the hydrogels in this thesis. The functional hydrogels with outstanding mechanical properties, conductivity, anti-freeze property, adhesion, and self-healing ability have been designed and prepared, and their applications in flexible sensors have been further studied.

In chapter 3, a double-network ionic conductive hydrogel has been designed and prepared via a simple one-pot approach. The unique microstructure ensures that the hydrogel has favorable toughness, resilience, and recovery along with less residual strain. The hydrogel also exhibits outstanding ionic conductivity (6.0 S/m). The combined mechanical performance and ionic conductivity of the prepared hydrogel results in its remarkable performance when used in sensors. The hydrogel-based sensor displays superior sensitivity, stability and durability towards both tensile and compressive deformation. In practical applications, the sensor demonstrates a broad strain window to detect both large and very small human activities, showing the excellent potential of this hydrogel in sensing and flexible devices. The approach in this research has also been optimized to potentially allow for large-area, low-cost fabrication.

In chapter 4, the anti-freeze performance of hydrogel has been realized by introducing a novel anti-freeze system based on ice structuring proteins and $CaCl_2$ to the hydrogel structure. Both formation of ice nuclei and ice growth of the hydrogel at sub-zero temperature could be inhibited. Supported by the anti-freeze system, the hydrogel revealed good flexibility, recovery and conductivity at both room temperature and sub-zero temperature. The low-temperature adaptability enabled the hydrogel to be used as strain and temperature sensors at both room temperature and sub-zero temperature. The anti-freeze system in this research is expected to open up a new avenue to promote the conductive hydrogel with low-temperature adaptability.

113

In chapter 5, the balance of good mechanical performance, adhesion and self-healing ability have been achieved in the novel PAA/Fe/PVP hydrogel. PVP, as the main components of adhesives in daily life, plays a significant role in improving adhesion of the hydrogel. The adhesion of the hydrogel reaches up to 64 kPa by adjusting the amount of PVP. The adhesion can also withstand multiple uses due to the good mechanical properties of the hydrogel. Furthermore, the hydrogel displays outstanding self-healing ability in terms of both mechanical properties and conductivity. Because of the good mechanical properties, robust adhesion and rapid self-healing ability, the hydrogel-based sensors have demonstrated stability, accuracy and reliability in real-time monitoring of subtle facial micro-expressions and large human activities. Moreover, benefiting from the common raw materials and simple preparation process, the method in this work has the potential for large-area, low-cost manufacturing.

Publications

Ⅰ．審査付投稿論文

(1) **<u>Chunyin Lu</u>**, Jianhui Qiu, Manxi Sun, Qifan Liu, Eiichi Sakai, Guohong Zhang, Simple preparation of carboxymethyl cellulose-based ionic conductive hydrogels for highly sensitive, stable and durable sensors. Cellulose, 28 (2021) 4253-4265. (IF=5.044)

(2) **<u>Chunyin Lu</u>**, Jianhui Qiu, Wei Zhao, Eiichi Sakai, Guohong Zhang, Rie Nobe, Makoto Kudo, Takao Komiyama, Low-temperature adaptive conductive hydrogel based on ice structuring proteins/$CaCl_2$ anti-freeze system as wearable strain and temperature sensor. International Journal of Biological Macromolecules, 188 (2021) 534-541. (IF=6.953)

(3) **<u>Chunyin Lu</u>**, Jianhui Qiu, Wei Zhao, Eiichi Sakai, Guohong Zhang, A tough hydrogel with fast self-healing and adhesive performance for wearable sensors. Colloids and Surfaces A: Physicochemical and Engineering Aspects, 632 (2021): 127793. (IF=4.539)

(4) **<u>Chunyin Lu</u>**, Bin Mu, Peng Liu, Stimuli-responsive multilayer chitosan hollow microspheres via layer-by-layer assembly. Colloids and Surfaces B: Biointerfaces, 83 (2011) 254-259. (IF=5.268)

(5) **<u>Chunyin Lu</u>**, Peng Liu, Effect of chitosan multilayers encapsulation on controlled release performance of drug-loaded superparamagnetic alginate nanoparticles. Journal of Materials Science: Materials in Medicine, 23 (2012) 393-398. (IF=3.896)

(6) Manxi Sun, Jianhui Qiu, **<u>Chunyin Lu</u>**, Shuping Jin, Guohong Zhang, Eiichi Sakai, Multi-Sacrificial Bonds Enhanced Double Network Hydrogel with High Toughness, Resilience, Damping, and Notch-Insensitivity. Polymers, 12 (2020) 2263. (IF=4.329)

(7) Bin Mu, **<u>Chunyin Lu</u>**, Peng Liu, Disintegration-controllable stimuli-responsive polyelectrolyte multilayer microcapsules via covalent layer-by-layer assembly.

Colloids and Surfaces B: Biointerfaces, 82 (2011) 385-390. (IF=5.268)

(8) Bin Mu, **Chunyin Lu**, Yun Dong, Peng Liu, Preparation and Characterization of PVC-based Photoresponsive Polymers Containing Azo-chromophores, Journal of Macromolecular Science, Part A: Pure and Applied Chemistry, 47 (2010) 833-838. (IF=2.168)

注：博士論文テーマ関連：3 編（(1) ～ (3)），その他：5 編（(4) ～ (8)）

Ⅱ． 国際会議論文・発表

（1）**Chunyin Lu**, Jianhui Qiu, Eiichi Sakai, Guohong Zhang. A novel 3D microporous structure hydrogel with stable mechanical properties and high elasticity and its application in sensing. The 2nd International Online Conference on Polymer Science - Polymers and Nanotechnology for Industry 4.0 (IOCPS 2021), Online, November 1-15, 2021.

注：博士論文テーマ関連：1 件

Ⅲ． 国内学会

(1) 陸　春因、邱　建輝、劉　啓凡、境　英一、張　国宏．優れた力学特性をもつダブルネットワーク **PAA** ヒドロゲルの設計と作製．**M&M2021** 材料力学カンファレンス、**2021 年 9 月 15 日**、オンライン．

注：博士論文テーマ関連：1 件

Acknowledgements